MONTHLY NOTICES

OF THE

ROYAL ASTRONOMICAL SOCIETY

Volume 121 No. 3 1960

Published and Sold by the

ROYAL ASTRONOMICAL SOCIETY
BURLINGTON HOUSE
LONDON, W.1

Price £1 4*s.* 0*d.*; *in U.S.A.* $3.50

Subscription for volume: £6 ; *in U.S.A.* $18

The Geophysical Journal

OF THE

ROYAL ASTRONOMICAL SOCIETY

Editors

A. H. Cook
M.A., Ph.D., F.R.A.S., F.G.S.
National Physical Laboratory
Teddington

T. F. Gaskell
M.A., Ph.D., F.R.A.S.
British Petroleum Company
London

Price £1 per number; in U.S.A. $3. Annual Subscription £3; in U.S.A. $9

Volume 3 No. 3 September 1960

CONTENTS INCLUDE :

Orders should be addressed to :

The Assistant Secretary

Royal Astronomical Society, Burlington House, London, W.1

NOTICE TO AUTHORS

Presentation of Papers at Meeting

At some meetings of the Society the background and conclusions of selected papers are presented and then discussed. In order to assist the Secretaries in the selection of papers for such meetings, authors are asked to let the Society know, when submitting papers, whether they would be willing to give an account of their paper, if requested.

The attention of authors resident abroad is drawn to the fact that the Society welcomes information about their work. The Secretaries would be happy to consider having such work described at a meeting, in accordance with the author's wishes, either by a Secretary or other Fellow.

Publication of Papers

1. *General.*—It is the aim of the Society to be of the greatest possible service in disseminating astronomical results and ideas to the scientific community with the utmost possible speed. Contributors are accordingly urged to give the most careful consideration to the presentation of their work, for attention to detail will assuredly result in a substantial saving of time.

It is the practice of the Society to seek a referee's opinion on nearly every paper submitted for publication in *Monthly Notices*; experience has shown that frequently the comments of referees have enabled authors to improve the presentation of their work and so increase its scientific value.

2. *Communication.*—Papers must be communicated to the Society by a Fellow. They should be accompanied by a summary at the *beginning* of the paper conveying briefly the content of the paper, and drawing attention to important new information and to the main conclusions. The summary should be intelligible in itself, without reference to the paper, to a reader with some knowledge of the subject; it should not normally exceed 200 words in length. **Authors are requested to submit MSS. in duplicate.** These should be typed using double spacing and leaving a margin of not less than one inch on the left-hand side. Corrections to the MSS. should be made in the text and not in the margin. By Council decision, MSS. of accepted papers are retained by the Society for one year after publication; unless their return is then requested by the author they are destroyed.

3. *Presentation.*—Authors are allowed considerable latitude, but they are requested to follow the general style and arrangement of *Monthly Notices*. References to literature should be given either in the traditional form of a numbered list at the end of the paper, or as prescribed in *Notes on the Preparation of Papers to be Communicated to the Royal Society*.

4. *Notation.*—For technical astronomical terms, authors should conform closely to the recommendations of Commission 3 of the International Astronomical Union (*Trans. I.A.U.*; Vol. VI, p. 345, 1938). Council has decided to adopt the I.A.U. 3-letter abbreviations for constellations where contraction is desirable (Vol. IV, p. 221, 1932). In general matters, authors should follow the recommendations in *Symbols, Signs and Abbreviations* (London: Royal Society, 1951) except where these conflict with I.A.U. practice.

5. *Diagrams.*—**These should be designed to appear upright on the page, drawn about twice the size required in print and prepared for direct photographic reproduction except for the lettering, which should be inserted in pencil.** Legends should be given in the manuscript indicating where in the text the figure should appear. Blocks are retained by the Society for 10 years; unless the author requires them before the end of this period they are then destroyed. **Rough copies or prints of the diagrams should accompany each manuscript.**

6. *Tables.*—These should be arranged so that they can be printed upright on the page.

7. *Proofs.*—Authors are liable for costs of alteration exceeding 5 per cent of composition. It is therefore in their own and the Society's interests to seek the maximum conciseness and simplification of symbols and equations consistent with clarity.

CONTENTS

Printed in London by Taylor & Francis, Ltd., 1960 October

MONTHLY NOTICES
OF THE
ROYAL ASTRONOMICAL SOCIETY
Vol. 121 No. 3

NOTE ON THE TRANSFERENCE OF ANGULAR MOMENTUM WITHIN THE GALAXY THROUGH THE AGENCY OF A MAGNETIC FIELD

F. Hoyle and J. G. Ireland

(Received 1960 March 10)

Summary

It is shown that, under favourable conditions, the conventional picture of the orientation of the magnetic field in the spiral arms of the Galaxy can explain the outward motion of gas at a radial speed of order 50 km sec^{-1} within the central regions of the Galaxy. Such a motion cannot arise, however, unless at a greater distance from the galactic centre there is a corresponding inward motion. The failure to observe such an inward motion casts doubt on the correctness of the conventional picture of the magnetic field.

1. *Introduction.*—In a previous paper (1) we have considered the magnetic field within the galactic plane, using in our work several assumptions that have become conventionally accepted:

(1) The magnetic field is orientated along the spiral arms.
(2) The intensity in the solar neighbourhood is $\sim 6 \times 10^{-6}$ gauss.
(3) Initially the field had the rough form of a bar that passed through the nucleus.
(4) The change with time of the angular momentum of rotation in the Galaxy of the interstellar gas is small and can be neglected.

Subject to these assumptions it was shown that the differential rotational velocity in the Galaxy winds the magnetic field into a clockspring-like structure, the degree of wrapping after a time interval of $\sim 5 \times 10^{7}$ years being comparable with the wrapping of the spiral arms inferred by observation.

It is proposed now to examine the fourth of the above assumptions. A clockspring winding of the magnetic field causes angular momentum to be transferred from the gas at one radial distance to the gas at another radial distance. Hence (4) is certainly not strictly satisfied. The question is evidently whether or not (4) is satisfied to a sufficient approximation for the former conclusions to be still applicable. In the following discussion it will be shown that this is indeed the case, provided (1), (2), (3) are satisfied, except possibly at two particular values of the radial distance.

2. *The transference of angular momentum.*—In Fig. 1 we have a spiral arm crossing a cylinder of radius r along the arc AB. The figure should be thought of as possessing unit thickness in the direction perpendicular to its own plane, which we take to be the plane of the Galaxy. We also take the magnetic intensity H to be uniform over AB. The magnetic stress across AB has a component $H^2 \cos\theta \sin\theta / 4\pi$ per unit length of AB in the direction transverse to the radius vector.

CONTENTS

Printed in Great Britain by [illegible]

MONTHLY NOTICES
OF THE
ROYAL ASTRONOMICAL SOCIETY
Vol. 121 No. 3

NOTE ON THE TRANSFERENCE OF ANGULAR MOMENTUM WITHIN THE GALAXY THROUGH THE AGENCY OF A MAGNETIC FIELD

F. Hoyle and J. G. Ireland

(Received 1960 March 10)

Summary

It is shown that, under favourable conditions, the conventional picture of the orientation of the magnetic field in the spiral arms of the Galaxy can explain the outward motion of gas at a radial speed of order 50 km sec^{-1} within the central regions of the Galaxy. Such a motion cannot arise, however, unless at a greater distance from the galactic centre there is a corresponding inward motion. The failure to observe such an inward motion casts doubt on the correctness of the conventional picture of the magnetic field.

1. *Introduction.*—In a previous paper (1) we have considered the magnetic field within the galactic plane, using in our work several assumptions that have become conventionally accepted:

(1) The magnetic field is orientated along the spiral arms.
(2) The intensity in the solar neighbourhood is $\sim 6 \times 10^{-6}$ gauss.
(3) Initially the field had the rough form of a bar that passed through the nucleus.
(4) The change with time of the angular momentum of rotation in the Galaxy of the interstellar gas is small and can be neglected.

Subject to these assumptions it was shown that the differential rotational velocity in the Galaxy winds the magnetic field into a clockspring-like structure, the degree of wrapping after a time interval of $\sim 5 \times 10^8$ years being comparable with the wrapping of the spiral arms inferred by observation.

It is proposed now to examine the fourth of the above assumptions. A clockspring winding of the magnetic field causes angular momentum to be transferred from the gas at one radial distance to the gas at another radial distance. Hence (4) is certainly not strictly satisfied. The question is evidently whether or not (4) is satisfied to a sufficient approximation for the former conclusions to be still applicable. In the following discussion it will be shown that this is indeed the case, provided (1), (2), (3) are satisfied, except possibly at two particular values of the radial distance.

2. *The transference of angular momentum.*—In Fig. 1 we have a spiral arm crossing a cylinder of radius r along the arc AB. The figure should be thought of as possessing unit thickness in the direction perpendicular to its own plane, which we take to be the plane of the Galaxy. We also take the magnetic intensity H to be uniform over AB. The magnetic stress across AB has a component $H^2 \cos\theta \sin\theta / 4\pi$ per unit length of AB in the direction transverse to the radius vector.

According to observation, the diameter d of a spiral arm varies only slowly with r. In the Galaxy $d \sim 500$ parsecs. It will be sufficient for our purpose to take the arc AB to be only a moderate fraction of a quadrant. At values of $r \gg d$ where angular momentum transfer is at all important, θ turns out to be sufficiently different from $\pi/2$ for this to be the case. Inspection of photographs of extra-galactic systems show indeed that in many cases, even near the nucleus, AB is short enough to be considered approximately straight, giving $AB \cong d \sec\theta$. The total force acting over AB in the transverse direction has magnitude $dH^2 \sin\theta/4\pi$ in this case.

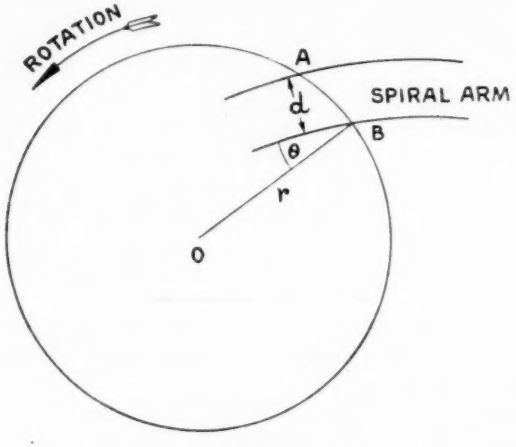

FIG. 1

Consider the gas enclosed between two cylinders of radii $r+dr, r$, the system again having unit thickness normal to the plane of the Galaxy. The net component of the force acting on the gas in the direction transverse to the radius vector is

$$\frac{1}{4\pi}\left[(H^2 d\sin\theta)_r - (H^2 d\sin\theta)_{r+dr}\right]. \qquad (1)$$

For θ defined as in Fig. 1, the expression (1) has positive sign when the force has the same sense as the rotation of the Galaxy.

Now both d, H vary slowly with r. If θ also varies slowly with r, the transverse force (1) turns out to be small and unimportant. If θ varies rapidly with r, however, as it can in a certain special circumstance to be considered below, the force (1) can become important in promoting angular momentum transfer. In such a case (1) may be written to sufficient accuracy as

$$-\frac{1}{4\pi} H^2 d\cos\theta \frac{d\theta}{dr}.dr. \qquad (2)$$

The mass of gas contained between the two cylinders (again with unit extension normal to the galactic plane) is $AB.\rho_g.dr \cong d\sec\theta\rho_g.dr$, where ρ_g is the gas density. Hence the transverse acceleration is of order

$$-\frac{1}{4\pi}\frac{H^2}{\rho_g}\cos^2\theta\frac{d\theta}{dr}, \qquad (3)$$

in the sense of galactic rotation.

Expression (3) shows the magnitude of the transverse force to be largest in the case $\theta = 0$ —i.e., when the arm points in the radial direction—and when

$|d\theta/dr|$ is as large as possible. This agrees with simple qualitative expectations. We consider next the special condition under which these requirements might arise.

3. *The rotational velocity curve.*—At some initial time let P_1, P_2 be the positions of two neighbouring elements of gas situated on the same magnetic line of force, P_1 at distance r from the galactic centre and P_2 at distance $r+dr$. If the gaseous elements move in accordance with a rotational velocity curve $V(r)$, then after a time interval T we have

$$\angle P_1OQ_1 = \frac{V(r)}{r}\,T, \bmod 2\pi,$$

$$\angle P_2OQ_2 = \frac{V(r+dr)}{r+dr}\,T, \bmod 2\pi,$$

where O is the galactic centre, and Q_1, Q_2 are the positions after time T of the two gaseous elements. For sufficiently small dr, we hence have

$$\angle Q_1OQ_2 = \angle P_1OP_2 - T\frac{d}{dr}\left(\frac{V}{r}\right)dr. \qquad (4)$$

This result shows that there is no bending of the line of force at central distance r if $d/dr\ (V/r) = 0$. This is the condition that rotation in the Galaxy shall not make the $\cos^2\theta$ factor in (3) small. We may express the condition in the form $dV/dr = V/r$, which shows that the tangent to the rotational velocity curve must pass through the origin. At such a point the value of θ is unchanged by galactic rotation. If $\theta = 0$ initially, in accordance with assumption (3) of the introductory section, then $\theta = 0$ at subsequent times. (To prevent $\cos^2\theta$ being small, this assumption is not strictly necessary—all that is required is for θ not to be close to $\pi/2$ at the initial time.)

To proceed further it is necessary to consider the likely form of the rotational velocity curve of the Galaxy. A plausible form is shown in Fig. 2. For central distance $r > \sim 3$ kpc, observation indeed gives a curve closely similar to Fig. 2. The novelty of Fig. 2 lies in the peak at $r = \sim 0{\cdot}25$ kpc. Recent work by the Dutch radio astronomers indicates the presence of high rotary speeds near the galactic centre, while the work of Walker has indicated a similar phenomenon in M31. These high speeds presumably arise from very high central condensations of mass—a mass of $\sim 2 \times 10^9 \odot$ being required to produce the peak shown in Fig. 2. In this connection it is worth noting that M31 possesses an inner nuclear region of very high surface brightness, such as would be expected to correspond to a high mass concentration. A mass $\sim 2 \times 10^9 \odot$ distributed uniformly throughout a sphere of radius 0·25 kpc yields a mass density comparable with the inner regions of globular clusters. Because of its larger dimension the inner galactic nucleus should therefore have a greater surface brightness than the globular clusters. This indeed appears to be the case for the inner nucleus of M31.

The high mass density cannot continue indefinitely with increasing r, however. Judging from surface brightness studies of M31, the mass density falls off sharply outside the inner nucleus. This implies a corresponding fall in the rotational velocity. Immediately outside the inner nucleus the rotational velocity must simply follow the Keplerian value in the gravitational field of the inner nucleus. That is to say, the rotational velocity falls as $r^{-1/2}$. Such a dependence is followed in Fig. 2 for $0{\cdot}25 < r < \sim 0{\cdot}75$ kpc.

Eventually however, the field of the inner nucleus declines in importance, while the main field of the Galaxy increases in importance. This causes the rotational velocity to increase again with r. Hence it seems that the rotational velocity curve of the Galaxy must possess two maxima separated by a minimum. The depth of the minimum is uncertain, however. The value given in Fig. 2 is an assumption.

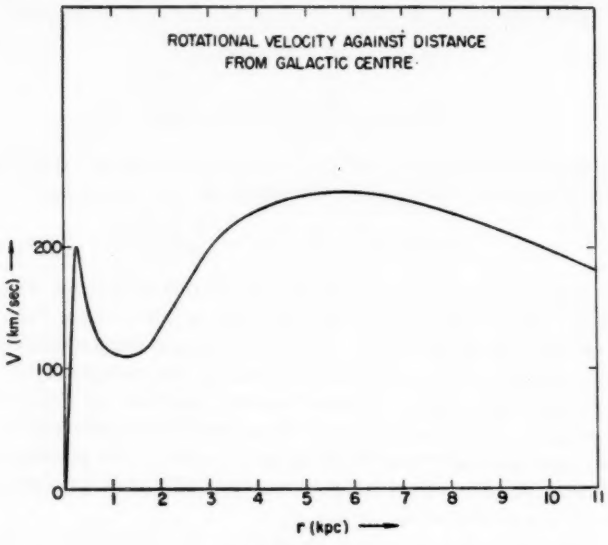

FIG. 2

Returning now to the question of satisfying the condition $d/dr\,(V/r)=0$, a point of inflexion must exist on the rotational velocity curve between the minimum and the outer maximum. If the tangent at this point of inflexion intersects the abscissa at $r>0$, there will be two points at which $d/dr\,(V/r)=0$ —one on either side of the inflexion. If, on the other hand, the tangent at the point of inflexion intersects the ordinate at $V>0$, there can be no such points. The limiting case is where the tangent at the point of inflexion passes through the origin. This is the case shown in Fig. 2. The condition

$$\frac{d}{dr}\left(\frac{V}{r}\right)=0$$

is then satisfied only at the inflexion.

It is of interest to consider the values of θ produced by the rotation curve of Fig. 2. This will be done for winding of magnetic lines of force over a time interval T, starting from an initial state in which $\theta\cong 0$ everywhere along the lines of force. Then $\angle P_1OP_2=0$ in (4). The two gaseous elements remain radially separated by dr throughout the winding. (We consider here only the effect of winding, with each element maintaining its radial distance r.) Hence

$$\tan\theta=-rT.\frac{d}{dr}\left(\frac{V}{r}\right). \qquad (5)$$

Values of $\theta(r)$ for $T=5\times10^8$ years are given in the following table. These were determined using the function $V(r)$ plotted in Fig. 2.

r(kpc)	1·75	2	2·25–2·5	2·75	3·0	4·0	6·0	8·0	10·0
θ	85°·1	51°·1	0°	55°·8	81°·5	87°·1	87°·4	87°·3	86°·5

Except close to the point of inflexion the field is wound in directions nearly transverse to the radius vector. For $2<r<3$ kpc we can use (3) to estimate the transverse acceleration, with

$$\frac{d\theta}{dr}\cong -1\,(\text{kpc})^{-1} \text{ for } 2<r\leqslant 2{\cdot}5\,\text{kpc}$$

and

$$\frac{d\theta}{dr}\cong 1\,(\text{kpc})^{-1} \text{ for } 2{\cdot}5<r<3\,\text{kpc}.$$

For other values of r, θ is so close to $\pi/2$ that our approximation used in determining (3)—that the spiral arm cuts the cylinder $r=$ constant over an arc appreciably less than a quadrant—becomes at best only a rough approximation. But this failure is quite unimportant, since angular momentum transfer at such values of r turns out to be negligible.

With

$$\left|\frac{d\theta}{dr}\right|\cong 1\,(\text{kpc})^{-1},\quad \cos^2\theta\cong 1,\quad \rho_g\cong 10^{-24}\,\text{gm cm}^{-3},$$

the transverse acceleration (3) has a magnitude of order $25H^2\,\text{cm sec}^{-2}$, where H is in gauss. This may be compared with the radial acceleration, which is

$$\sim 4\times10^{14}/r\,\text{cm sec}^{-2},$$

with r in cm. Putting $r=10^{22}$ cm, i.e., $r\sim3$ kpc, we see that the tangential acceleration is comparable with the radial acceleration if $H\cong4\times10^{-5}$ gauss.

4. *Discussion.*—Subject to the assumptions (1), (2), (3), set out in the introductory section, we can now assess the conditions required to produce the outward gaseous motions observed by van Woerden, Rougoor, and Oort (**2**). For $2<r<3$ kpc it is sufficiently accurate to use the following formula for the angular momentum h per unit mass about the galactic centre:

$$h=rV=2\times10^{-15}r^2, \tag{6}$$

in c.g.s. units. At $r=10^{22}$ cm $\cong3$ kpc this relation gives $V\cong2\times10^7\,\text{cm sec}^{-1}$, which agrees with the curve of Fig. 2. Also we note that over the range $2<r<3$ kpc we have $V(r)$ approximately proportional to it, thereby yielding $h\propto r^2$.

Now for a transverse acceleration $\sim25H^2\,\text{cm sec}^{-2}$, acting at radial distance r, the change of angular momentum Δh occurring in a time interval Δt sec is $\sim25H^2r\Delta t\,\text{cm}^2\,\text{sec}^{-1}$. From (6) we also have

$$\Delta h\cong4\times10^{-15}r\Delta r,$$

so that

$$\pm25H^2\Delta t\cong4\times10^{-15}\Delta r. \tag{7}$$

This relation requires that as r changes the gas moves always in an orbit close to the circular orbit corresponding to the rotational velocity curve. Since the transverse acceleration is applied smoothly around the orbit this should be the case to a tolerable approximation. The + sign in (7) must be used for $d\theta/dr<0$, the − sign for $d\theta/dr>0$. To obtain $|\Delta r/\Delta t|\cong50\,\text{km sec}^{-1}$ we require $H\cong3\times10^{-5}$ gauss.

Before we go on to discuss whether or not this constitutes a plausible explanation of the results of the Dutch astronomers we note that similar effects become very weak indeed for $r > 4$ kpc. The differential obtained from (1) contains a term

$$-\frac{1}{4\pi}\sin\theta\frac{d}{dr}(H^2d).dr \tag{8}$$

which is now considerably greater than the $d\theta/dr$ term. Using (8), the transverse acceleration becomes of order

$$-\frac{1}{4\pi\rho_0 d}\sin\theta\cos\theta\frac{d}{dr}(H^2d). \tag{9}$$

With

$$\frac{d}{dr}(H^2d)\cong\frac{H^2d}{r}$$

it can readily be estimated that (9) is numerically less than the case discussed above by a factor $\sim 10^{-2}$. Hence the magnetic stress can produce radial motions only of $\sim 0{\cdot}5$ km sec^{-1} in the outer parts of the Galaxy. Such motions give no appreciable redistribution of material in the time scale required to produce the observed degree of winding of the spiral arms of the Galaxy, viz., 5×10^8 years.

The question now arises as to whether the form of magnetic stress considered above yields a satisfactory explanation of the origin of the large radial motions observed by the Dutch astronomers in the inner regions of the Galaxy. The requirement that H be of order 3×10^{-5} gauss is not a severe one. It is true that if the diameter d of the spiral were strictly independent of r, and if the magnetic flux along the arm were constant, then H at $r\sim2{\cdot}5$ kpc would only have the same value as it has at the solar distance, $r\sim8$ kpc, $H\sim6\times10^{-6}$ gauss. But d probably increases with r, implying higher values of H at small r. Moreover, it is possible that magnetic lines of force escape from the spiral arms into the halo (1), and this would permit the flux along the arm to be greater at small r than it is at the solar distance. Hence it does not seem unreasonable that the magnetic intensity might be 5 times greater at $r\cong2{\cdot}5$ kpc than it is at $r\cong8$ kpc.

More serious is the requirement

$$\frac{d}{dr}\left(\frac{V}{r}\right)=0.$$

It was this condition that permitted $\theta\cong0$ in the range $2{\cdot}25<r<2{\cdot}5$ kpc. If the minimum of the rotational velocity curve were appreciably shallower than it is in Fig. 2, the tangent at the point of inflexion would intersect the ordinate axis at $V>0$, in which case large radial motions would not arise.

Still more serious, a large outward motion cannot arise by the present process without there being a corresponding large inward motion. For outward motion we require $d\theta/dr<0$, which occurs at $r\cong2$ kpc, whereas at $r\cong2{\cdot}75$ kpc we have $d\theta/dr>0$. Thus the motion is outwards at 2 kpc and inwards at 2·75 kpc. This change in the sense of the motion is a consequence of the need for conservation of angular momentum. Subject to the assumptions (1), (2), (3) of the introductory section, the gaseous material at one value of r can only gain angular momentum at the expense of material at other values of r. This conservation requirement is introduced implicitly into the θ-values worked out above, for these θ-values are only correct if sufficient gaseous material exists at

all values of r. The essential requirement is that to a tolerable approximation the gaseous material follows the rotational velocity curve. This implies that the gas density must be sufficiently high for the magnetic lines of force to be wound in accordance with the rotational velocity curve—the latter being determined essentially by the gravitational field of the stars.

A radial outflow of gas in the Galaxy is observed near $r = 3$ kpc (**2**). Probably our result that the outflow should occur at smaller r, namely $r \cong 2$ kpc, is not an overriding objection to the above theory—the rotational velocity curve could take a form that would increase the theoretical value, whereas the observational value could possibly be too large. A far more serious objection is that the corresponding inflow of material does not seem to have been observed. It is true that radial velocities of recession from the Sun are observed, also of order 50 km sec^{-1}, but these appear to arise from gas on the far side of the galactic nucleus (**3**) which would hence also be in outward motion. Since the observations are made in the 21 cm line of neutral atomic hydrogen a failure to observe inward motion would be understandable if the inward moving material were ionized. There is no very obvious reason why this should be so, however.

The failure to observe the inward motion seems indeed to be so serious as to make doubtful the above explanation of the outward motion. Yet within the terms of reference of the assumptions (1), (2), and (3) of the introductory section there seems to be no other way in which a rapid outward drift of gas can arise through the agency of the magnetic field. Hence we are led to question very seriously whether these assumptions are in fact correct. This question will form the subject of a further communication.

Conclusions in regard to the transfer of angular momentum in the Galaxy (subject to (1), (2), (3) *of the introduction*).—The rotation curve of the Galaxy probably possesses at least one point of inflexion at central distance in the range $2 < r < 3$ kpc. If the tangent at the inflexion passes close to the origin, or if it intersects the abscissa at $r > 0$, there is a region between 2 and 3 kpc from the centre where a spiral arm remains essentially unwound. On the other hand for $r < 2$ kpc and $r > 3$ kpc the winding of a spiral arm causes the angle θ made by the arm with the radius vector to become close to $\pi/2$. Transfer of angular momentum is then slow and unimportant and assumption (4) of the introduction is satisfied. But for values of r in the range 2 to 3 kpc the value of $|d\theta/dr|$ can be of order 1 (kpc)$^{-1}$. The transfer of angular momentum can then be very appreciable. Angular momentum is conserved through a compensation between inward and outward motion. If, however, the tangent at the point of inflexion intersects the ordinate axis at a value of the velocity V appreciably > 0, the angle θ is everywhere close to $\pi/2$, transfer of angular momentum is always small, and assumption (4) of the introduction is everywhere satisfied.

St John's College,
Cambridge:
1960 *March* 7.

Emmanuel College,
Cambridge.

References

(1) Hoyle, F., and Ireland, J. G. (1960), *M.N.*, **120**, 173.
(2) van Woerden, H., Rougoor, W., and Oort, J. H. (1957), *Compt. Rend.*, **244**, 1691.
(3) van de Hulst, H. C., (1958), *Rev. Mod. Phys.*, **30**, 913.

NOTE ON THE BRIGHTNESS FLUCTUATION IN THE SOLAR GRANULATION

J. Gaustad and M. Schwarzschild

(Communicated by Lyman Spitzer, Jr., Director of the Princeton University Observatory)

(Received 1960 March 21)

Summary

On photographs of the solar granulation obtained with a balloon-borne telescope, Blackwell, Dewhirst and Dollfus (1) measured a r.m.s. brightness fluctuation of 4·6 per cent. From this measurement they deduced a true r.m.s. brightness fluctuation of 18 per cent. This deduction was based on an accurate measurement of the contrast transmission function of their instrument, but on an approximate application of this transmission function to the granulation. This note aims to show that, using the same observed r.m.s. brightness fluctuation, the same measured instrumental transmission function, and the same value of 1·4 seconds of arc for the average granule diameter, a more detailed analysis gives a true r.m.s. brightness fluctuation not of 18 per cent, but of only about 7 per cent. The overestimate by Blackwell *et al.* appears to have resulted from their identifying the granule diameter with a wave-length rather than half a wave-length.

Recently two rather discrepant values have been published for the true r.m.s. brightness fluctuation in the solar granulation, one by Blackwell *et al.* (1) of 18 per cent and the other by Schwarzschild (3) of at most 8 per cent (corresponding to a temperature fluctuation of 100°). The purpose of this note is to show that this discrepancy can be eliminated by applying a different granulation model to the observations by Blackwell *et al.*

As a simple model we will consider the granulation as consisting of a set of circular disks of equal size randomly distributed over the solar surface, each differing from the mean brightness by a constant intensity $\pm I_0$. The reduction in the r.m.s. brightness fluctuation for this distribution will be the same as that for a single disk.

The general development used here follows closely that of Uberoi (2). We define the two-dimensional covariance function $R(\xi)$ of the brightness fluctuation $I(r)$ by

$$R(\xi) = N \int\int I(r) I(r+\xi) dr, \tag{1}$$

where N is a normalization factor. The r.m.s. brightness fluctuation is proportional to the square root of $R(0)$;

$$\sqrt{\langle (I)^2 \rangle} \propto \sqrt{R(0)}. \tag{2}$$

The spectral density $P(k)$ is the Fourier transform of R;

$$P(k) = \frac{1}{2\pi} \int\int R(\xi) e^{ik \cdot \xi} d\xi. \tag{3}$$

In any telescope the image is smoothed by diffraction and other causes. It can be shown that the observed spectral density $P^*(k)$ is

$$P^*(k)=2\pi S(k)P(k), \tag{4}$$

where the sensitivity spectrum $S(k)$ is given by

$$S(k)=\frac{1}{2\pi}\int\int \Psi(y)e^{iky}dy, \tag{5}$$

where

$$\Psi(y)=\int\int W(r)W(r+y)dr \tag{6}$$

and $W(r)$ is the instrumental profile of the telescope. (The sensitivity spectrum S is proportional to the square of the contrast transmission function as used by Blackwell *et al.*) The observed covariance at zero displacement is then

$$R^*(0)=\int\int S(k)P(k)dk. \tag{7}$$

Finally we define a reduction factor β as the ratio of the observed to the true r.m.s. brightness fluctuation;

$$\beta=\frac{\sqrt{\langle(I^*)^2\rangle}}{\sqrt{\langle(I)^2\rangle}}=\frac{\sqrt{R^*(0)}}{\sqrt{R(0)}}. \tag{8}$$

We now apply these general equations to our specific problem. For the granule model which we are considering, a disk of radius s and constant intensity I_0, the true spectrum $P(k)$ is

$$P(k)=2\pi N\left[\frac{I_0 s}{k}J_1(ks)\right]^2, \tag{9}$$

and the true covariance at zero displacement is

$$R(0)=\pi N I_0^2 s^2. \tag{10}$$

For the instrumental profile we shall consider two cases, first the theoretical diffraction pattern of an ideal telescope, and second the actual measured profile of the instrument used by Blackwell *et al.* The theoretical diffraction pattern for an aperture of radius a at an effective wavelength λ is

$$W(r)=(\pi r^2)^{-1}J_1^2\left(\frac{k_0 r}{2}\right)$$

with

$$k_0=\frac{4\pi a}{206,265\,\lambda}(\text{sec of arc})^{-1}, \tag{11}$$

and the sensitivity spectrum defined by equations (5) and (6) is

$$S(k)=\frac{2}{\pi^3}\left[\cos^{-1}\left(\frac{k}{k_0}\right)-\frac{k}{k_0}\left(1-\left(\frac{k}{k_0}\right)^2\right)^{1/2}\right]^2 \tag{12}$$

for $k<k_0$, and $S(k)=0$ for $k>k_0$.

The observations of Blackwell *et al.* were made with an instrument of 29 cm diameter at an effective wavelength of 5300 A. They measured a mean granule diameter ($2s$) of 1·4 seconds of arc. By introducing these values of the parameters into equations (9) and (12) we obtain the true granule spectrum and the ideal sensitivity spectrum. Then introducing these two functions into equation

(7) and executing the quadrature numerically gives the observed zero displacement covariance $R^*(0)$. Finally, by inserting this result as well as the value of $R(0)$ from equation (10) into equation (8) we obtain for the reduction factor β in the ideal case

$$\beta_{\text{ideal}} = 0{\cdot}76.$$

In the second case the procedure is the same except that the sensitivity spectrum is derived not from equation (12) for the ideal diffraction pattern, but from the square of the contrast transmission function actually measured by Blackwell *et al.* Thus one finds for the actual reduction factor

$$\beta_{\text{actual}} = 0{\cdot}63,$$

which is somewhat smaller than the ideal value, but considerably larger than the value of 0·25 which Blackwell *et al.* used in correcting their measured r.m.s. fluctuation.

Using this actual reduction factor, the corrected r.m.s. brightness fluctuation becomes

$$\sqrt{\langle (I)^2 \rangle} = 7{\cdot}3 \text{ per cent},$$

which corresponds to a temperature fluctuation of

$$\sqrt{\langle (\Delta T)^2 \rangle} = 89°.$$

This is consistent with Schwarzschild's estimate (3) that the r.m.s. temperature fluctuation on the surface of the Sun probably does not exceed 100°.

By comparing these values of the reduction factor β with the contrast transmission function curves given by Blackwell *et al.*, it can be seen that the reduction factor is approximately equal to the contrast transmission function at a spatial wavelength of 2·8 seconds of arc. Thus the effective transmission function is approximately that corresponding to a wavelength twice the average granule diameter, rather than to a wavelength equal to this diameter as used in the approximation by Blackwell *et al.*

It is clear that the result of the present note is correct only to the degree in which the model of randomly distributed circular disks of the size given by Blackwell *et al.* represents the actual granulation. It should be hoped that the present result can be superseded by a detailed analysis based on the observed autocorrelation function rather than on a granulation model.

Princeton University Observatory,
Princeton, New Jersey:
1960 *March* 5.

References

(1) Blackwell, D. E., Dewhirst, D. W. and Dollfus, A., *M.N.*, **119**, 98, 1959.
(2) Uberoi, M. S., *Ap. J.*, **122**, 466, 1955.
(3) Schwarzschild, M., *Ap. J.*, **130**, 345, 1959.

THE SCORPIO-CENTAURUS ASSOCIATION

1. Radial Velocities of 120 Bright Stars

William Buscombe and Pamela M. Morris

(Received 1960 April 2)

Summary

Newly determined radial velocities are given for 2 stars of spectral type O, 104 of type B and 14 of type A, all brighter than magnitude 7·0. They are part of a programme covering the region of the Scorpio–Centaurus moving stream, between galactic longitudes 200° and 300°. Each star has been classified on the revised Yerkes luminosity system.

At least three spectrograms of each star have been measured, except in a few cases where previous results were merely confirmed. For 39 stars the statistical reliability of previously published mean velocities is increased. Eighteen new velocities are announced, of which nine are constant and nine variable. Observations have been resumed on 64 stars previously known to have variable velocity, including 5 double-lined binaries.

Revised orbital elements are derived for the spectroscopic binaries HD 79351 and 81188, and velocity curves are presented for five separate cycles of the pulsating star θ Ophiuchi. Two of these stars are members of the association.

Selection of programme stars.—Blaauw (1) described in detail the motions of early B-type stars in the region of the southern stream, usually called the Scorpio-Centaurus Cluster. Earlier contributions to this study are fully reviewed in his monograph, and the recent literature may be traced by reference to the *Catalogue of Star Clusters and Associations* (2) and annual supplements (3). After establishing the stream motion, Blaauw compared the predicted and observed velocity components of stars with spectral types B5 or earlier. Within statistical limits of error, he showed that 40 stars brighter than visual magnitude 5·5 are certain members and 50 more are probable members. For a large number a definite decision cannot be made until more precise values of the radial velocities are available. Blaauw indicated certain regions in which fainter members of spectral types later than B5 should be sought.

While construction of the three-prism spectrograph for the Cassegrain focus of the 30-inch reflector was in progress, Dr Gollnow and Dr Buscombe planned the first observing programme of about 100 stars brighter than visual magnitude 6·0, listed by Blaauw, for which membership of the Scorpio–Centaurus stream could be more certainly decided if the mean radial velocity were more accurately determined. Initial observations with the instrument during 1954 showed that many of these dwarf stars of spectral type B have such broad, diffuse absorption lines that improved velocity measures might be very difficult to obtain. In 1955 and 1956, while Dr Gollnow's time was largely occupied with problems of instrumental adjustments and photographic processing, he agreed that Buscombe should add some fainter stars to the programme. The wider selection included a number of stars of types B8 to A5 whose proper motions were found to be parallel

to the stream by Rasmuson (4) or Kulikowsky (5), but for which either no radial velocity or only a very uncertain value was available. In 1957 the entire list was divided so that individual observers might complete sections of the programme for publication as early as possible.

Velocity system.—Following Professor Struve's personal suggestion, Gollnow and Buscombe selected ten certain or probable members of the cluster with reliable constant radial velocities to be used as internal velocity standards. These stars are marked with an asterisk in Table I. The mean difference in velocity in the sense Stromlo—*General Catalogue of Stellar Radial Velocities* (6) for the 81 spectrograms is $0 \pm 0{\cdot}5$ (p.e.) km/s. When it became apparent that the velocity of τ Sco (HD 149438) varies irregularly with a small amplitude, this star was withdrawn from further study. The internal probable error of measurement for a single spectrogram of a dwarf B star (usually between 3 and 5 km/s) masks this small variation. For giants and supergiants, which have sharper lines, the error is usually smaller.

On each spectrogram of a B star between 10 and 12 lines were measured, and for A stars between 18 and 20. However, in the velocities of HD 105435, 120324, 141556 and 178322 the probable errors are abnormally high, because only six lines could be measured on each plate.

In a previous communication (7) to the Society, we have outlined the technique of observation and measurement, our experience with the choice of absorption lines recommended by Petrie (8), and the general consistency of measures of standard-velocity stars of later spectral types. These stars are still observed and measured regularly, and continue to show no significant deviations from the adopted standard values.

Stars with variable velocity.—For convenience in future studies of spectroscopic binary or pulsating stars, the individual plate velocities for 75 stars are given in Table II, with references to previous work. An orbit has already been computed (9) for HD 170523, and observations are nearly complete for analyses of the velocity variations of HD 134687, 170465 and 180885.

Table III lists new observations of the single-lined binary HD 79351 (a Carinae), for which Curtis (10) derived a provisional orbit based on 25 spectrograms obtained during 1904-07 at Santiago, Chile. The additional data make possible the derivation of a more accurate period, but, as Table IV shows, little alteration to the other orbital elements is necessary. Miss Morris has solved the orbit graphically by the method of Lehmann-Filhes, but the data do not warrant the computation of least-squares corrections. The velocity variation is shown graphically in Fig. 1.

Recent observations of HD 81188 (κ Velorum) indicate that the preliminary value of its orbital period should be increased to 116·776 days. As shown by Fig. 2, the fitting of both old and new measurements to the radial velocity curve is improved by slight changes in the longitude and epoch of periastron to 92°·60 and JD 2416456·66 respectively.

At the request of Professor van Hoof, Buscombe has obtained spectra of the β Canis Majoris-type star θ Ophiuchi (HD 157056), covering several complete cycles of its pulsation. The primary period is $3^{h}24^{m}$, with a beat period of about 75 days (11). Both the mean value and amplitude of the radial velocity vary from cycle to cycle, and a slight variation in brightness has been reported privately by van Hoof. References to previous spectroscopic studies of this star are listed in

Table II. Radial velocities from 55 spectrograms on this programme are presented in Table V and Fig. 3. On the last night of observations a slightly distorted maximum of the velocity curve is seen just two cycles after the sharp one reported by McNamara (**12**) from his coudé spectrograms. It seems quite clear that future progress in unravelling the complex behaviour of this and similar stars will depend on spectra of high dispersion. We cannot report any further observation of Ca II emission at the K line, as this region of the spectrum is not brought in good definition by the usual adjustment of the spectrograph.

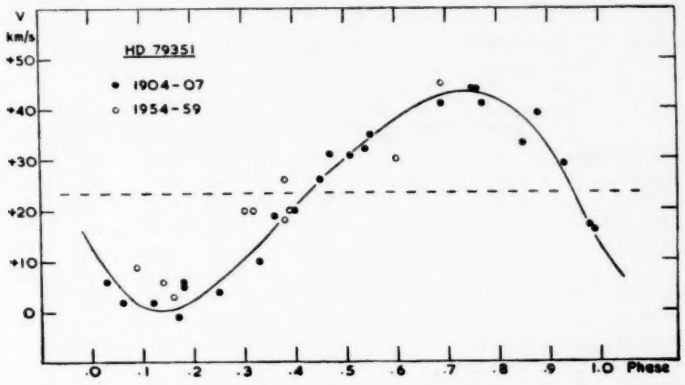

FIG. 1.—*The velocity curve of HD* 79351.

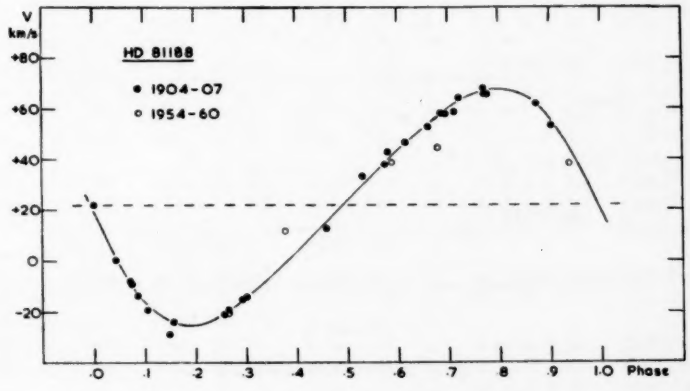

FIG. 2.—*The velocity curve of HD* 81188.

Further studies.—In forthcoming communications in this series, Miss Morris will present additional luminosity classifications for about 200 stars now being studied, while Dr Gollnow and Dr Przybylski will present other velocity determinations. Spectrograms are being taken of some stars fainter than 6th magnitude in the region of the association for spectrophotometry of absorption lines. Some of these objects, with proper motions and distance moduli which relate them to the association are being observed further for radial velocity determinations.

Computations are in hand for a rediscussion of the kinematics of the system as new data become available.

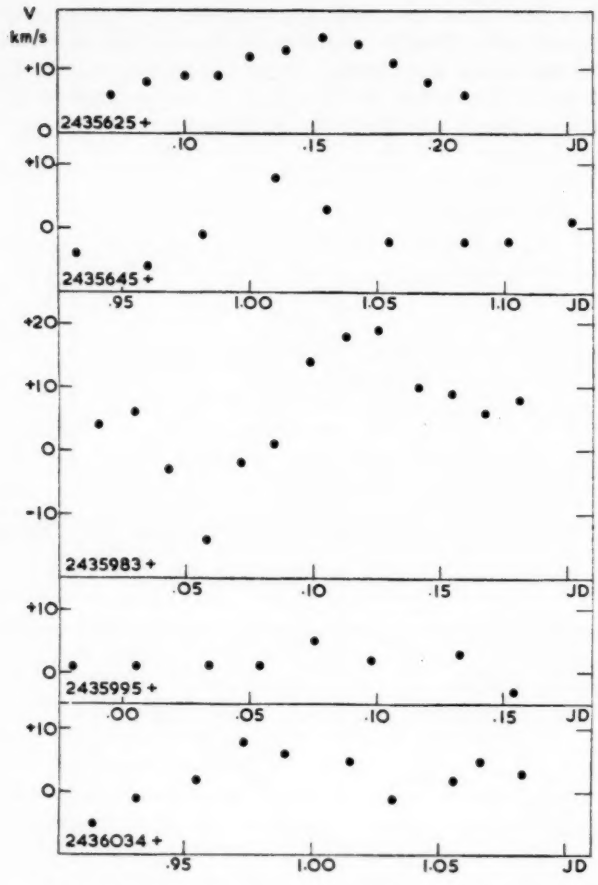

FIG. 3.—*Velocity curves for θ Ophiuchi on five nights in* 1956–57.

TABLE I

Stars with constant velocities

Column

1 Number in Henry Draper Catalogue (*Harvard Annals*, **91–99**).

2 Constellation designation. For stars lacking a Greek Bayer letter, the Gould number is quoted from Uranometria Argentina (*Cordoba Resultados*, **1**).

3 Visual apparent magnitude, from the Henry Draper Catalogue.

4 Spectral type of the MK system, determined from Mount Stromlo spectrograms by A. de Vaucouleurs (*M.N.*, **117**, 449, 1957) or P. M. Morris (unpublished).

5 Mean radial velocity relative to the Sun from Mount Stromlo spectrograms, to nearest integral kilometre per second.

6 Probable error of the mean, from deviations of individual plate velocities, in km/sec.

7 Number of plates measured.

TABLE I (*continued*)

Column

8 Mean of individual radial velocity determinations published previously, as given in references. The lower case letters denote quality by internal consistency of the individual plate measurements, on the system used in Wilson's *Catalogue* (6). The succeeding digit indicates the number of measurements included. The final upper case letters denote the observatories whose measurements are contained in the mean.

9 References to publications giving previous velocity measurements.

(1) HD	(2) Star	(3) m_v	(4) Sp	(5) $\bar{V}$ km/s	(6) p.e. ±	(7) n	(8) Previous mean vel.	(9) References
49336	30G Pup	6·10	B3 V	+15	0·8	4		
62747	161G Pup	5·53	B1 V	+15	2·0	4		
66591	77G Car	4·96	B3 IV	+23	0·4	3	+21 b 4 L	*Lick Publ.* 16
67536	79G Car	6·42	B4 Vn	0	1·2	5	0 c 3 L	*Lick Bull.* 15
75149	68G Vel	5·54	B2 II	+30	2·4	2	+25 b 6 L	*Lick Publ.* 16
*77002	109G Car	5·08	B3 IV	+29	1·4	5	+25 a 5 L	*Lick Publ.* 16
*79447	119G Car	4·18	B3 IV	+18	0·5	9	+17 b 5 L	*Lick Publ.* 16
91533	206G Car	6·19	A2 I	+10	0·5	4		
*93845	δ^2Cha	4·62	B3 V	+24	2·1	6	+22 b 7 L	*Lick Publ.* 16
99556	33G Cen	5·39	B5 IV	+10	1·6	3	+ 9 b 4 L	*Lick Bull.* 15
100929	50G Cen	5·70	B3 IV	+12	2·6	5	+ 9 b 4 L	*Lick Bull.* 15
							+13 a 3 R	*Mem. R.A.S.* 67
105382	92G Cen	4·51	B6 III	+15	1·1	4	+16 b 4 L	*Lick Publ.* 16
106983	ζ Cru	4·06	B3 IV	+16	1·2	4	+19 b 7 L	*Lick Publ.* 16
110335	39G Cru	5·02	B7 IV	+14	2·1	2	+12 c 6 L	*Lick Publ.* 16
111613	47G Cru	5·74	A1 Ia	−20	1·8	3	−22 b 3 L	*Lick Publ.* 16
112092	μ^1 Cru	4·06	B3 IV	+16	2·5	5	+12 b 5 L	*Lick Publ.* 16
116226	210G Cen	6·46	B7 IV	−41	0·7	3		
120640	278G Cen	5·87	B4 III	− 4	0·6	4	− 6 c 3 L	*Lick Bull.* 15
*120709	3 CenA	4·60	B5 IV	+10	1·3	6	+14 b 4 L	*Lick Publ.* 16
*120908	283G Cen	5·96	B5 V	+ 6	0·9	8	+ 8 b 3 L	*Lick Bull.* 15
*122980	χ Cen	4·41	B2 V	+10	1·5	9	+12 b 5 L	*Lick Publ.* 16
							+10 a 4 R	*Mem. R.A.S.* 68
125288	υ Cen	4·41	B5 II	+ 7	2·0	4	+ 5 b 6 L	*Lick Publ.* 16
*125823	a Cen	4·42	B5 III	+ 9	1·0	6	+ 9 b 7 L	*Lick Publ.* 16
							+ 8 a 4 R	*Mem. R.A.S.* 68
129954	22G Cir	6·05	B2 V	+19	2·8	5		
130807	o Lup	4·38	B6 III	+10	1·9	6	+ 7 b 6 L	*Lick Publ.* 16
132955	45G Lup	5·45	B4 IV	+ 8	1·8	4	+ 6 b 3 L	*Lick Publ.* 16
135160	40G Cir	5·95	B1 Ve	+ 4	2·6	4		
141168	12G Nor	5·96	B8 V	+12	3·0	4	+21 b 3 L	*Lick Bull.* 15
141318	14G Nor	5·84	B2 III	0	0·9	5	− 3 d 5 L	*Lick Bull.* 15
							+ 2 c 3 R	*Mem. R.A.S.* 67
142250	6G Sco	6·01	B7 V	+ 1	0·4	3		
147084	o Sco	4·54	A5 II	− 6	1·2	2	− 8 a 6 L	*Lick Publ.* 16
148937		6·89	O6f††	−53	1·9	5		
*149438	τ Sco	2·85	Bo V	+ 3	1·1	8	− 1 a10 L	*Lick Publ.* 16
							− 6 c 4 Y	*Ap. J.* 64
							− 1 b 7 W	*Ap. J.* 97 & 111
							+ 4 c 3 Mi	*Mich. Pub.* 5
							+ 4 a21 R	*Mem. R.A.S.* 68
149711	62G Nor	6·14	B3 IV	0	1·7	3	+ 2 b 3 L	*Lick Bull.* 15
150898	9G Ara	5·76	Bo Ib	−53	0·9	5	−51 b 9 L	*Lick Publ.* 16
							−62 a 3 R	*Mem. R.A.S.* 68

TABLE I (*continued*)

(1) HD	(2) Star	(3) m_v	(4) Sp	(5) $\bar{V}$ km/s	(6) p.e. ±	(7) n	(8) Previous mean vel.	(9) References
156325	140G Sco	6·41	B6 IV	−13	1·3	5	−14 d 4 L	*Lick Bull.* **15**
156838	46G Ara	5·88	B2 V	+10	0·6	6	− 1 c 6 L	*Lick Bull.* **15**
							+ 3 c 3 R	*Mem. R.A.S.* **67**
159358	6G Ser	5·56	B8 V	− 8	2·7	4		
165024	θ Ara	3·90	Bo·5 II	+ 4	1·2	2	+ 3 b 5 L	*Lick Publ.* **16**
*172910	91G Sgr	4·82	B3 V	+ 5	0·8	13	+ 3 a 5 L	*Lick Publ.* **16**
							+ 1 b 3 R	*Mem. R.A.S.* **68**
175191	σ Sgr	2·14	B4 IV	−12	2·8	3	−12 c 8 L	*Lick Publ.* **16**
							− 7 c 3 Y	*Ap. J.* **64**
*175362	31G CrA	5·41	B8 IV	0	1·0	11	+ 3 b 4 L	*Lick Publ.* **16**
							+ 3 a 4 R	*Mem. R.A.S.* **68**
186837	73G Pav	6·42	B5 V	−15	1·1	5	−16 c 3 L	*Lick. Bull.* **15**

* Internal velocity standard.
† Kindly communicated by B. Westerlund in advance of publication.

TABLE II

Stars with variable velocities

Column
1 Henry Draper number and constellation designation. } As in Table I
2 Visual magnitude and spectral type. }
3 Julian date and decimal for time of mid-exposure.
4 Radial velocity relative to the Sun.
5 Internal probable error of deviations from the mean velocity for the plate to velocities for the individual lines.
6 Previous mean velocity, as in Table I.
7 References.

(1) HD Star	(2) m_v Sp	(3) JD 243	(4) V km/s	(5) p.e. ±	(6) Previous mean vel.	(7) References
57593	5·84	5086·230	+16	4·4		
158G CMa	B3 V	6150·237	+38	7·7		
		6264·954	+ 1	3·8		
		6911·194	+16	2·9		
70839	6·07	6238·047	+ 3	4·4	+15 c 3 L	*Lick Bull.* **15**
87G Car	B3 III	6264·991	−11	3·4	+37 b 4 R	*Mem. R.A.S.* **68**
		6914·220	+17	3·9		
		6955·092	+13	1·8		
79351	3·56	orbit:			+23 a 25 L	*Lick Bull.* **4**
a Car	B2 IV	see Table III				
80094	6·06	5882·087	+ 9	4·4	+ 7 c 3 L	*Lick Bull.* **15**
124G Car	B7 IV	6954·141	+24	2·3		
		6972·076	+28	1·5		
		7003·976	+27	1·9		
81188	2·45	orbit:			+22 a 27 L	*Lick Bull.* **4**
κ Vel	B2 IV	4821·979	−21	4·5		
		6236·097	+12	3·2		
		6260·957	+39	7·1		
		6972·095	+45	4·9		
		7001·988	+38	6·2		

TABLE II (*continued*)

(1) HD Star	(2) m_v Sp	(3) JD 243	(4) V km/s	(5) p.e. ±	(6) Previous mean vel.	(7) References
83944	4·67	4820·006	+20	4·6	+24 b 8 L	*Lick Publ.* **16**
m Car	B9 V	6238·128	+ 4	3·2		
		6265·044	+16	3·9		
		6319·896	+12	5·3		
		6321·897	+13	4·3		
84461	5·71	5531·065	− 2	2·1	+ 6 d 2 L	*Lick Bull.* **15**
154G Vel	Ao V	5537·031	+13	1·4		
		5826·237	+24	1·6		
84816	5·68	5527·046	−14	5·6	− 8 c 5 L	*Lick Bull.* **15**
157G Vel	B3 V	5919·039	−33	2·7		
		6949·210	+27	2·7		
		7002·005	+19	2·7		
88206	5·10	5882·116	+20	4·6	+23 c 5 L	*Lick Publ.* **16**
Q Vel	B2 V	5914·988	− 2	4·4		
		6238·146	+26	4·1		
		6263·146	+ 8	3·9		
		6319·908	− 2	3·2		
		6322·913	− 2	3·2		
88955	4·09	under observation			+ 8 c 8 L	*Lick Bull.* **5**
q Vel	A2 V	for orbit				
89080	3.33	4822·008	+14	3·9	+ 4 c 6 L	*Lick Publ.* **16**
ω Car	B7 IV	6322·921	0	4·4		
		6972·177	+30	5·2		
		7002·036	− 2	3·0		
93237	6·18	6319·927	+49	5·6	0 c 3 L	*Lick Bull.* **15**
24G Cha	B5 Ve	6322·939	+42	4·8		
		6331·921	+16	3·0		
98718	3·92	4818·094	0	4·4	+16 c 3 L	*Lick Publ.* **16**
π Cen	B6 V	5527·142	− 1	6·8		
		6708·891	−11	7·3		
102776	4·52	4855·996	+26	3·5	+37 c 4 L	*Lick Publ.* **16**
j Cen	B3 Vne	6238·198	+31	7·1		
		6263·106	+16	4·9		
		6318·988	+31	4·4		
		6319·968	+ 5	3·3		
103884	5·55	5203·010	− 2	4·5	+16 c 6 L	*Lick Bull.* **15**
1G Cru	B3 V	5527·127	+45	6·2		
		5884·201	+40	6·7		
		6238·215	+22	5·3		
		6263·118	+ 4	7·2		
		6319·979	+10	6·4		

TABLE II (*continued*)

(1) HD Star	(2) m_V Sp	(3) JD 243	(4) V km/s	(5) p.e. ±	(6) Previous mean vel.	(7) References
104878	5·33	5919·104	+60	2·0 A	+23 c 4 L	*Lick Publ.* **16**
25G Mus	Ao V+B		−12	2·8 B		
		5938·040	+74	6·3 A		
			−14	5·0 B		
		6972·204	+40	2·0 A		
			+15	4·7 B		
		6979·154	+44	2·8 A		
			+34	6·2 B		
		7002·113	+33	2·6 A		
			− 3	5·1 B		
105416	5·58	6238·242	+11	1·4	+ 6 e 1 L	*Lick Bull.* **15**
93G Cen	A1 V	6263·137	+28	1·3		
		6265·151	+ 1	2·4		
		6319·001	−20	2·2		
		6322·983	−12	2·5		
		6736·854	+ 6	2·8		
105435	2·58	5259·912	+ 1	4·3	+ 9 d 13 L	*Lick Publ.* **16**
δ Cen	B3 Vne	5588·022	+ 8	4·8		
105937	3·97	4818·117	+32	3·0	+21 c 4 L	*Lick Publ.* **16**
ρ Cen	B4 V	6736·867	−12	5·2		
		6765·849	− 6	3·5		
107696	5·59	6263·154	+13	2·5	+ 1 c 2 L	*Lick Bull.* **15**
24G Cru	B8 Vp	6320·004	−14	2·7		
		6323·001	− 8	2·2		
		6331·946	−15	2·1		
		6736·879	−16	7·4		
108257	4·87	5240·980	−36	6·4	+24 d 4 L	*Lick Publ.* **16**
119G Cen	B5 Vn	5586·012	−26	4·0	+10 c 3 R	*Mem. R.A.S.* **67**
		6710·958	−11	6·4		
109668	2·70	4873·992	+45	4·3	+18 c 5 L	*Lick Publ.* **16**
α Mus	B2 IV	5265·921	−23	3·3		
		6708·945	+ 8	7·9		
111597	5·01	5612·974	− 3	3·0	+18 c 3 L	*Lick Publ.* **16**
p Cen	Ao IV	6332·001	− 2	2·2		
		6355·914	−28	2·4		
		6998·189	+ 8	2·3		
112091	5·26	5266·915	− 5	4·5	+19 c 5 L	*Lick Publ.* **16**
μ^2 Cru	B5 Ve	5555·114	+40	5·3		
		6738·883	−22	5·3		
113314	5·02	5984·980	+12	2·5	−10 c 5 L	*Lick Publ.* **16**
ξ^1 Cen	Ao V	6263·192	+39	2·1		
		6265·187	+36	2·2		
		6323·038	+12	2·1		
		6356·936	−24	3·0		
		6708·988	− 6	3·8		
		6736·899	−17	2·7		

TABLE II (*continued*)

(1) HD Star	(2) m_V Sp	(3) JD 243	(4) V km/s	(5) p.e. ±	(6) Previous mean vel.	(7) References
115823	5·53	5236·008	+30	2·7 B	+ 6 b 5 L	*Lick Bull.* **15**
202G Cen	B5 III		−25	1·6 A		
	+A1:	6004·923	+ 5	8·4 B		
			+18	4·4 A		
		6268·194	+ 5	5·3 B		
			+50	1·6 A		
		6334·021	+ 6	6·0 B		
			−16	2·2 A		
		6712·002	+ 7	5·5 B		
			+19	3·0 A		
116087	4·52	4854·083	−16	2·5	+26 d 4 L	*Lick Publ.* **16**
208G Cen	B5 V	5265·935	− 9	6·4		
		5555·131	+ 1	3·9		
		5995·947	−31	5·0		
118978	5·53	5893·216	+21	2·3	−30 c 2 L	*Lick Bull.* **15**
251G Cen	B9 IV	5994·949	−20	2·9		
		6319·069	− 1	2·7		
		6323·051	− 2	2·4		
		6718·005	+ 8	1·4		
		6736·951	−14	3·3		
120324	3·2v	5241·004	− 5	4·6	+13 b 5 L	*Lick Publ.* **16**
μ Cen	B3 Ve	5268·921	− 4	5·5		
		5588·035	**+11**	**13·2**		
		5995·963	−14	5·0		
121190	5·84	6263·230	+31	5·2	+ 8 b 4 L	*Lick Bull.* **15**
288G Cen	B8 V	6265·201	+38	5·8		
		6320·032	+42	5·0		
		6323·071	+37	3·9		
121743	3·86	4827·165	+11	2·1	+ 7 b 7 L	*Lick Publ.* **16**
ϕ Cen	B2 V	6004·940	−16	3·3		
		6712·037	+19	5·1		
		6766·901	−11	7·3		
121790	3·92	5266·928	+14	3·0	+ 7 c 7 L	*Lick Publ.* **16**
v^1 Cen	B3 IV	5268·927	− 3	3·0		
		5586·088	+ 5	4·0		
		5650·938	+ 1	5·0		
		6649·209	+48	7·6		
		6712·053	−13	5·1		
		6766·864	+ 9	5·3		
		6766·905	−44	6·0		
123335	6·43	5265·956	−14	4·0	+ 3 c 3 L	*Lick Bull.* **15**
318G Cen	B5 IV	5585·084	+39	5·4	−18 c 3 R	*Mem. R.A.S.* **67**
124367	5·20	5203·124	− 1	6·4	+19 d 6 L	*Lick Publ.* **16**
328G Cen	B3 Ve	5290·941	+ 2	6·1	+11 d 4 R	*Mem. R.A.S.* **67**
		5588·071	+21	6·5		
		5998·968	−11	4·7		

TABLE II (*continued*)

(1) HD Star	(2) m_V Sp	(3) JD 243	(4) V km/s	(5) p.e. ±	(6) Previous mean vel.	(7) References
124771	5·20	5265·982	− 2	3·4	+ 5 d 5 L	*Lick Publ.* **16**
ϵ Aps	B4 IV	5591·128	+28	3·0	− 4 c 4 R	*Mem. R.A.S.* **68**
		5995·990	+18	5·8		
129056	2·33	4826·201	− 2	1·2	+ 8 b 10 L	*Lick Bull.* **5**
α Lup	B1 III	5260·112	+12	2·5	+ 5 a 6 L	*Lick Publ.* **16**
		7002·217	+ 7	1·4	+ 4 a 74 R	*M.N.* **116**
129116	4·00	4858·124	− 4	4·8	+ 8 c 3 L	*Lick Publ.* **16**
368G Cen	B3 IV	6355·995	− 2	4·1		
		6709·059	− 8	4·7		
		6717·994	+ 3	6·7		
		6765·868	+ 3	3·2		
131492	5·42	5267·001	+12	3·8	− 4 d 5 L	*Lick Publ.* **16**
θ^1 Cir	B3 Vne	5290·954	+ 6	8·1	+ 6 c 5 R	*Mem. R.A.S.* **67**
		5586·129	+24	5·0		
		5998·981	− 9	8·7		
132058	2·69	4822·227	− 1	6·1	0 b 7 L	*Lick Publ.* **16**
β Lup	B2 V	5268·965	− 8	3·3		
		5585·139	+15	5·8		
		6711·023	− 4	4·8		
133242–3	4·02	5267·017	−16	5·5	+17 c 4 L	*Lick Publ.* **16**
π Lup	B5 IV	5268·999	−15	5·2		
		5591·140	+ 1	4·9		
		5996·033	0	5·7		
133955	4·11	5267·028	+17	4·6	+18 c 8 L	*Lick Publ.* **16**
λ Lup	B3 IV	5269·003	+ 8	3·6	+ 9 b 11 C	*M.N.* **119**
		5591·167	+ 7	7·5		
		5998·992	−15	4·8		
134687	4·92	under observation			+11 c 6 L	*Lick Publ.* **16**
66G Lup	B3 III	for orbit			+ 6 d 4 R	*M.N.* **116**
135737	6·28	6356·019	+21	3·6		
7G TrA	B3 V	6736·984	−13	3·3		
		6738·967	−12	3·3		
		6798·876	−10	1·8		
136504	3·40	5297·964	− 9	3·8 B	+ 4 c 10 L	*Lick Publ.* **16**
ϵ Lup	B3 IV		+28	2·6 A		
	+A1:	6793·876	−19	8·8 B		
			+ 4	3·0 A		
		6798·856	−21	8·4 B		
			+ 8	2·2 A		
137432	5·46	5269·014	+18	5·5	+ 7 c 5 L	*Lick Bull.* **15**
100G Lup	B4 V	5651·008	− 8	4·8		
		5999·014	− 9	6·0		
		6322·137	+ 6	1·8		
138690	2·80	4971·879	− 9	4·6	+ 6 c 5 L	*Lick Publ.* **16**
γ Lup	B3 V	5996·058	+ 2	6·7	−16 c 7 C	*M.N.* **119**

TABLE II (*continued*)

(1) HD Star	(2) m_V Sp	(3) JD 243	(4) V km/s	(5) p.e. ±	(6) Previous mean vel.	(7) References
138764	5·15	5211·151	+ 4	1·2	− 5 b 5 L	*Lick Publ.* **16**
90G Lib	B6 IV	5999·030	−12	3·7	− 8 c 4 V	*Pub. D.A.O.* **5**
		6720·020	−64	3.2	+ 2 a 4 Y	*Ap. J.* **64**
			+13	2·6	− 4 b 4 W	*Ap. J.* **42**
		6736·006	− 5	4·0		
		6748·960	0	3·5		
139160	6·03	6356·997	+26	9·2		
94G Lib	B9 IV	6392·947	+28	8·5		
		6718·043	+ 4	4·7		
		6765·894	−12	6·3		
139365	3·63	4829·215	+ 5	7·7	+ 5 d 7 L	*Lick Publ.* **16**
τ Lib	B4 V	5586·160	+44	5·2	−10 c 3 Y	*Ap. J.* **64**
141556	4·11	4826·251	+ 8	2·6	−18 c 6 L	*Lick Publ.* **16**
χ Lup	Ao III –IV	5555·246	−70	4·7		
			+63	4·0		
		5613·086	−51	2·2		
			+24	2·4		
		5897·285	+14	6·2		
			+119	11·5		
141637	4·65	5211·161	+42	5·2	−10 c 6 L	*Lick Publ.* **16**
1 Sco	B3 V	5612·092	−14	2·9		
		5996·087	+32	7·0		
		6263·272	+27	8·1		
142139	5·76	6354·069	+12	2·6		
19G TrA	A1 V	6720·046	−12	1·9		
		6737·023	−24	1·9		
		6739·004	−18	2·0		
		6765·923	−12	2·3		
142165	5·44	5211·177	+25	4·0	+13 e 4 L	*Lick Publ.* **16**
4G Sco	B6 Vn	6005·999	− 8	5·4		
		6711·111	− 2	4·6		
		6736·018	− 9	3·4		
		6748·972	−35	4·4		
142184	5·46	5586·171	+48	5·8	−27 e 1 L	*Lick Publ.* **16**
5G Sco	B3 Vne?	5612·139	+ 2	3·0		
		6006·026	0	6·9		
		6736·030	+15	7·1		
		6766·966	− 2	5·6		
142990	5·41	6319·174	+ 3	4·9	−11 b 4 L	*Lick Publ.* **16**
11G Sco	B8 V	6323·152	−17	3·7		
		6357·049	− 1	4·8		
		6768·929	−30	7·2		
145482	4·60	5635·048	−14	5·0	+ 9 c 3 L	*Lick Publ.* **16**
13 Sco	B3 Vn	5646·047	−26	3·9	+10 d 3 W	*Ap. J.* **115**
		5996·099	+ 7	4·2		
147971	4·80	4971·911	− 6	3·3	−12 c 8 L	*Lick Bull.* **9**
ϵ^1 Nor	B3: V	5291·032	+ 9	4·2		
		5313·938	− 4	5·3		

TABLE II (*continued*)

(1) HD Star	(2) m_V Sp	(3) JD 243	(4) V km/s	(5) p.e. ±	(6) Previous mean vel.	(7) References
148379	5·46	6037·954	− 7	2·1	−19 b 4 L	*Lick Publ.* **16**
59G Nor	B2 Ia	6320·131	0	3·1		
		6322·189	− 1	3·8		
		6326·154	− 8	2·7		
148605	4·80	5211·201	+35	6·7	− 5 b 4 L	*Lick Publ.* **16**
i Sco	B2 V	5555·290	+49	12·6	− 2 c 3 W	*Ap. J.* **70**
		6003·073	−22	4·2		
		6035·964	−43	6·0		
		6319·188	+49	6·3		
		6323·173	+80	7·5		
148703	4·25	5291·054	0	3·7	0 b 10 L	*Lick Publ.* **16**
72G Sco	B2 V	5292·996	+31	3·2		
		6709·124	+ 8	4·1		
		6737·044	+ 2	2·0		
149757	2·56	4943·967	−10	2·7	−35 d 6 Y	*Ap. J.* **64**
ζ Oph	O9.5 Vnk	5296·025	− 6	6·7	−20 d 4 L	*Lick Publ.* **16**
		5647·038	+12	8·5	+30 a 2 V	*Pub. D.A.O.* 5
153613	5·06	5623·109	+ 1	5·1	+15 c 5 L	*Lick Publ.* **16**
117G Sco	B8 V	5914·280	+ 2	5·0		
		5995·091	−11	3·3		
		6379·042	−18	5·2		
154481	6·20	5350·909	−41	2·8		
80G Oph	Ao III–IV	6037·972	−26	1·5		
		6720·089	−10	2·1		
		6737·066	−17	1·7		
155450	6·00	5211·219	+14	5·0	+ 7 d 3 L	*Lick Bull.* **15**
130G Sco	B1 III	5265·101	+33	6·0	+33 a 3 R	*Mem. R.A.S.* **67**
		5555·308	+ 3	1·0		
		5635·127	0	4·0		
157056	3·37	see Table V			−15 c 45 O	*Pub. D.O.* **8**
θ Oph	B2 IV				+ 2 b 4 Y	*Ap. J.* **64**
					− 1 a 8 L	*Lick Publ.* 16
					− 4 b182 Md	*Ap. J.* **124** & 128
					+ 2a 20 Wc	*P.A.S.P.* **69**
157243	5·10	5623·131	+19	4·1	+ 8 c 7 L	*Lick Publ.* **16**
146G Sco	B6 V	5995·106	− 7	4·2		
			+78	6·4		
		6711·179	−14	3·3		
			+56	10·0		
157246	3·32	4848·240	+22	4·9	− 4 c 4 L	*Lick Publ.* **16**
γ AraA	B1 III	4943·977	−19	3·4		
		5266·062	+11	4·6		
		5291·010	−14	4·9		
		5647·049	+21	6·3		
		5999·075	+ 4	6·4		

TABLE II (*continued*)

(1) HD Star	(2) m_V Sp	(3) JD 243	(4) V km/s	(5) p.e. ±	(6) Previous mean vel.	(7) References
158408	2·70	5914·309	+ 1	3·9	+18 c 8 L	*Lick Publ.* **16**
v Sco	B3 Ib	5919·308	− 1	3·0		
		6709·171	+ 7	3·1		
		6737·084	− 7	2·3		
158926	1·60	4965·935	−44	7·2	+ 1 d 11 Lw	*Lowell Bull.* **1**
λ Sco	B2 IV	5293·052	− 2	6·2	− 7 d 3 L	*Lick Publ.* **16**
160578	2·39	4944·001	−30	3·4	−10 c 9 L	*Lick Publ.* **16**
κ Sco	B2 IV	4970·913	−44	2·9		
		4973·912	−40	2·1		
		5269·089	+19	4·3		
161756	6·16	6036·021	−23	3·1		
4G Sgr	B3 IV	6037·993	−18	6·2		
		6320·183	+20	4·2		
		6322·224	+36	6·0		
		6720·125	+30	4·4		
167128	5·54	5586·257	+58	3·5	+12 d 5 L	*Lick Bull.* **15**
6G Tel	B3 V	5995·144	+34	2·7		
		6718·160	+39	4·5		
		6737·100	−33	3·3		
		6768·051	− 9	3·9		
167356	6·08	5627·160	+29	2·2	− 1 c 4 W	*Ap. J.* **111**
45G Sgr	Ao Ia	6379·090	−10	2·3		
		6720·154	+ 6	1·4		
		6804·940	− 7	2·1		
170465	5·05	under observation			−15 d 11 L	*Lick Publ.* **16**
δ^1 Tel	B6 IV	for orbit				
170523	5·33				− 6 d 11 L	*Lick Publ.* **16**
δ^2 Tel	B5 IV				− 6 d 5 R	*Mem. R.A.S.* **67**
		orbit:			− 8 a 24 St	*M.N.* **116**
171034	5·38	5290·078	+10	4·9	−17 c 4 L	*Lick Publ.* **16**
77G Sgr	B3 IV	6323·208	+29	4·8		
		6353·160	+14	3·5		
		6356·180	+38	6·0		
		6393·077	+ 9	3·1		
173117	5·76	5612·212	+34	2·0		
94G Sgr	B5: V	5985·171	− 6	6·9		
		5987·173	+36	4·0		
		5997·167	+15	3·6		
173948	4·42	4856·286	− 1	3·7	+20 b 4 L	*Lick Publ.* **16**
λ Pav	B1 Ve	4966·057	− 7	5·0	+14 c 4 R	*Mem. R.A.S.* **68**
		5293·108	−13	6·7		
		5314·006	+ 4	2·3		
		5999·117	0	5·8		

TABLE II (*continued*)

(1) HD Star	(2) m_v Sp	(3) JD 243	(4) V km/s	(5) p.e. ±	(6) Previous mean vel.	(7) References
178322	5·86	4966·026	− 3	4·9	+ 6 d 3 L	*Lick Bull.* **15**
45G CrA	B5 V	5260·172	−38	6·8		
		5314·026	+30	9·8		
		5715·947	−32	6·7		
		5996·176	−15	3·5		
180885	5·61	under observation			−10 c 5 L	*Lick Bull.* **15**
162G Sgr	B4 IV	for orbit			− 9 c 3 R	*Mem. R.A.S.* **67**
182180	5·94	5999·153	+14	3·0		
179G Sgr	B5 IV	6036·071	− 3	4·1		
		6038·046	+30	4·3		
		6066·988	−19	4·4		
186219	5·52	5291·133	+ 5	2·3	o d 4 L	*Lick Publ.* **16**
70G Pav	Am	5356·948	−31	3·7		
		6737·181	+15	2·4		
		6768·087	−10	2·4		

TABLE III

Radial velocities of HD 79351

JD 243	V km/s	p.e. ±
4793·058	+ 6	2·7
5585·890	+45	1·9
5826·216	+20	3·6
5882·052	+30	3·1
5894·030	+18	6·4
6238·081	+20	5·1
6263·040	+ 9	3·5
6318·938	+26	3·0
6331·903	+20	4·4
6647·969	+ 3	6·7

TABLE IV

Orbital elements of HD 79351

		Provisional	Revised
	Period	$6^d{\cdot}744$	$6^d{\cdot}74469$
γ		+23·3	+23·3 km/sec
K		21·5	21·5 km/sec
T		JD 2416533·81	JD 2416534·215
e		0·18	0·18
ω		115°·84	112°·97
$a \sin i$		$1{\cdot}96 \times 10^6$	$1{\cdot}96 \times 10^6$ km

TABLE V

Radial velocities of θ Ophiuchi

JD 243....	V km/s	p.e. ±	JD 243....	V km/s	p.e. ±
5260·027	+12	2·6	5983·085	+ 1	4·3*
			·099	+14	5·9*
			·113	+18	4·1
5613·140	+15	2·4	·126	+19	4·1*
			·142	+10	3·7*
5625·071	+ 6	4·5	·155	+ 9	1·9*
·085	+ 8	2·6	·168	+ 6	3·5*
·100	+ 9	1·6	·182	+ 8	3·3*
·113	+ 9	3·0			
·126	+12	3·2			
			5987·099	+ 4	3·6
·140	+13	1·8	·141	+13	3·7
·154	+15	2·8			
·168	+14	3·3			
·182	+11	1·5	5994·981	+ 1	3·4
·196	+ 8	2·4	5995·006	+ 1	2·9
·210	+ 6	2·0*	·034	+ 1	2·0
			·054	+ 1	2·5
			·076	+ 5	2·8
5645·933	− 4	1·9			
·960	− 6	1·9	·098	+ 2	2·6
·982	− 1	3·0	·133	+ 3	3·0
5646·011	+ 8	2·5	·154	− 3	1·5
·031	+ 3	2·6			
·055	− 2	1·9	6034·913	− 5	3·7
·085	− 2	2·1	·931	− 1	3·3
·102	− 2	1·9	·954	+ 2	3·7
·128	+ 1	3·1	·973	+ 8	2·7
			·989	+ 6	2·9
5983·016	+ 4	5·3*	6035·015	+ 5	2·6
·030	+ 6	5·9	·032	− 1	4·3
·043	− 3	2·5	·056	+ 2	4·0
·058	−14	2·7	·067	+ 5	2·8
·072	− 2	1·9	·083	+ 3	3·1

* Under-exposed

TABLE VI

Observers and measurers

Name	Observed	Measured
W. Buscombe	310	411
H. Gollnow	88	0
G. Hagemann	2	42
W. Heintz*	16	0
P. Morris	68	182
A. Przybylski	105	0
Totals	589	635

* Munich Observatory: guest observer, 1954–55.

Acknowledgments.—The great enthusiasm of Professor Woolley acted as a stimulus to our original interest in this study. In discussion and correspondence, Professor Blaauw and Dr Thackeray have contributed helpful ideas. We thank the colleagues named in Table VI for their co-operation in obtaining the observations, and Mr Hunt for his care with the photographic processing.

Mount Stromlo Observatory,
Canberra, Australia:
1960 *March.*

References

(1) A Blaauw, *Publ. Kapteyn Astr. Lab.*, Groningen, no. 52, 1946.
(2) G. Alter, J. Ruprecht and V. Vanysek, Czechoslovak Academy of Sciences, Prague, 1958.
(3) G. Alter *et al.*, Appendix to *B.A.C.*, 10 (3), 1959.
(4) N. H. Rasmuson, *Lund. Medd.*, ser. II, no 26, 1921.
(5) P. G. Kulikowsky, *Sternberg Bull.*, no. 2, 1940.
(6) R. E. Wilson, *Carnegie Inst. Pub.*, no. 601, Washington, 1953.
(7) W. Buscombe and P. M. Morris, *M.N.*, **118**, 609, 1958.
(8) R. M. Petrie, *Publ. Dom. Astrophys. Obs.*, **9**, 297, 1953.
(9) W. Buscombe, *M.N.*, **116**, 262, 1956.
(10) H. D. Curtis, *Lick Bull.*, **4**, 153, 1907.
(11) A. van Hoof, *P.A.S.P.*, **69**, 179, 1957.
(12) D. H. McNamara, *P.A.S.P.*, **69**, 570, 1957.

THE EMISSION SPECTRUM OF THE NIGHT SIDE OF VENUS

B. Warner

(Communicated by the Director of the University of London Observatory)

(Received 1960 April 5)

Summary

The measurements given by Kozyrev of features in the spectrum of the night side of Venus are examined. The existence of nitrogen bands is confirmed and evidence is presented identifying emission lines of neutral and ionized oxygen.

In a recent paper (**1**) concerned with the night side of Venus, N. A. Kozyrev lists 50 features observed by him in the emission spectrum of the Ashen Light. Of these, 22 features are tentatively identified as being produced by the N_2 and N_2^+ molecules, the others being left unidentified. A further study of the Kozyrev spectrum has shown that many of the latter may be due to atomic oxygen emission.

1. *Kozyrev's spectrum.*—The spectrum obtained by Kozyrev contains features that are at the limit of detection of his instruments; consequently the reality of many of these may be questioned until further evidence is produced. An attempt to confirm the Kozyrev spectrum has been made by Newkirk (**4**) and is briefly described in Section 4. In the present paper it is necessary to accept the reality of the whole spectrum as Kozyrev gives no indications of the objectivity of individual features.

In Kozyrev's paper, a list of wavelengths of spectral features is given which distinguishes between 'lines' and 'bands'. In fact, it is evident from the reproduction of the spectrogram that the 'lines' have a width of several angstroms and there is a gradual transition in width from 'lines' to 'bands'. The latter are better termed emission 'strips' since the features identified by him (N_2 and N_2^+ band heads) coincide with 'lines' in his spectrum.

From the data given in (**1**) the line-width due to the slit is found to be 1·25 A, while the photographic resolution could not be less than about 2·5 A. From the reproduction and data it would appear that the actual resolution is 4–5 A, thus suggesting that the emission strips may be due to unresolved lines and hence can be caused by atomic transitions.

Accordingly, a search has been made for atoms capable of producing the observed features. To do this, Kozyrev's measurements are compared with wavelengths taken from Moore's tables (**2**). To test whether the number of coincidences between these two tabulations is significant the number expected on chance is computed as shown in Section 2. For completeness the coincidences with bands in the N_2 and N_2^+ spectra are also treated quantitatively, taking data from Pearse and Gaydon (**3**). Throughout this investigation only strong lines and bands in the listed spectra are considered.

2. *Statistical considerations.*—We shall count a coincidence whenever a laboratory line falls within x units of an observed line. Then, if there are M observed

lines within a spectral region of X units, the chance of coincidences for one laboratory line from the same region is

$$p = \frac{2Mx}{X}.$$

If there are N lines in the laboratory spectrum then the total number of expected coincidences C is given by

$$C = Np$$
$$= \frac{2MNx}{X}.$$

For emission strips the corresponding formula is

$$C' = \frac{2M'N'(x + \frac{1}{2}w)}{X'}$$

where w is the average width of the strips (10 A) and x is measured from the edge of a strip (A). The average interval between lines (X/M) is 44 A and the average interval between strips (X'/M') is 61 A.

In Tables I to V an asterisk (*) is placed whenever the number of observed coincidences (O, O') is significantly greater than C, C' at a 5 per cent level. For a real correlation, O, O' should remain nearly constant as x increases. From a study of the results given in Tables I to V this is found to be the case for O in Tables I and II and O' in Tables IV and V.

3. *Comparison of numbers of observed and calculated coincidences*

(i) *Nitrogen.*—The three important systems of bands in the N_2 and N_2^+ spectra are the Main System (MS), the Second Positive Group (2PG), and the Vegard-Kaplan System (VK). These are treated separately and compared first with lines (O and C) and then with emission strips (O' and C') in the Ashen Light emission spectrum. Tables I to III give the results.

TABLE I

N_2 (2PG)

x	O	C	O'	C'
0	–	–	2	2·0
1	4*	0·6	2	2·4
2	5*	1·3	2	2·8
3	7*	1·9	2	3·1
4	7*	2·5	3	3·5

TABLE II

N_2^+ (MS)

x	O	C	O'	C'
0	–	–	0	1·8
1	4*	0·6	1	2·2
2	4*	1·3	1	2·5
3	4	1·9	1	2·9
4	5	2·5	1	3·2

TABLE III

N_2 (VK)

x	O	C	O'	C'
0	–	–	1	1·8
1	0	0·4	2	2·2
2	1	0·8	2	2·5
3	2	1·2	2	2·9
4	2	1·6	2	3·2

It is clear that the coincidence of N_2 (2PG) and N_2^+ (MS) bands with observed lines is significantly above chance and O is approximately constant as expected. There is no evidence for the emission of the N_2 (VK) system. Both of these results confirm Kozyrev's results. The N_2 and N_2^+ bands do not seem to coincide with the strips.

No other molecules have been found that give significant results, so the search has been extended to atomic lines with the justification of Section 1.

The only atom found that gives any significant coincidence is oxygen.

(ii) *Oxygen.*—The 4 O I lines of intensities 8 or greater and the 31 O II lines of intensities 7 or greater (within the required spectral region) have been compared with Kozyrev's list. The numbers of coincidences are given in Tables IV and V.

TABLE IV

O I

x	O	C	O'	C'
0	–	–	1	0·7
1	0	0·2	1	0·8
2	2*	0·4	1	0·9
3	2	0·5	1	1·0
4	3*	0·7	1	1·2

TABLE V

O II

x	O	C	O'	C'
0	–	–	12*	5·1
1	0	1·4	13*	6·1
2	2	2·8	13*	7·1
3	3	4·2	13*	8·1
4	5	5·6	13	9·1
5	5	7·0	14	10·2
6	6	8·4	14	11·2

Table V is more extensive than the previous ones as the evidence for the presence of oxygen rests mainly on it.

It appears from these two tables that there is some evidence for the presence of O I and strong evidence for O II, the latter contributing mainly to the emission strips. The O' for O II are significantly greater than the C' for small x and O' is virtually constant even to $x = 6$ A.

TABLE VI

Identification of features in the emission spectrum of Venus

Venus Lines and strips	I	Identification		
		Probable	Possible	Absent
3528	2		3532·6(MS)[1,0]	
3536	2	3536·7(2PG)[8]		
				3548·9(MS)[3, 0]
				3563·9(MS)[4, 0]
3577	2	3576·9(2PG)[10]		
3583	2	3582·1(MS)[4, 3]		
3616–3630	1			
3646	1		3641·7(2PG)[3]	
3655	1			
3665	2			
				3671·9(2PG)[6]
3686	2			
3700	1			
3710–3716	2	3712·8 O II[7], 3710·5(2PG)[8]		
3724–3732	2	3727·3 O II[8]		
3746–3756	2	3749·5 O II[9], 3755·4(2PG)[10]		
3781	1			
3805	1	3804·9(2PG)[10]		
3825	1	3823·5 O I[10]		
3836	1		3835·4(MS)[1, 1]	
3860	2	3857·9(2PG)[5]		
				3882·2 O II[7]
3888	2		3884·3(MS)[3, 1]	
				3894·6(2PG)[7]
3900	1			

TABLE VI—*continued*

Venus Lines and strips	I	Identification Probable	Possible	Absent
3914	3	3914·4(MS)[6, 0], 3912·0 O II[10]		
3946	2–3	3947·3 O I[10], 3943·0(2PG)[8]		
				3954·4 O II[7]
3958	1	3954·7 O I[10]		
				3973·3 O II[10]
4000	1	3998·4(2PG)[9]		
4024–4038	1			
4052–4056	1		4059·4(2PG)[8]	
				4072·2 O II[8]
				4075·9 O II[10]
4090	1		4094·8(2PG)[4]	
				4105·0 O II[7]
				4119·2 O II[8]
4128	1			
4141	1	4141·8(2PG)[5]	4140(MS)[2, 0]	
				4153·3 O II[7]
				4166·8(MS)[3, 0]
4184–4192	2	4185·5 O II[8], 4189·8 O II[10]		
				4199·1(MS)[4, 2]
				4200·5(2PG)[6]
4206–4219	2			
				4236·5(MS)[7, 5]
4250	3	4253·7 O II[8]		
4264	3		4269·7(2PG)[5]	
4278	3	4278·1(MS)[8, 6]		
4314–4330	2	4317·1 O II[8], 4319·6 O II[8]		
4340–4350	2	4345·6 O II[7], 4349·4 O II[8]		
4363–4370	3	4366·9 O II[7], 4368·3 O I[10]		
4390–4395	2	4396·0 O II[7]		
4410–4420	2	4415·0 O II[10], 4417·0 O II[8]	4416·7(2PG)[3]	
4430–4440	2			
4450–4462	2			
4496–4504	2			
				4515·9(MS)[6, 0]
				4554·1(MS)[4, 0]
				4591·0 O II[9]
				4596·2 O II[8]
				4599·7(MS)[6, 2]
4612–4616	2			
4640	1	4641·8 O II[9]		
4652	1	4651·8(MS)[4, 13], 4649·1 O II[10]		
				4661·6 O II[9]
4670	2		4676·2 O II[8]	
				4699·2 O II[7]
				4705·4 O II[8]
4710–4720	2	4709·2(MS)[4, 2]		
4760–4780	2			
4856	2			

Having established, on statistical grounds, the probable presence of certain nitrogen and oxygen emission features it is possible to construct a list of identifications—Table VI. In this table the first column is a reproduction of Kozyrev's published wavelength measurements, which have a probable error of 2–3 A.

Single numbers denote 'lines', and pairs of numbers, 'strips'. The second column gives his estimates of the intensities of the features. Column three is a list of probable identifications. The square brackets signify the intensities—for the M.S. the first number gives the intensity in a discharge through helium containing a trace of nitrogen, the second the intensity through nitrogen at low pressure (**3**). The oxygen and nitrogen intensities are not on the same scale. The next column gives possible identifications and the final column absent features.

The reason why oxygen and not nitrogen causes apparent 'bands' in the emission spectrum is due to the resolving power of the optical system used and the multiplet structure of the oxygen spectrum. It can be seen from Table VI that all but one of the pairs of features that cause emission strips have separations less than 4·5 A, i.e. less than the probable resolving power of Kozyrev's instrument.

4. *Conclusion.*—By statistical means we have found evidence for the presence of N_2, N_2^+ and O II in the atmosphere of Venus, and shown the presence of O I to be probable. The absent strong lines (see last column of Table VI) are a cause for concern. However it should be remembered that the detection of all the features in the Ashen Light spectrum has been marginal and some detection failures must be expected. Moreover, differences of relative intensities in the laboratory and the Ashen Light might result in the non-appearance of some lines whose laboratory intensities are thought to be above threshold. In the O II spectrum all but three of the lower excitation lines (low E.P. < 24 eV) and only four of the higher excitation lines have been detected. This suggests that the laboratory excitation temperature was higher than that of the Ashen Light. If the lower excitation O II lines only had been used in the statistics the calculated significance of O II presence would have been much greater.

The attempt to confirm Kozyrev's work by Newkirk (**4**) provides no additional evidence in favour of oxygen, the one extra feature discovered by him still being unidentifiable. Newkirk provided a criterion for deciding the reality of the emission features in his spectra, but this throws no light on the fainter features in Kozyrev's spectrum as Newkirk's apparatus had a lower dispersion. Two of the brighter bands (due to N_2^+) are confirmed.

One might conclude that the reality of the emission features in Kozyrev's spectrum is much strengthened by their independent identification with oxygen lines.

The writer's thanks are due to Mr T. Kiang for advice relating to the statistical problems concerned in this paper.

University of London Observatory,
Mill Hill Park,
London, N.W.7:

1960 *April* 4.

References

(1) Kozyrev, N. A., *Szv. Krym. Astrofiz. Obs.*, **12**, 169, 1954.
(2) Moore, C. E., *A Multiplet Table of Astrophysical Interest*, Princeton, N. J., 1945.
(3) Pearse, R. W. B., and Gaydon, A. G., *The Identification of Molecular Spectra*, Chapman and Hall, 1950.
(4) Newkirk, G., *Planetary and Space Science*, **1**, 32, 1959.

THE DETERMINATION OF THE INCIDENT FLUX OF RADIO-METEORS

T. R. Kaiser

(Received 1960 April 7)

Summary

The observed rate of radio-meteors depends on a number of factors which include: (i) the incident flux and distribution in magnitude of the meteors, (ii) the radiant co-ordinates, (iii) the variation in ionization along a meteor trail, (iv) the nature of the radio reflection process and (v) the parameters of the radio-echo equipment. The present work represents a considerable simplification over previous attempts (**5, 6**) to relate the radio echo rate to the actual flux of meteoroids. Simple formulae are derived relating these two quantities which, when used together with suitable graphical representation of the directional properties of the aerial system and of the reflection geometry, enable the incident flux of shower meteors to be deduced from the observed rate. The fact that the variation with time of the shower rate obtained with a fixed aerial beam may be predicted is relevant in connection with a method (**7, 8**) for shower radiant determination. Limitations due to the approximations in the theory, and to the simplified ablation theory on which it is based, are discussed.

---

1. *Introduction.*—The study of radio reflections from meteor trails has yielded a considerable amount of information concerning the properties and distribution of interplanetary matter and the physical processes accompanying the entry into the atmosphere of meteoric particles (meteoroids). A virtue of the technique is its inherent objectivity; the mechanism and geometry of reflection are fairly well understood and the essential equipment parameters (transmitted power, receiver sensitivity, aerial gain, etc.) are amenable to precise determination. It may therefore seem at first sight surprising that relatively little effort has been devoted to the problem of deducing the absolute incident flux of meteoroids from the observed echo rate. The following are the major difficulties which arise: (1) The reflection process is selective; echoes are only observed from trails which produce sufficient ionization in the vicinity of the specular reflection point (where a vector from the observer makes a normal intersection with the trail). (2) The sensitivity varies with direction in the aerial beam and with range. (3) In the case of sporadic meteors the relation between incident flux and echo rate depends on the orbital distribution. In view of the additional complication resulting from (3) the present discussion is limited to the case of shower meteors.

In former theoretical work (**1, 2**) concerned with the distribution of reflection points it was shown that they should be confined to a relatively narrow height interval about a mean height near 100 km and in spite of certain simplifying assumptions (particularly as concerns the meteor ablation process) fair agreement with observation has been obtained (**3, 4**). A previous extension of the theory to the present problem (**5, 6**) suffered through involving unduly complicated integrals which only in limiting cases (e.g. for a narrow, gaussian aerial beam)

led to manageable formulae. In the present work simple formulae are derived which combined with a suitable graphical procedure enable the magnitude distribution and incident flux of shower meteors to be derived from the observed echo rates. The theory enables the variation in echo rate due to the diurnal motion of the meteor radiant to be predicted and hence it has some importance in connection with the method for shower radiant determination developed by Clegg (**7**), particularly as modified by Keay (**8**) for high echo rates.

2. *The geometry of meteor reflections.*—On account of the specular condition all reflection points lie in the 'echo plane' ABCD (Fig. 1), which is normal to the radiant direction and passes through the observing station, O. The elevation of ABCD above the horizontal at O is thus equal to the radiant zenith distance, χ_0, measured at O. The reflection points are further limited to a band corresponding to a relatively narrow height range about a mean height $\bar{h}$ which defines the locus SS^1 in the figure (we will call SS^1 the 'echo line').

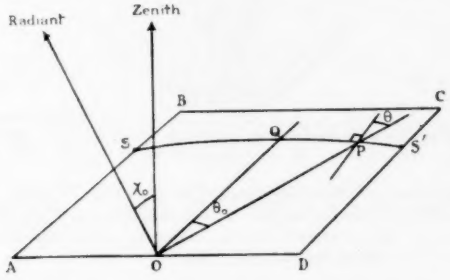

FIG. 1.—*The echo plane* ABCD *which is normal to the radiant direction and contains the echo line* SS^1.

The minimum detectable line density, α_P, in a meteor trail which intersects the echo plane at P is related to the system parameters by (**5, 9, 10**)*.

$$\alpha_P = \left(\frac{32\pi^2 R^3 P_R}{P_T G \lambda^3}\right)^{1/2} \left(\frac{mc^2}{e^2}\right) \quad \text{for} \quad \alpha_P < 2{\cdot}4 \times 10^{12} \text{ cm}^{-1} \text{ (decay type echoes)} \quad (1)$$

and

$$\alpha_P = \left(\frac{54\pi^3 R^3 P_R}{P_T G \lambda^3}\right)^{2} \left(\frac{mc^2}{e^2}\right) \quad \text{for} \quad \alpha_P > 2{\cdot}4 \times 10^{12} \text{ cm}^{-1} \text{ (persistent echoes).} \quad (2)$$

Here, $R = OP$, P_R = minimum detectable echo power, P_T = transmitted power, $G = \sqrt{G_T G_R}$ where G_T and G_R are the transmitting and receiving aerial gains respectively, λ = wave-length, m, e, and c are respectively the mass and charge of the electron and the velocity of light (in c.g.s. gaussian units).

From (1) and (2) we may deduce the variation in sensitivity for meteor detection, i.e. of α_P, along the echo line SS^1. However, since the echo plane moves through the aerial beam due to the daily motion of the radiant, it is more convenient to use the representation of Clegg (**7**) in which the contours of constant α_P are plotted on a sphere (the 'echo surface') at height $\bar{h}$ above the Earth's surface. This is illustrated in Fig. 2 for one of the rhombic aerials at

* The echo enhancement due to plasma resonance (**9**) with transverse polarization has been ignored in (1). The numerical factor in (2) has been modified in accordance with a correction to the original theory due to Manning (**11**).

Sheffield with $\bar{h}=100$ km. The projection is such that the radial coordinate is proportional to the distance R_S measured in the echo surface from its intersection with the observer's zenith; the normalized sensitivity contours are represented by lines of constant $\rho=\alpha_{P0}/\alpha_P$, where α_{P0} is the minimum value of α_P and depends on the equipment parameters as well as the aerial gain*. The error in scaling distances in the curved echo surface directly from the projection of Fig. 2 is negligible.

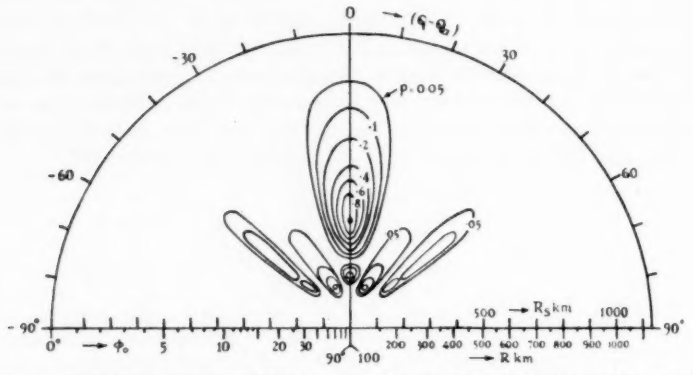

FIG. 2.—*Normalized meteor sensitivity contours for one of the Sheffield rhombic aerials, projected onto the echo surface at 100 km height. R_S=radial distance measured in the echo surface from its intersection with the observer's zenith, R=slant range, ϕ_0=elevation, φ=azimuth, φ_a= azimuth of beam axis (azimuths measured E of N).*

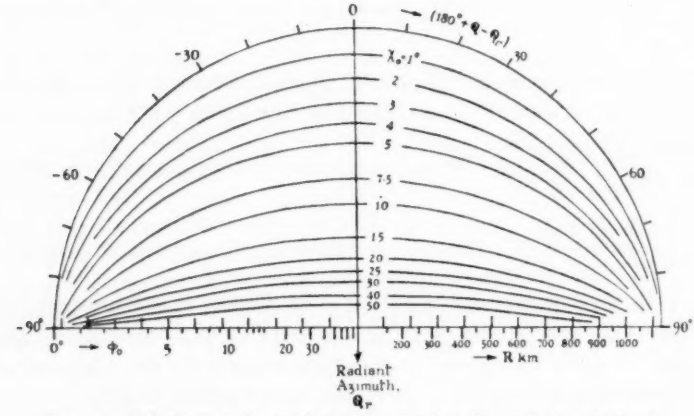

FIG. 3.—*Echo lines on the 100 km echo surface (similar projection to Fig. 2).*

The echo lines may also be represented on the echo surface as shown in Fig. 3. Given the radiant zenith distance (χ_0) and azimuth (φ_T), Fig 3 can be superimposed on Fig. 2, and oriented so as to dispose correctly the radiant azimuth relative to that of the beam maximum, thus giving the intersection of the echo line with the sensitivity contours. In this way the variation of α_P along an

* Provided $\alpha_{P0} \ll 10^{12}$ it is sufficient only to employ (1) in evaluating ρ, since in this case the contribution of persistent echoes to the total rate will be small.

echo line is obtained. The Geminid echo lines at various times relative to radiant transit are shown in Fig. 4 for an observer at Sheffield (latitude 53° 23′)*.

If the echo rate is sufficiently high, considerable simplification may be achieved by considering only echoes within a restricted range interval centred on some range R (e.g. the range at which $\rho = 1$). In this case a set of curves of the type shown in Fig. 5 will be useful. These are loci of constant azimuth and zenith

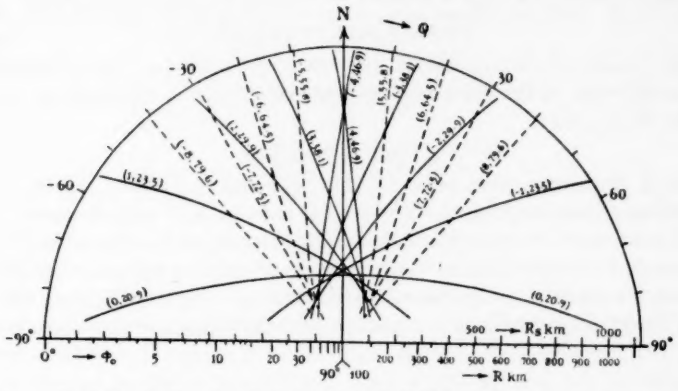

FIG. 4.—*Geminid echo lines for the latitude of Sheffield* (53°23′*N*) *in a similar projection to Figs.* 2 *and* 3. *The figures on the curve are* (T, χ_0) *where* T *hr. is the radiant hour angle and* χ_0 *degrees is the zenith distance.*

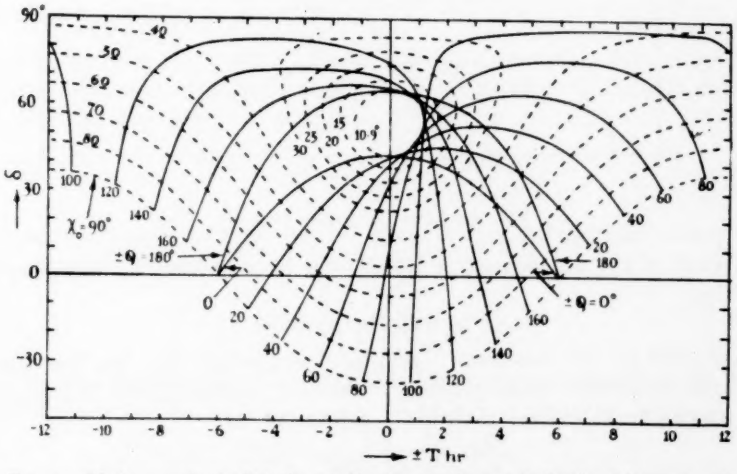

FIG. 5.—T=*hour angle at which the echo line for a radiant at declination* δ *intersects azimuth* φ(*E of N*) *at slant range* R=450 *km* (ϕ_0=10·9°, *latitude* 53°23′*N*). *The broken curves are loci of constant zenith distance,* χ_0.

distance of a point on the echo line at the fixed range R, plotted in radiant declination–hour angle coordinates. Given a set of such curves, together with the sensitivity contours of Fig. 2, the sensitivity factor ρ and zenith distance χ_0

* Formulae relating χ_0 and φ_T to the celestial coordinates of the radiant and for calculating the echo lines in the projection of Fig. 3 are given in the Appendix.

can be determined as a function of hour angle for any specified radiant declination. In particular the time at which the echo line intersects the point of maximum sensitivity (on the beam axis) is easily ascertained. A method for computing these curves will be found in the Appendix.

3. *The representation of the incident flux of shower meteors.*—An approximate relation for the electron line density α cm^{-1} produced by a spherical meteoroid travelling through a rarefied isothermal atmosphere is (**12**):

$$\alpha = \alpha_m (p/p_m)(1 - \tfrac{1}{3}p/p_m)^2 \qquad (3)$$

where the maximum line density α_m occurs at pressure p_m; α_m is proportional to the initial mass of the meteoroid and to $\cos\chi$. If the pressures p, p_m occur at heights h, h_m, then

$$h - h_m = H \ln (p/p_m) \qquad (4)$$

where H is the exponential scale height. (3) and (4) define the line density as a function of height (Fig. 6). Weiss (**13**) has obtained a more exact equation and has considered the effect of a linear height gradient of H. However in neither case is the form of the electron density profile altered to an extent which would be serious for the present purposes. Indeed major departures from the simple ablation theory are more likely to come from processes such as fragmentation (**14**).

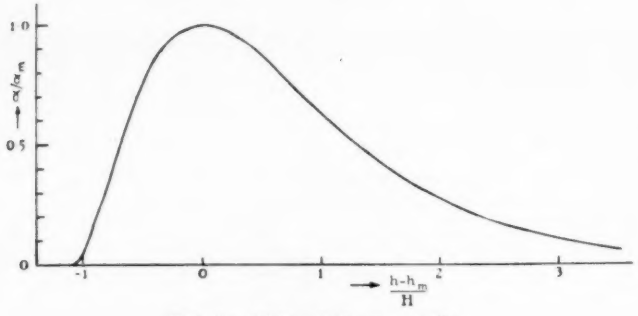

FIG. 6.—*Meteor ionization profile.*

In view of the dependence of α_m on χ it is convenient to introduce the quantities

$$\alpha_z = \alpha_m (\cos\chi)^{-1} \qquad (5)$$

which we will call the maximum "zenithal" line density (i.e. the line density which the meteoroid would produce if incident vertically) and the absolute radio magnitude M which is defined by Kaiser (**10**) as

$$M = -2{\cdot}5 \log_{10} \alpha_z + 35. \qquad (6)$$

Decay type echoes occur for $M > +5$

The incident flux of meteoroids (per unit time across unit area normal to the radiant direction) can thus be represented by:

$\Phi(\alpha_z)\,d\alpha_z$ = flux producing zenithal line densities between α_z and $\alpha_z + d\alpha_z$,

$\Theta(\alpha_z)$ = flux producing zenithal line densities greater than α_z,

$A(M)\,dM$ = flux producing meteors with magnitude between M and $M + dM$,

$B(M)$ = flux producing meteors brighter than magnitude M.

In many cases we can approximate to the distribution function Φ by the power law

$$\Phi(\alpha_z) = c\alpha_z^{-s} \tag{7}$$

where c and s are constants. Such a law appears to hold for sporadic meteors over a wide range of magnitudes with s close to 2·0 (**2, 5**). In a study of the major showers (**6**) s was found to have some dependence on α_z and to be generally less than 2, at least for the sub-visual radio meteors. If (7) is valid we obtain:

$$\Theta(\alpha_z) = \frac{c}{(s-1)\alpha_z^{s-1}} \tag{8}$$

and

$$\mathrm{B}(M) \propto \mathrm{A}(M) \propto a^M \tag{9}$$

where $s = 1 + 2{\cdot}5 \log a$. For $s = 2$ we get $a = 2{\cdot}51$ which corresponds to a constant total mass of meteoric material per unit magnitude interval.

4. *The echo rate per unit length of echo line.*—With the help of the geometrical considerations in Section 2 we can now relate the observed shower echo rate to the actual incident flux of meteoroids.

Consider those meteoroids incident upon a strip of the echo plane at P (Fig. 1) which is normal to the echo line and is of width dl, and let the height and atmospheric pressure at burn-out be h_0 and p_0 respectively. Equation (3) may thus be re-written:

$$\alpha/\alpha_m = \frac{27}{4} u(1-u)^2 \tag{10}$$

where $u = p/p_0 = \exp(-x/H)$, $x = h - h_0$. The number of meteors passing through the interval of the strip between heights x and $x + \mathrm{d}x$ above h_0 and with maximum line densities in excess of α_m is simply

$$\mathrm{d}N = \Theta\left(\frac{\alpha_m}{\cos\chi}\right)\frac{\mathrm{d}l\,\mathrm{d}x}{\sin\chi}. \tag{11}$$

The radio-echoes from these will be detected provided the line density at the echo plane is in excess of α_p, i.e. provided*

$$\alpha_m \geqslant \frac{4}{27}\alpha_p u^{-1}(1-u)^{-2}. \tag{12}$$

The total number of echoes obtained from meteors intersecting the strip is therefore

$$N_1\,\mathrm{d}l = \frac{H\,\mathrm{d}l}{\sin\chi}\int_0^1 \Theta(\alpha_{zz})\frac{\mathrm{d}u}{u}. \tag{13}$$

Where $\alpha_{zz} = \frac{4}{27}\frac{\alpha_P}{\cos\chi}u^{-1}(1-u)^{-2}$; it is the maximum zenithal line density of the faintest detectable meteor at height $h_0 + x$. Thus N_1 is the observed echo rate per unit length of echo line.

* If the height interval from which echoes are obtained is reasonably small compared with the mean height $\bar{h}$ we can treat the minimum detectable line density as constant over the strip and equal to its value α_P on the mean echo line.

If $\Theta(\alpha_z)$ can be represented by equation (8) we get the simple result:

$$N_1 = \frac{HI}{\sin\chi}\,\Theta\left(\frac{\alpha_P}{\cos\chi}\right) \tag{14}$$

where

$$I = \left(\frac{27}{4}\right)^{s-1}\int_0^1 u^{s-2}(1-u^2)^{s-1}\,du = \left(\frac{27}{4}\right)^{s-1}\frac{\Gamma(s-1)\Gamma(2s-1)}{\Gamma(3s-2)} \tag{15}$$

and is plotted in Fig. 7.

HI is simply the area of the normalized distribution in height of the reflecting points in the strip of the echo plane and I is identical with the integral

$$I_1 = \int_{-\infty}^{\infty}\left[\frac{3e^{x}}{2e^{3x/2}+1}\right]^{3(s-1)}dx$$

which appears in earlier work (**1, 2, 5, 6**). $HI/\cos\chi$ may be regarded as an average effective length of the trails of radio-meteors.

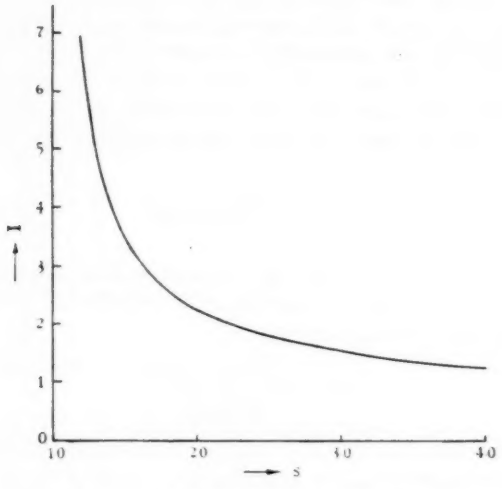

FIG. 7.—$I = \left(\frac{27}{4}\right)^{s-1}\int_0^1 u^{s-2}(1-u^2)^{s-1}\,du$.

The zenith distance χ in the above is the value at the point P on the echo line and it differs from the value χ_0 at the observer. To a close approximation we may substitute (see Appendix):

$$\cos\chi \simeq \cos\chi_0, \qquad \sin^2\chi \simeq \sin^2\chi_0 + 2\bar{h}/R_E$$

where R_E is the Earth's radius, whence we obtain

$$N_1 = Hf_1(\chi_0, s)\Theta(\alpha_P) \tag{16}$$

where

$$f_1(\chi_0, s) = I(\cos\chi_0)^{s-1}(\sin^2\chi_0 + 2\bar{h}/R_E)^{-1/2}. \tag{17}$$

$f_1(\chi_0, s)$ is given in Fig. 8 as a function of χ_0 for a range of values of s (with $\bar{h} = 100$ km).

Using the method of Section 2, the sensitivity factor ρ may be determined at all points along the echo line, hence the echo rate N over part or the whole of the echo line can be obtained, by numerical integration, from

$$N = Hf_1(\chi_0, s)\Theta(\alpha_{P0}) \int \rho^{s-1}\, dl. \tag{18}$$

The echo rate between specific range limits can be found by evaluating the integral in (18) along the appropriate intercept of the echo line.

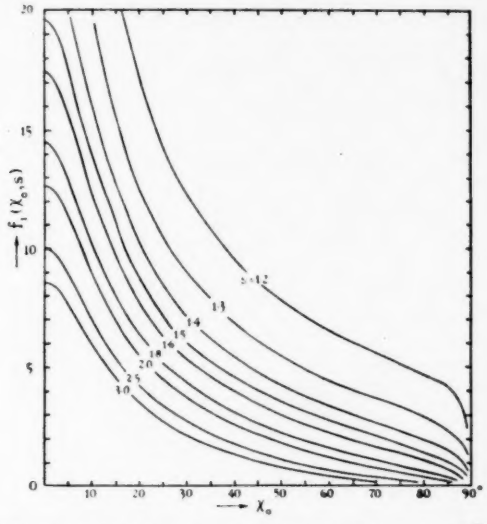

FIG. 8.—*The rate factor* $f_1(\chi_0, s)$ *as a function of* χ_0 *for various* s ($\bar{h}$ = 100 *km*).

The value of s can be found from the distribution in amplitude of the shower meteor echoes or from the dependence of echo rate on equipment sensitivity (**5, 6, 15**). By substituting it into (18) we obtain the factor relating N to Θ and hence the incident flux may be deduced from the observed echo rate.

5. *The echo rate per unit range interval.*—In Fig. 1, θ is the angle between OP and the normal to the echo line at P. ϕ, ϕ_0 are the elevation of OP above a horizontal plane at P and O respectively. θ_0 is the angle QOP where OQ is the intersection between the echo plane and the plane through O, the zenith and radiant point.

We have $\sin\theta = dR/dl$ where dR is the range interval corresponding to the element dl of the echo line. Thus if $N_2\, dR$ is the rate of echoes with ranges between R and $R + dR$ we obtain, using (14),

$$N_2 = \frac{HI}{\sin\theta \sin\chi}\,\Theta\left(\frac{\alpha_P}{\cos\chi}\right). \tag{19}$$

To a sufficient order of approximation (see Appendix),

$$\sin\theta \sin\chi \simeq \sqrt{(\sin^2\chi_0 - \sin^2\phi_0)}, \qquad \cos\chi \simeq \cos\chi_0,$$

hence

$$N_2 = Hf_2(\chi_0, s)\Theta(\alpha_p) \tag{20}$$

where

$$f_2(\chi_0, s) = I(\cos\chi_0)^{s-1}(\sin^2\chi_0 - \sin^2\phi_0)^{-1/2}; \tag{21}$$

N_2 depends on R through $\sin\phi_0 \simeq \frac{h}{R} - \frac{R}{2R_E}$.

Equation (20) gives the rate per unit range; it can be applied to a finite range interval provided the sensitivity factor ρ does not vary appreciably along the intercept of echo line. It clearly fails when ϕ_0 approaches χ_0, when the echo line becomes tangent to the circle of constant range R (i.e. when P and Q in Fig. 1 coincide). In this case we must revert to the method of Section 4 and evaluate the integral of ρ^{s-1} along the echo line (for the result to be valid the range interval must be sufficiently large to encompass the range spread due to the finite dispersion in height of the reflection points). In this manner the mean rate $\bar{N}$ between 400 and 500 km has been evaluated, for echo lines intersecting the beam axis of the Sheffield rhombics at range 450 km*. The result is illustrated in Fig. 9 where the full curves give $\bar{N}/[H\Theta(\alpha_{p0})] = \bar{f}_2(\chi_0, s)$; they may be compared with $f_2(\chi_0, s)$ evaluated for $R = 450$ km, given as broken curves.

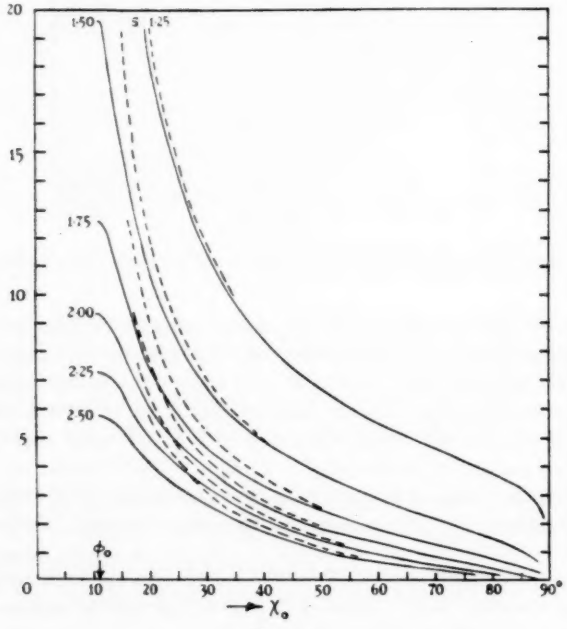

FIG. 9

———$\bar{f}_2(\chi_0, s)$ *evaluated for the Sheffield rhombic aerials with* $400 < R < 500$ *km.*
— — —$f_2(\chi_0, s)$ *for* $R = 450$ *km* ($\phi_0 = 10{\cdot}9°$).

6. *The determination of shower radiants.*—The method of Clegg (7) and its modification due to Keay (8) rests essentially on the assumption that the

* This will be approximately the condition for maximum rate per unit range at $R = 450$ km (but see Section 6).

maximum shower echo rate at a given range occurs when the echo line intersects the beam axis at that range. Referring to Fig. 5 we see that the radiant declination and right ascension can be estimated from the times of maximum rate on two aerials at different azimuths. It is clear from the above, however, that the zenith distance will be changing as the echo line moves through the beam causing a displacement in the time of maximum rate which will occur earlier or later depending upon whether χ_0 is an increasing or decreasing function of T. The magnitude of the displacement will depend, *inter alia*, on the azimuthal width of the aerial beams (being greater, the wider the beam) and on the radiant declination. It is clear that the present theory enables these time displacements to be estimated and appropriate corrections to be made.

7. *An alternative approach to the problem.*—If we consider again a narrow strip in the echo plane, normal to the echo line at P, we see that a meteor trail with maximum line density α_m can be detected over a height range $H \ln (u_1/u_2)$ where u_1, u_2 $(u_1 > u_2)$ are the positive solutions of the cubic equation (10) with $\alpha = \alpha_p$. The quantity $\ln (u_1/u_2)$ is thus a function of α_m (for given α_p) and may be regarded as a weighting factor which when multiplied by the differential distribution function $\Phi(\alpha_m/\cos\chi)$ gives the distribution of maximum line densities of the meteor trails which are actually observed (see Fig. 10).

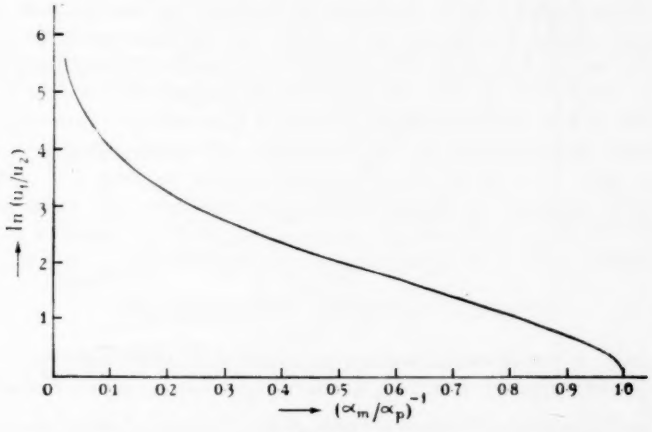

FIG. 10

Thus the number of echoes observed per unit length of echo line at P from meteors with line densities between α_m and $\alpha_m + d\alpha_m$ is $n(\alpha_m)\, d\alpha_m$ where

$$n(\alpha_m) = \frac{H}{\sin\chi \cos\chi} \ln\frac{u_1}{u_2} \Phi\left(\frac{\alpha_m}{\cos\chi}\right). \qquad (22)$$

For the special case when Φ may be represented by the power law we get

$$n(\alpha_m) \propto z^{-s} \ln (u_1/u_2) \qquad (23)$$

where $z = \alpha_m/\alpha_p$. When $z \gg 1$, $u_1/u_2 \simeq 27z/4$. Fig. 11 illustrates how $n(\alpha_m)$ from (23) varies with α_m. For $s = 2$ the most frequently observed meteor has maximum line density about 1·3 times the threshold value, α_p.

The total observed rate per unit length of echo line, for any distribution Φ is obtained by integrating (22) giving

$$N_1 = \frac{H\alpha_P}{\sin\chi\cos\chi}\int_1^\infty \ln\frac{u_1}{u_2}\,\Phi\left(\frac{z\alpha_P}{\cos\chi}\right)dz. \tag{24}$$

Equation (24) enables the observed rate to be predicted if Φ is known but unfortunately it is of little value in deducing Φ from the observations. It is nevertheless instructive in showing that only for the power law does N_1 have the same functional dependence as Θ on the limiting line density, α_P; in this case (24) becomes

$$N_1 = \frac{(s-1)H}{\sin\chi}\,\Theta\left(\frac{\alpha_P}{\cos\chi}\right)\int_1^\infty z^{-s}\ln(u_1/u_2)\,dz. \tag{25}$$

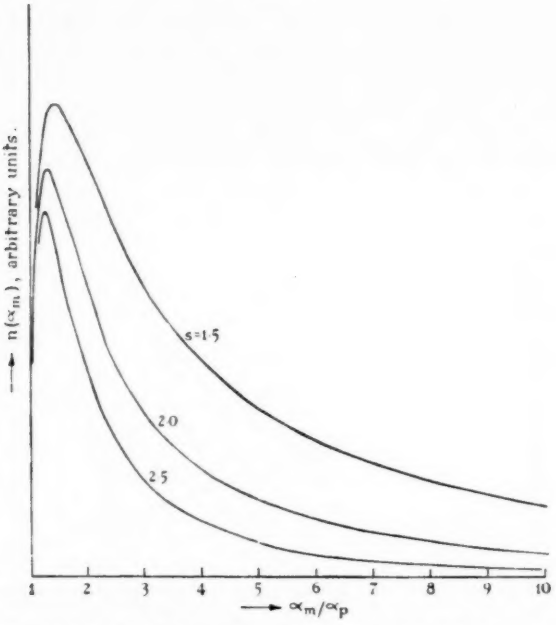

FIG. 11.—*Differential distribution in maximum electron line density of observed meteors for an incident distribution satisfying an inverse power law with exponent s.*

8. *Discussion.*—A number of approximations have been made in order to secure the simplest procedure for deducing the incident flux of meteoroids from the observed radio-echo rates. To whatever extent this may limit the absolute accuracy of the result, the above treatment should prove of considerable value for comparison of the incident fluxes and magnitude distributions in the various meteor showers.

Errors will clearly result if the ablation process deviates from the theoretical model; for instance if the phenomenon of fragmentation (**14**) is important for the faint radio-meteors the factor *HI* in the echo rate equations will be an overestimate. Rapid diffusion of meteor trails will limit the height to which they can be observed, particularly on short wave-lengths, while on longer wave-lengths

($\lambda > 15$m) ionospheric D-region absorption and Faraday rotation may at times have a significant effect on the rate (Baldwin and Kaiser (unpublished) have observed a marked decrease in the echo rate on 17 Mc/s associated with a short-wave radio fade-out). The effects of rapid diffusion will be most marked for fast meteors (which tend to ionize at greater heights) and for showers with values of s markedly less than 2, when the theory predicts a substantial proportion of echoes from meteors considerably brighter than the threshold for detection (and which may therefore be seen to greater heights).

Deviation of the distribution of maximum line densities from the simple power law with constant exponent s will lead to error since it was shown in Section 7 that only in this case does the echo rate have the same functional dependence as Θ on α_p. Observations of sporadic meteors made at Sheffield (unpublished) give s near to 2·0 down to 11th radio magnitude, with no significant seasonal or diurnal variation. However, considerable deviations from a power law are found in the case of a number of meteor showers. In these cases the exponent deduced from the variation of echo rate with equipment sensitivity (or from the echo amplitude distribution) will be close to the true value only if s varies sufficiently slowly with α_z, this condition being more stringent the smaller the value of s. In fact, provided s is not too small, most observed meteors will have magnitudes near to the limit of detection in which case the threshold value of s may be used in the echo rate equations without serious error.

It has been assumed that the echoes all originate in a narrow band about a mean height $\bar{h}$ (which will tend to be higher the larger the meteor velocity and the more sensitive the apparatus) and that the limiting sensitivity is constant across this band. In fact the minimum detectable line density will tend to increase with height across the echo band (due to increased range) and this will again cause the present theory slightly to overestimate the echo rate. The representation of the echo band by a mean echo line on a constant height surface introduces an additional limitation since the echoes corresponding to the point P on this line will actually be spread in range over an interval ΔR where

$$\Delta R \sim HI(\sin\phi)^{-1} \simeq HI(\sin^2\phi_0 + 2h/R_E)^{-1/2}.$$

This will not be serious provided (*a*) the sensitivity factor ρ does not vary substantially over the range interval ΔR and (*b*) that if χ_0 approaches ϕ_0 the range interval within which the echoes are counted is at least a few times ΔR.

It has been further supposed that the shower has a well defined point radiant. A spread in the radiant will not be serious provided it is reasonably small compared with the aerial beam width, except when χ_0 approaches ϕ_0 when the range interval needs to be large enough to encompass any additional range spread due to the finite radiant area.

A final difficulty can arise in subtracting the sporadic rate from the total in order to obtain the shower rate. Since s is generally smaller for shower than for sporadic meteors the ratio (shower rate : sporadic rate) decreases with increasing equipment sensitivity (increasing total rate) until eventually the shower may be scarcely observed against the sporadic background. In these cases it may be difficult to estimate shower rates unless some method for selecting shower meteors (e.g. by velocity) is used to distinguish them from the background.

Appendix

(i) *Transformation of the radiant coordinates.*

Let

l = latitude of observer,

δ = radiant declination,

T = radiant hour angle,

φ_r = radiant azimuth (E of N),

χ_0 = radiant zenith distance.

A convenient form for the solution to the astronomical triangle is

$$f(\chi_0) - \sin\chi_0(1-\cos\varphi_r) = f(\delta - l) \tag{26}$$

where

$$f(x) = \sin x + \tan l \cos x.$$

Given the latitude l, $f(x)$ may be presented in tabular or graphical form and used to evaluate δ for any given χ_0, φ_r. The hour angle can then be obtained from either of the relations

$$\sin T = -\frac{\sin\chi_0 \sin\varphi_r}{\cos\delta} \tag{27}$$

or

$$\cos T = \frac{\cos\chi_0 - \sin l \sin\delta}{\cos l \cos\delta}. \tag{28}$$

(ii) *Equations for the echo line*

If ϕ_0, φ are the elevation and azimuth from O of the point P on the echo line (Fig. 1) then it can be shown that

$$\tan\phi_0 = -\tan\chi_0 \cos(\varphi_r - \varphi). \tag{29}$$

The slant range R and the curved distance R_s (see Fig. 12) are related to ϕ_0 through

$$R \simeq R_E\left(\sqrt{\sin^2\phi_0 + \frac{2\bar{h}}{R_E}} - \sin\phi_0\right) \tag{30}$$

and

$$R_s \simeq R\cos\phi_0 \tag{31}$$

where R_E is the Earth's radius.

Equations (29), (30), (31) give the coordinates (R_s, φ) of the point P on the echo line for any given zenith distance χ_0. They have been used for the construction of Fig. 3.

(iii) *Equations for the curves of Fig.* 5

We wish to determine the radiant hour angle when the echo line corresponding to a radiant at declination δ intersects a point on the echo surface at azimuth φ and slant range R. R is related to ϕ_0 by (30) and φ is obtained as a function of ϕ_0 from (29). δ is then obtained as a function of T through the procedure in (i) (note that $\chi_0 \geqslant \phi_0$).

(iv) *Relations between* ϕ, ϕ_0, χ, χ_0, θ (*see Sections* 4, 5)

Consider the triangle OPC (Fig. 12) where C is the centre of the Earth. It will be recalled that ϕ is the elevation of OP above the horizontal at P, thus the angle OPC is equal to $\pi/2-\phi$ and we obtain

$$\frac{\cos\phi_0}{\cos\phi} = 1 + \frac{h}{R_E} \simeq 1 \tag{32}$$

from which it follows that

$$\sin^2\phi \simeq \sin^2\phi_0 + \frac{2h}{R_E}. \tag{33}$$

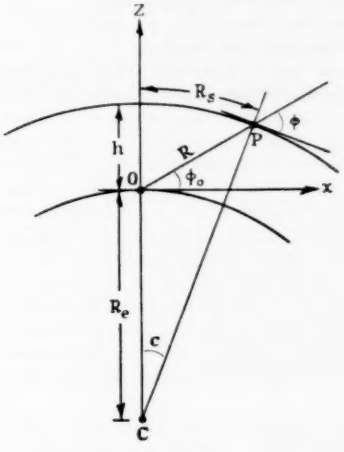

FIG. 12

In the right-handed coordinate system Oxz of Fig. 12, let the radiant have direction cosines (l, m, n) where $n = \cos\chi_0$. The direction cosines of OP and CP are $(\cos\phi_0, 0, \sin\phi_0)$ and $(\sin c, 0, \cos c)$ respectively. Now χ is the radiant zenith distance at P, hence

$$\cos\chi = l\sin c + \cos\chi_0\cos c$$

and since the radiant direction is normal to OP,

$$0 = l\cos\phi_0 + \cos\chi_0\sin\phi_0.$$

Eliminating l from the above two equations, and putting $\phi = \phi_0 + c$, we get

$$\left.\begin{aligned} &\frac{\cos\chi_0}{\cos\chi} = \frac{\cos\phi_0}{\cos\phi} = 1 + \frac{h}{R_E} \simeq 1 \\ \text{and}\quad &\sin^2\chi \simeq \sin^2\chi_0 + \frac{2h}{R_E}. \end{aligned}\right\} \tag{34}$$

Referring to Fig. 1 we see that $\sin\chi\cos\theta = \sin\phi$, whence, using (34), we obtain

$$\sin\chi\sin\theta = \left(1 + \frac{h}{R_E}\right)^{-1}\sqrt{(\sin^2\chi_0 - \sin^2\phi_0)}. \tag{35}$$

The University,
Sheffield:
1960 *April.*

References

(1) Kaiser, T. R., *M.N.*, **114**, 39, 1954.
(2) Kaiser, T. R., *M.N.*, **114**, 52, 1954.
(3) Evans, S., *M.N.*, **114**, 63, 1954.
(4) Weiss, A. A., *Aust. J. Phys.*, **12**, 54, 1959.
(5) Kaiser, T. R., *Adv. Phys.* (*Phil. Mag. Supp.*), **2**, 495, 1953.
(6) Kaiser, T. R., " Meteors " ed. T. R. Kaiser (Pergamon Press: London), p. 119, 1955.
(7) Clegg, J. A., *Phil. Mag.*, **34**, 577, 1948.
(8) Keay, C. S. L., *Aust. J. Phys.*, **10**, 471, 1957.
(9) Kaiser, T. R., and Closs, R. L., *Phil. Mag.*, **43**, 1, 1952.
(10) Kaiser, T. R., " Meteors " ed. T. R. Kaiser (Pergamon Press: London), p. 55, 1955.
(11) Manning, L. A., *J. Atmos. Terr. Phys.*, **4**, 219, 1953.
(12) Herlofson, N., *Phys. Soc. Rep. Prog. Phys.*, **11**, 444, 1948.
(13) Weiss, A. A., *Aust. J. Phys.*, **11**, 591, 1958.
(14) Jacchia, L. G., " Meteors " ed. T. R. Kaiser (Pergamon Press: London), p. 36, 1955.
(15) Browne, I. C., Bullough, K., Evans, S., and Kaiser, T. R., *Proc. Phys. Soc.*, B **69**, 83, 1956.

OSCILLATOR STRENGTHS OF NEUTRAL ATOMS OF THE IRON-GROUP

C. W. Allen

(Received 1960 May 11)

Summary

Measurements from various sources of the relative oscillator strengths of multiplets in Sc, Ti, V, Cr, Mn, Fe, Co, Ni have all been reduced to a consistent absolute scale. This makes it possible to compare experimental accuracy, make certain corrections, and tabulate mean measurements. The measurements are then compared with calculations based mainly on an elaboration of the *f*-sum rule. The character of the results differs for three sets of multiplets as follows:—

(*a*) For the transition types A, E, F, G, H, which involve non-equivalent electrons only, the log (observed/calculated) intensity is almost independent of excitation potential or wave-length. The scatter is probably due to unsuitability of the designations or to the interaction of terms. When absolute *f*-value measurements (for Cr, Mn, Fe, Co, Ni only) are used to convert these multiplets to a measured absolute scale, all atoms are within a factor 3 of the calculated scale. The high (obs./calc.) value in Mn is discussed. There is only a small systematic difference between observation and calculation.

(*b*) For the transition types B, C, which involve equivalent electrons, the scatter of the results is much larger. Multiplets with an upper excitation potential less than 4 eV have *f*-values below the calculations, while above 4 eV values agree with the calculated absolute scale.

(*c*) Measured values of multiplets violating *LS*-coupling vary erratically between zero and an empirically calculated value.

Recommended corrections for putting the mean values onto the best absolute scale are given.

---

1. *Introduction.*—The atoms that give rise to the greatest number of absorption lines in stellar spectra are mainly in the first long period of the elements. Of these, Sc, Ti, V, Cr, Mn, Fe, Co, and Ni have rather similar spectroscopic properties typified by their most abundant member Fe. They may be called the iron-group atoms. Since these elements have such rich spectra the oscillator strengths of their lines are in strong demand for astrophysical analysis. Unfortunately oscillator strength measurements of these atoms on an absolute scale are attended by considerable difficulty and possible error. Moreover the atoms are too complex to allow reliable calculations. Both measurements and calculations are being used and it is not certain which gives the best absolute values.

The object of the present work is to compare the experimental and calculated oscillator strengths in the iron-group atoms. We thus obtain an indication of what regularities and general trends occur and what values are reliable.

Although measurements and calculations may be applied to individual spectrum lines the number of lines concerned is too great for convenient tabulation and analysis. The situation may be relieved by using data for complete multiplets only. The values of the weighted oscillator strengths gf, where g is the statistical weight and f the oscillator strength, may readily be added within each multiplet to give the weighted oscillator strength of the multiplet g_tf. The subscript t implies that the values refer to complete terms and multiplets, not levels and lines. The symbol g_tf must refer to the multiplet as a whole since f is not the same for each line. When summing gf to give g_tf an allowance can be made for missing or unreliable lines by using the rules for intensities of lines within multiplets (Condon and Shortley 1935, p. 241; Allen 1955, p. 55). Usually the best measured or calculated lines are the strong ones and the contribution from the rest of the multiplet does not give rise to much ambiguity. If the intensity rules do not apply, as for multiplets forbidden in *LS*-coupling, the eye estimates of intensity in the Revised Multiplet Table (Moore 1945) usually lead to a suitable estimate of the conversion from gf to g_tf. In the present paper all values are expressed as g_tf or $\log g_tf$.

2. *Measurements.*—Some relative oscillator strength measurements have been made for all of the eight iron-group atoms. There are satisfactory absolute measurements in Cr, Mn, and Fe, and also some absolute values have been obtained for Co and Ni by quantitative comparisons made in arc spectra of diluted copper alloys. Only relative values are available for Sc, Ti, and V.

In order to compare and average the experimental relative g_tf values it is important that they should be systematically reduced to the same scale. The ideal would be to convert them all to an experimental absolute scale, but for some atoms no absolute values exist and for the others the absolute values are likely to change as better measurements become available. In order to achieve some stability and consistency I have converted all the *measured relative* values to a *calculated absolute* scale. Simple methods of obtaining calculated values are given in Section 3.

First the experimental values have been converted to $\log g_tf$ in the units of the published experimental work. Where the results are quoted as intensity I the value used is $\lambda^3 I$ with λ in microns, or where transition probability A is quoted we use $\lambda^2 gA$. Sometimes a Boltzmann factor or a correction to a Boltzmann factor has been applied. A reduction factor has then been found by plotting experimental against calculated values. In doing so, greater weight was given to the higher values of g_tf and to the types of transition found to give more regular results (see Section 4). The reduction factors and any Boltzmann corrections or factors are given in Tables I and II.

Both measured and calculated values of g_tf are set out in Table I. The columns are: the Multiplet Number from the "Revised Multiplet Table" (Moore 1945); the designations of the lower and upper terms from "Atomic Energy Levels" (Moore 1949, 1952); the type of transition using the notation of Section 3; the lower and upper excitation potentials; the wave-lengths λ of the leading lines; relative measurements of $\log g_tf$ reduced to a calculated absolute scale (the asterisk * implies a temperature adjustment has been made); mean values of $\log g_tf$ on the same scale (the experimental results have been used almost entirely but a little weight has been given to calculated values in a

few cases where this seemed appropriate); calculated values of $\log g_i f$ from the f-sum rule (Section 3); and calculated values from the Bates-Damgaard (1949) procedure. Except for a possible absolute scale adjustment the "mean" column is intended as the best available estimate of true $\log g_i f$.

Sources of experimental values for various atoms and the author abbreviations are as follows:—

KK	King and King (1938)	Ti, Fe
King	King (1947, 1948)	V, Ni
HK	Hill and King (1951)	Cr
KPDO	King, Parnes, Davis and Olsen (1955)	Co
OPP	Ostrovsky, Parchevsky and Penkin (1956)	Ti, Mn
OP	Ostrovsky and Penkin (1957a, 1957b)	Cr, Sc
Ost	Ostrovsky (1958)	V, Co
AA	Allen and Asaad (1957)	Cr, Mn, Fe, Co, Ni
Mit	Mitrofanova (1952, 1954, 1955, 1958)	Fe, Cr, Ti, Sc
vSS	van Stekelenburg and Smit (1948)	Ti
AHB	Aarts, Harting and Bakker (1954)	Fe
Car	Carter (1949)	Fe
vD	van Driel (1935). Data from King (1948)	Ni
OB	Ornstein and Bouma (1930)	Co, Ni
HD	Heid and Dieke (1954)	Ni

The more accurate and reliable values of $\log g_i f$ are quoted to two places of decimals. For the "mean" column, reliability is determined by interagreement of experimental results or agreement with calculations.

All measurements of oscillator strengths require a Boltzmann factor to allow for the declining population of higher levels. The factor may be very large and may cause serious error if the excitation temperature T is not well determined. The factor is usually applied in the form

$$\log g_i f \text{ (final)} = \log g_i f \text{ (as measured)} + E(5040/T)$$

where E is excitation potential in volts. If the experimentally determined $(5040/T)$ is unsuitable the final $\log g_i f$ results require a correction $E\,\Delta(5040/T)$. Corrections have been made for some atoms (labelled *) in Table I. In order to keep the temperature correction and scale correction as independent as possible the temperature correction has been pivoted on a representative excitation potential for which we adopt 1 volt for E_1 (lower E.P.) or 4 volts for E_2 (upper E.P.). Thus the corrections to $\log g_i f$ are

for absorption lines $\quad \Delta(5040/T)(E_1 - 1{\cdot}0)$,

for emission lines $\quad \Delta(5040/T)(E_2 - 4{\cdot}0)$.

TABLE I

Mult. No.	Terms	Transition	E.P. Volts	λ A	log $g_t f$ measured: Individual observers OP	Mit	Mean	log $g_t f$ calculated: f-sum	B.D.
Sc	($n=2$)				−4·48	−3·3			
1	a^3D–z^4F^0	Bic	0·0–2·0	6362	−2·13		−2·1	<0·4	
2	z^3D^0	B1	2·0	6305	−1·19		−1·2	+0·07	+0·10
3	z^4D^0	Bic	2·0	6231	−1·63		−1·6	<0·4	
5	z^2F^0	B1	2·6	4779	−1·58	−1·2	−1·5	+0·20	+0·24
6	y^3P^0	B3	3·0	4082	−0·49	−0·6	−0·51	+0·32	+0·35
7	y^3D^0	B3	3·1	4023	−0·72	−0·4	−0·65	+0·55	+0·57
8	y^3F^0	B3	3·2	3911	−0·61	−0·3	−0·55	+0·69	+0·72
9	x^3P^0	dj	3·8	3273	+0·19		+0·2	<0·4	
10	x^3F^0	dj	4·1	3019	−0·03		0·0	<0·4	
12	a^4F–z^4G^0	A	1·4–3·6	5671	+0·84	+1·1	+0·89	+0·93	+1·04
14	y^4D^0	A	4·0	4743	+0·85	+0·4	+0·75	+0·67	+0·83
15	a^2F–z^2G^0	A	1·9–4·1	5520	+0·56		+0·58	+0·63	+0·78
16	x^2F^0	A	4·1	5481	+0·62		+0·59	+0·52	+0·68
Ti	($n=3$)				KK	OPP	vSS	Mit	
					−3·22	−4·15	−1·24	−3·1	
3	a^3F–z^5D^0	Bic	0·0–2·3	5460	−2·23				−2·2	<0·7	
4	z^3F^0	B2	2·4	5210	−0·44	−0·48	−0·49	−0·6	−0·46	+0·52	+0·40
5	z^3D^0	B2	2·5	5064	−0·61	−0·55		−0·4	−0·56	+0·37	+0·26
6	z^3G^0	B2	2·7	4681	−0·71	−0·76	−0·73	−0·8	−0·74	+0·62	+0·57
7	z^1D^0	Bic	2·7	4562	−2·55				−2·5	<0·7	
9	z^1G^0	Bic	3·0	4112	−1·61			−1·4	−1·55	<0·7	
11	z^5S^0	Bic	3·1	4009	−1·18	−1·22			−1·20	<0·7	
12	y^3F^0	B4	3·1	3998	+0·38	+0·21	+0·38	−0·2	+0·32	+0·81	+0·87
13	y^3D^0	B4	3·2	3958	+0·22	+0·05			+0·16	+0·67	+0·74
14	z^3P^0	Bip	3·2	3947	−0·89	−0·96		−0·6	−0·90	<0·7	
15	y^5D^0	Bic	3·2	3914	−0·92			−0·7	−0·89	<0·7	

17	x^3F^0	dj	3·3	3752	+0·33	+0·25	+0·33	−0·3	+0·29	<0·7	
18	x^3D^0	dj	3·4	3689	−0·93	−0·83			−0·89	<0·7	
19	y^3G^0	dj	3·4	3653	+0·55	+0·44	+0·56		+0·52	<0·7	
20	z^3P^0	Bip	3·4	3635	−1·62				−1·6	<0·7	
21	y^1D^0	Bip	3·4	3604	−2·25				−2·2	<0·7	
22	y^3F^0	dj	3·6	3506	−1·76	−1·7			−1·71	<0·7	
23	w^3D^0	Bip	3·7	3385	+0·17	+0·09	+0·18		+0·16	<0·7	
24	x^3G^0	B4	3·7	3371	+0·47	+0·36	+0·47		+0·43	+0·92	+1·00
25	x^3D^0	dj	3·7	3369	−0·39				−0·4	<0·7	
26	v^3D^0	Bip	3·8	3243	−1·48				−1·5	<0·7	
27	w^3G^0	Bip	3·9	3199	+0·53	+0·41	+0·51		+0·49	<0·7	
35	$a^5F-y^5F^0$	Cic	0·8–3·1	5361	−1·85				−1·8	<0·9	
37		C	3·2	5238	−1·28				−1·3	+0·7	
38	y^5G^0	A	3·3	4981	+1·04	+1·23	+1·05	+0·4	+1·08	+1·02	+1·05
42	y^5F^0	A	3·6	4533	+1·02		+1·03	+0·4	+1·00	+0·91	+1·03
43	w^3D^0	Cic	3·7	4314	−0·16			−0·7	−0·2	<0·9	
44	x^5D^0	A	3·7	4305	+0·75			+0·2	+0·72	+0·76	+0·90
48	$a^1D-z^1D^0$	Bip	0·9–2·7	6743	−1·54				−1·5	<0·1	
49	z^1F^0	Bip	2·8	6599	−2·04				−2·0	<0·1	
53	y^1D^0	B2	3·4	4840	−0·56			−0·9	−0·60	+0·37	+0·40
56	y^1F^0	B2	4·1	3904	+0·14	+0·29			+0·28	+0·51	+0·72
57	z^1P^0	B2	4·2	3786	−0·06	+0·09			+0·08	+0·15	+0·36
58	y^1P^0	Bip	4·3	3610	−0·29				−0·3	<0·1	
61	v^3G^0	dj	4·6	3299	−0·8				−0·8	<0·1	
62	x^1F^0	Bip	4·6	3292	−0·19				−0·2	<0·1	
66	x^1P^0	dj	4·8	3141	−0·58				−0·6	<0·1	
67	w^1D^0	dj	4·8	3123	−0·48				−0·5	<0·1	
69	$a^3P-z^3S^0$	B4	1·1–3·1	6126	−0·93				−0·9	−0·03	−0·17
71	z^3P^0	B4	3·2	5918	−1·01				−1·0	+0·45	+0·33
72	y^3D^0	Bip	3·2	5866	−0·42				−0·4	<0·3	
74	x^3D^0	dj	3·4	5295	−0·95				−0·9	<0·3	
75	w^5D^0	B4	3·7	4691	−0·45			−0·1	−0·40	+0·67	+0·75
77	x^5D^0	dj	3·7	4675	−1·4				−1·4	<0·3	
80	x^3P^0	B2	4·1	4078	+0·22			+0·2	+0·21	+0·15	+0·21
83	y^3S^0	B2	4·4	3725	+0·07			0·0	+0·05	−0·33	−0·18

TABLE I (*continued*)

Mult. No.	Terms	Transition	E.P. Volts	λ A	log $g_t f$ measured: Individual observers KK	OPP	vSS	Mit	Mean	log $g_t f$ calculated: f-sum	B.D.
Ti	($n=3$)				−3·22	−4·15	−1·24	−3·1			
84	a^3P–w^3P^0	dj	1·1–4·6	3480	−0·10				−0·1	<0·3	
86	u^3D^0	B2	4·7	3382	0·00				0·0	+0·37	+0·60
87	t^3D^0	dj	4·8	3314	+0·50				+0·5	<0·3	
90	s^3D^0	dj	4·9	3213	−0·17				−0·2	<0·3	
102	b^3F–x^3F^0	A	1·4–3·3	6556	−0·56				−0·5	+0·69	+0·72
104	y^3G^0	A	3·4	6258	+0·13				+0·2	+0·80	+0·84
106	w^3D^0	C	3·7	5512	+0·23				+0·3	+0·5	
107	x^5D^0	Aic	3·7	5449	−0·71				−0·7	<0·7	
108	x^3G^0	C	3·7	5474	−0·68				−0·7	−0·1	
109	v^3D^0	C	3·8	5145	−0·05			+0·5	0·0	+0·5	
110	w^3G^0	C	3·9	5035	+0·58			+0·5	+0·56	−0·1	
113	v^3F^0	C	4·2	4457				+0·9	+0·9	+0·5	
129	a^1G–y^1G^0	B2	1·5–4·4	4186				+0·2	+0·2	+0·62	
130	x^1F^0	B2	4·6	3919				−1·3	−1·3	+0·51	
131	x^1G^0	dj	4·8	3724	+0·31			−0·5	+0·3	<0·3	
145	a^5P–w^5D^0	A	1·7–4·4	4617	+0·78			+0·8	+0·78	+0·76	+0·85
146	y^5P^0	A	4·5	4481	+0·77			+0·7	+0·73	+0·54	+0·63
154	a^3G–z^3H^0	C	1·9–3·9	5953	+0·26				+0·2	−0·46	
156	v^3F^0	C	4·2	5265	+0·27				+0·3	+0·6	
157	y^3H^0	A	4·4	4885	+0·72			+0·5	+0·72	+0·89	+0·96
160	v^3G^0	A	4·6	4449				+1·0	+1·0	+0·80	
162	t^3F^0	A	4·8	4263				+1·1	+1·0	+0·69	
179	z^5G^0–g^5G	J	2·0–5·8	3226	+1·54				+1·55	+1·66	
185	z^5F^0–e^5G	F	2·1–5·2	4030				+1·2	+1·2	+1·16	+0·96
188	e^5D	F	5·2	4003				+0·1	+0·2	+0·63	+0·42
218	b^3P–r^3D^0	A	2·2–5·0	4404				+0·6	+0·6	+0·54	
231	a^3H–z^3I^0	A	2·2–4·8	4856				+0·4	+0·6	+0·96	

233	x^3H^0	A	4·8	4759			+1·3	+1·1	+0·89	
235	u^3G^0	A	5·1	4318			+1·1	+1·0	+0·80	
240	$b^1G-y^1G^0$	C	2·3–4·4	5644	+0·30			+0·3	0·0	
252	$z^5D^0-c^5D$	F	2·3–5·2	4256			+0·7	+0·7	+0·93	+0·73
276	$a^1P-w^1P^0$	A	2·5–4·8	5206	+1·00			+1·0	−0·15	
283	$b^1D-w^1F^0$	A	2·5–5·0	4975			+0·6	+0·5	+0·21	
290	$a^1H-x^1H^0$	A	2·6–5·4	4369			+0·6	+0·6	+0·48	

V ($n=4$)

					King	Ost				
					−3·73	−4·73				
–	$a^4F-z^6G^0$	Bic	0·1–2·1	6109	−3·60			−3·6	<0·8	
1	z^6D^0	Bic	2·3	5632	−2·76			−2·8	<0·8	
2	z^6F^0	Bic	2·3	5515	−2·84			−2·8	<0·8	
3	z^4D^0	B_3	2·6	4881	−0·12	−0·22		−0·17	+0·54	+0·40
4	z^4G^0	B_3	2·7	4594	−0·15	−0·27		−0·21	+0·80	+0·71
5	z^4F^0	B_3	2·9	4352	−0·22	−0·36		−0·29	+0·69	+0·64
6	z^2D^0	Bic	2·9	4234	−1·65			−1·6	<0·8	
7	y^4F^0	dj	3·2	3902	+0·26	+0·21		+0·24	<0·8	
8	z^2G^0	Bic	3·2	3876	−0·50	−0·53		−0·52	<0·8	
9	y^4D^0	dj	3·3	3855	+0·42	+0·36		+0·39	<0·8	
10	y^6D^0	dj	3·3	3817	−1·50			−1·5	<0·8	
11	z^2F^0	Bic	3·4	3713	−2·23			−2·2	<0·8	
12	y^4G^0	Bip	3·8	3298	−0·65			−0·6	<0·8	
13	x^4F^0	Bip	3·9	3249	−1·55			−1·6	<0·8	
14	x^4G^0	B_5	3·9	3185	+0·96	+1·12		+1·04	+1·02	+1·20
15	x^4D^0		4·0	3091	−0·83	−0·7		−0·80		
16	z^2P^0	ic	4·0	3063	−0·93			−0·9		
17	w^4F^0	B_5	4·1	3066	+0·69	+0·81		+0·77	+0·91	+1·19
19	$a^6D-z^6D^0$	C	0·3–2·3	6243	−0·53			−0·5	+0·8	
20	z^6F^0	C	2·3	6150	−1·16			−1·2	+0·64	
21	z^6P^0	A	3·1	4460	+0·25	+0·28		+0·27	+0·62	+0·68
22	y^6F^0	A	3·1	4379	+1·21	+1·07		+1·12	+0·99	+1·06
23	z^4P^0	Aic	3·1	4381	−1·28			−1·3	<0·8	
24	y^4F^0	Aic	3·2	4209	−0·94			−0·9	<0·8	

TABLE I (*continued*)

Mult. No.	Terms	Transition	E.P. Volts	λ A	log $g_t f$ measured: Individual observers King	log $g_t f$ measured: Individual observers Ost	log $g_t f$ measured: Mean	log $g_t f$ calculated: f-sum	log $g_t f$ calculated: B.D.
V	(n=4)				−3·73	−4·73			
25	a^4D–z^2G^0	Cic	0·3–3·2	4179	−1·17		−1·2	<0·8	
26	y^4D^0	Aic	3·3	4136	−1·70		−1·7	<0·8	
27	y^6D^0	A	3·3	4111	+0·99	+0·94	+0·95	+0·85	+0·94
28	x^6D^0	C	3·5	3794	+0·18	+0·22	+0·20	+0·8	
29	y^6P^0	C	3·6	3703	+0·61	+0·71	+0·64	+0·62	
31	a^4D–z^4F^0	C	1·1–2·9	6753	−1·35		−1·4	+0·3	
33	y^6F^0	Aic	3·1	6097	−1·99		−2·0	<0·7	
34	z^4P^0	A	3·1	6090	+0·08		+0·1	+0·45	+0·48
35	y^4F^0	A	3·2	5727	+0·55		+0·6	+0·81	+0·87
36	z^2G^0	Cic	3·2	5670	−0·27		−0·3	<0·7	
37	y^4D^0	A	3·3	5627	+0·06		+0·1	+0·67	+0·73
38	y^6D^0	Aic	3·3	5547	−1·22		−1·2	<0·7	
39	y^4P^0	C	3·7	4670	−0·25		−0·2	+0·3	
40	x^4F^0	C	3·9	4423	−0·59		−0·6	+0·3	
41	w^4F^0	C	4·1	4090	+0·54	+0·76	+0·64	+0·3	
42	w^4D^0	C	4·2	3934	+0·39		+0·4	+0·5	
43	v^4F^0		4·3	3872	−0·33		−0·3		
44	v^4D^0	C	4·3	3840	+0·14		+0·2	+0·5	
45	x^4P^0	Aip	4·5	3583	−1·1		−1·1	<0·7	
46	t^4D^0	Aip	4·7	3400	−0·13		−0·1	<0·7	
48	a^4P–z^4P^0	dj	1·2–3·1	6531	−0·79		−0·8	<0·4	
49	y^4D^0	dj	3·3	6002	−1·50		−1·5	<0·4	
50	y^4P^0	B_3	3·7	4925	−0·39		−0·4	+0·33	+0·18
52	w^4D^0	B_3	4·2	4113	−0·16		−0·1	+0·55	+0·57
53	t^4D^0	dj	4·7	3533	+0·35		+0·3	<0·4	
54	w^4P^0	B_5	4·9	3377	+0·26		+0·3	+0·55	+0·85
55	x^4S^0	B_3	4·9	3329	−0·11		−0·13	−0·15	+0·08

56	v^4P^o		5·2	3106	+0·2		+0·2			
57	r^1D^o	B5	5·2	3083	+0·17		+0·2	+0·77	+1·12	
60	$a^3G-z^3F^o$	Bip	1·4–3·4	6106	−1·51		−1·5	<0·6		
62	y^2G^o		4·1	4501	−0·56		−0·6			
63	x^2G^o	dj	4·5	3930	+0·2		+0·2	<0·6		
64	w^4G^o	Bic	4·5	3886	−0·28		−0·3	<0·6		
66	x^2F^o		4·6	3871	+0·08		+0·1			
68	v^2G^o	dj	4·6	3806	−0·13		−0·1	<0·6		
69	w^2F^o	dj	4·6	3790	−0·30		−0·3	<0·6		
70	x^2H^o	dj	4·7	3686	−0·04		0·0	<0·6		
71	t^2G^o	B1	5·1	3284	−0·13		−0·1	+0·32	+0·38	
72	u^2F^o	Bip	5·2	3233	−0·16		−0·2	<0·6		
73	u^2H^o	B1	5·2	3212	+0·63		+0·6	+0·41	+0·49	
74	t^2F^o	B1	5·4	3050	−0·0		0·0	+0·21	+0·26	
77	$a^3P-z^3S^o$		1·7–3·9	5558	−0·87		−0·9			
82	$a^3D-y^3P^o$	B1	1·8–4·5	4537	−0·5		−0·5	−0·15		
84	$a^4H-y^4G^o$	C	1·9–3·8	6326	−0·27		−0·3	+0·9		
86	y^3H^o		4·6	4501	+0·5		+0·5			
87	z^4I^o	A	4·6	4452	+0·99		+1·02	+1·08	+1·16	
88	x^4H^o	A	4·7	4268	+1·08		+1·05	+1·01	+1·10	
89	u^4G^o	A	4·9	3998	+1·07		+1·04	+0·93	+1·03	
92	$b^4P-x^4D^o$		1·9–4·1	5772	−0·30		−0·3			
94	x^4P^o	A	4·5	4751	−0·29		−0·3	+0·45		
99	$a^2H-v^2G^o$	dj	1·9–4·6	4524	+0·16		+0·2	<0·7		
100	z^4I^o	dj	4·6	4515	−0·4		−0·4	<0·7		
101	z^2I^o	dj	4·6	4474	+0·38		+0·4	<0·7		
102	w^2F^o	dj	4·6	4468	−0·43		−0·4	<0·7		
103	x^2H^o	dj	4·7	4354	−0·09		−0·1	<0·7		
104	u^2H^o	Bip	5·2	3708	+0·31		−0·3	<0·7		
109	$b^4F-v^4G^o$	A	1·9–4·7	4545	+0·88		+0·89	+0·92	+0·98	
110	t^4D^o	A	4·7	4474	+0·69		+0·68	+0·67	+0·74	
111	u^4F^o	A	4·9	4232	+0·75		+0·77	+0·81	+0·90	
112	s^4D^o	Aip	4·9	4104	+1·0		+1·0	<0·8		
113	$z^4G^o-e^6F$	E	2·1–4·7	4807	+0·93		+0·9	+0·66	+0·49	
114	e^6H	F	5·5	3695	+1·53		+1·54	+1·57		

TABLE I (*continued*)

Mult. No.	Terms	Trans-ition	E.P. Volts	λ A	log $g_t f$ measured: Individual observers				Mean	log $g_t f$ calculated: f-sum	B.D.
	V ($n=4$)				King						
115	z^6G^0–f^6G	F	2·1–5·5	3676	−3·73						
118	a^4G–y^4H^0	C	2·1–4·6	4904	+0·79				+0·85	+1·02	
119	x^4H^0	Aip	4·7	4706	+0·1				+0·1	+0·2	
120	w^4H^0	A	5·0	4291	+0·17				+0·2	<0·9	
121	t^4G^0	A	5·2	4051	+0·96				+0·89	+1·01	+1·10
125	z^6F^0–e^6F	E	2·3–4·7	5193	+0·87				+0·98	+0·92	+1·03
127	b^2P–y^2P^0	C	2·4–4·5	5748	+0·73				+0·68	+0·56	+0·46
129	b^2H–v^2G^0	A	2·4–4·6	5487	+0·9				+0·9	−0·2	
130	z^2I^0	A	4·6	5415	+0·38				+0·45	+0·62	+0·68
131	x^2H^0	A	4·7	5240	+0·57				+0·62	+0·78	+0·85
135	a^2F–x^2G^0	A	2·4–4·5	5725	+0·65				+0·67	+0·71	+0·80
					+0·3				+0·4	+0·62	
	Cr ($n=5$)				HK*	OP	AA*	Mit*			
					−3·58	−0·18	+0·22	−3·3			
1	a^7S–z^7P^0	A	0·0–2·9	4254	+0·09	+0·20	+0·13		+0·14	+0·69	+0·74
2	z^5P^0	Aic	3·3	3732	−1·69		−2·0		−1·80	<0·2	
3	z^7D^0	Cml	3·4	3615	−2·29				−2·3	<0·2	
4	y^7P^0	C	3·4	3578	+0·62	+0·73	+0·36		+0·59	+0·74	
5	y^5P^0	Cic	3·7	3351	−1·85				−1·8	<0·2	
6	a^5S–z^7P^0	Aic	0·9–2·9	6330	−2·83				−2·9	<0·1	
7	z^5P^0	A	3·3	5208	+0·38	+0·46			+0·41	+0·54	+0·61
8	z^7D^0	Cic	3·4	5021	−2·18				−2·2	<0·1	
9	y^7P^0	Cic	3·4	4942	−1·90				−1·9	<0·1	
10	y^5P^0	C	3·7	4496	−0·72	−0·80	−0·64		−0·72	+0·2	
11	z^5D^0	Cml	4·2	3833	−2·19				−2·2	<0·1	
13	z^3D^0	Cic	4·8	3192	−1·62				−1·6	<0·1	

16	a^5D–z^7P^0	dj	1·0–2·9	6580	−2·71				−2·7	<0·8	
18	z^5P^0	dj	3·3	5409	−0·21	−0·17			−0·19	<0·8	
19	z^7D^0	Bic	3·4	5122	−2·26				−2·3	<0·8	
20	y^7P^0	Bic	3·4	5093	−2·15				−2·2	<0·8	
21	y^5P^0	B6	3·7	4646	−0·14	−0·23	0·0	−0·2	−0·15	+0·62	+0·69
22	z^5F^0	B6	3·9	4351	+0·17	+0·06	+0·17	−0·2	+0·12	+0·99	+1·09
23	z^5D^0	B6	4·2	3919	−0·02		+0·10	0·0	+0·02	+0·85	+1·03
24	z^3P^0	Bic	4·2	3831	−0·92		−1·20		−1·02	<0·8	
25	z^3D^0	Bic	4·8	3266	−0·91				−0·9	<0·8	
30	a^5G–x^5P^0	Cml	2·5–5·1	4872	−0·57				−0·6	<1·0	
31	y^5F^0	C	5·1	4789	+0·24				+0·2	+0·8	
32	z^5H^0	C	5·2	4571	+0·45		+0·2		+0·35	+0·6	
33	z^5G^0	A	5·3	4526	+1·07		+1·0		+1·04	+1·02	+1·03
34	x^5D^0	Cml	5·3	4466	−0·4				−0·4	<1·0	
35	y^5G^0	C	5·5	4126	+0·48			+0·3	+0·43	+0·8	
36	x^5F^0	C	5·6	4033	0·00				0·0	+0·8	
37	z^3H^0	Aic	5·6	4027	+0·25			+0·2	+0·24	<1·0	
38	y^5H^0	A	5·6	3963	+1·49		+1·66	+1·3	+1·52	+1·11	+1·05
40	w^5F^0	A	5·8	3817	+0·4		+0·5		+0·48	+0·91	+0·99
43	x^5G^0	C	5·8	3743	+1·48		+1·46		+1·47	+0·8	
46	v^5D^0	Aip	5·9	3656	+1·27				+1·3	<1·0	
47	u^5F^0	C	5·9	3639	+1·27		+1·00		+1·18	+0·8	
48	x^5H^0	C	5·9	3619	+0·4				+0·4	+0·6	
49	t^5F^0	C	5·9	3632	+0·94				+0·9	+0·8	
51	w^3G^0	Cic	6·1	3445	+1·21		+0·8		+1·08	<1·0	
52	w^5G^0	C	6·1	3433	+1·38		+1·3		+1·34	+0·8	
53	x^3F^0	Aip	6·1	3435	+0·45				+0·4	<1·0	
54	s^5F^0	C	6·2	3362	+0·99				+1·0	+0·8	
58	a^5P–y^5F^0	Cm	2·7–5·1	5225	−0·61				−0·6	<0·5	
59	x^5P^0	C	5·1	5206	−0·27				−0·3	+0·3	
60	y^5D^0	C	5·2	5013	−0·10				−0·1	+0·3	
62	z^5S^0	C	5·3	4697	−0·07				−0·1	+0·1	
63	w^5P^0	A	5·5	4459	+0·05				0·0	+0·54	+0·58
64	v^5P^0	C	5·6	4295	+0·44				+0·4	+0·3	
65	y^3D^0	Aic	5·7	4108	+0·22				+0·2	<0·5	

TABLE I (*continued*)

Mult. No.	Terms	Transition	E.P. Volts	λ A	log $g_i f$ measured				log $g_i f$ calculated	
					Individual observers			Mean	f-sum	B.D.
	Cr ($n=5$)				HK*	OP	AA*	Mit*		
					−3·58	−0·18	+0·22	−3·3		
66	a^5P–w^5D^0	A	2·7–5·7	4066	+0·23			+0·2	+0·21	+0·76	+0·84
67	u^5P^0	C	5·8	3992	+0·55		+0·5	+0·6	+0·54	+0·3	
69	v^5D^0	Aip	5·9	3841	+1·23		+1·21		+1·22	<0·5	
70	u^5F^0	Cml	5·9	3819	+0·54		+0·6		+0·56	<0·5	
71	t^5F^0	Cml	5·9	3815	+0·26		+0·2		+0·24	<0·5	
74	t^5P^0	Aip	6·1	3574	+1·10				+1·1	<0·5	
75	y^5S^0	A	6·2	3572	+0·79				+0·8	+0·07	+0·18
81	a^3P–y^3P^0	dj	2·9–5·6	4619	+0·38				+0·4	<0·3	
82	y^3D^0	dj	5·7	4527	−0·14				−0·1	<0·3	
83	w^5D^0	dj	5·7	4491	+0·22				+0·2	<0·3	
84	u^5P^0	Bic	5·8	4387	+0·1				+0·1	<0·3	
93	z^7P^0–e^7S	G	2·9–4·6	7462	−0·27				−0·3	+0·25	+0·24
94	e^7D	H	5·2	5328	+0·97				+1·0	+1·25	+1·09
95	f^7S	Gh	5·6	4514	+0·18				+0·2		−0·62
96	f^7D	dj	5·8	4261	+0·45				+0·4	<0·7	
97	g^7D	Hh	5·9	4129	+0·97				+1·0		+0·42
99	a^3H–z^3H^0	dj	3·0–5·6	4727	+0·48				+0·5	<0·9	
100	y^3F^0	dj	5·7	4543	−0·1				−0·1	<0·9	
102	w^5F^0	dj	5·8	4442	−0·07				−0·1	<0·9	
103	z^3G^0	B4	5·8	4387	+0·39			+0·4	+0·39	+0·92	
104	y^3G^0	dj	5·8	4374	+0·59			+0·6	+0·59	<0·9	
105	z^3I^0	B4	5·9	4255	+0·22				+0·2	+1·08	
106	x^5H^0	Bic	5·9	4175	+0·7			+1·0	+0·75	<0·9	
108	y^3H^0	B4	6·0	4123	+0·18			+0·3	+0·21	+1·01	
125	b^5D–y^3D^0	Aic	3·0–5·7	4566	+0·2				+0·2	<0·8	
126	w^5D^0	Aip	5·7	4515	+0·19				+0·2	<0·8	

127	w^5F^o	Aip	5·8	4458	+0·52			+0·5		<0·8	
128	z^3G^o	Cml	5·8	4403	+0·1			+0·1		<0·8	
129	u^3P^o	C	5·8	4424	+0·76			+0·8		+0·4	
131	v^3D^o	A	5·9	4238	+0·25			+0·3		+0·76	+0·81
132	u^3F^o	C	5·9	4217	+0·56		+0·7	+0·60		+0·4	
133	t^5F^o	C	5·9	4211	+0·29			+0·30		+0·4	
134	w^3G^o	Cml	6·1	3945	−0·4			−0·4		<0·8	
135	x^3F^o	Aic	6·1	3945	−0·1			−0·1		<0·8	
136	t^3P^o	A	6·1	3915	+0·60			+0·60		+0·54	+0·63
138	s^5F^o	C	6·2	3849	+1·24			+1·2		+0·4	
139	u^5D^o	C	6·2	3804		+1·40		+1·4		+0·5	
143	a^3G–z^3H^o	A	3·1–5·6	4922	+0·68			+0·70		+0·89	+0·94
145	y^3F^o	A	5·7	4756	+0·89		+1·1	+0·95		+0·69	+0·76
146	y^3D^o	Aip	5·7	4698	−0·4			−0·4		<0·8	
147	w^5D^o	Aic	5·7	4656	+0·2			+0·2		<0·8	
150	y^5G^o	A	5·8	4540	+0·72			+0·74		+0·80	+0·90
154	y^3H^o	C	6·0	4271	+0·1			+0·1		+0·3	
155	x^5G^o	C	6·0	4209	+0·3			+0·3		+0·6	
166	a^3F–z^3H^o	dj	3·1–5·6	4954	+0·2			+0·2		<0·7	
171	w^5F^o	dj	5·8	4640	0·0			0·0		<0·7	
179	x^5D^o	B4	6·1	4142	+0·50			+0·5		+0·67	+0·61
186	z^7F^o–f^7D	E	3·1–5·8	4718	+1·27		+1·4	+1·30		+0·62	+0·42
191	b^5P–y^5P^o	A	3·3–5·6	5400	−0·06			−0·1		+0·32	+0·34
193	w^5D^o	Aic	5·7	5221	+0·5			+0·5		<0·3	
197	y^5S^o	A	6·1	4492	+0·42			+0·4		−0·15	−0·04
201	z^7D^o–f^7D	E	3·4–5·8	5224	+1·32			+1·3		+0·47	+0·38
207	b^3G–y^3G^o	dj	3·4–5·8	5196	+0·41			+0·4		<0·8	
225	y^7P^o–f^7D	E	3·4–5·8	5255	+0·60			+0·6		+0·25	+0·21
234	a^3D–w^3P^o	A	3·5–6·3	4413			+1·0	+1·0		+0·32	
248	a^3I–w^3H^o	C	3·8–6·8	4193			+0·6	+0·6		+0·8	
268	a^5F–y^5G^o	A	3·9–6·9	3989			+1·0	+1·0		+1·02	
293	c^3D–y^5G^o	dj	4·2–6·9	4488			+1·2	+1·2		<0·5	
305	b^3H–w^3I^o	A	4·4–7·4	4161			+0·8	+0·8		+0·96	

TABLE I (*continued*)

Mult. No.	Terms	Transition	E.P. Volts	λ A	log $g_t f$ measured: Individual observers					Mean	log $g_t f$ calculated: f-sum	B.D.
					AA	OPP						
Mn	($n=6$)				−0·32	−0·42						
1	a^6S–z^8P^0	Bic	0·0–2·3	5394		−3·70				−3·7	<0·1	
2	z^6P^0	B7	3·1	4030	−0·56	−0·53				−0·54	+0·69	+0·68
3	z^4P^0	Bic	3·8	3224		−2·73				−2·7	<0·1	
–	y^6P^0	B5	4·4	2795		+0·47				+0·49	+0·54	
5	a^6D–z^6D^0	A	2·1–5·2	4041	+0·92					+0·90	+0·85	+0·88
6	z^6F^0	A	5·4	3806	+1·02					+1·01	+0·99	+1·05
8	x^6P^0	A	5·6	3577	+0·85					+0·80	+0·62	+0·69
16	z^8P^0–e^8S	E	2·3–4·9	4823	+0·23					+0·25	+0·31	+0·09
18	e^8D	F	5·8	3569	+1·31					+1·31	+1·31	+1·05
21	a^4D–z^4F^0	A	2·9–5·5	4762	+0·73					+0·75	+0·81	
22	z^4D^0	A	5·7	4451	+0·72					+0·71	+0·67	+0·78
Fe	($n=7$)				KK	AA*	AHB	Car	Mit*			
					−3·38	−0·10	−3·45	−3·65	−3·9			
1	a^5D–z^7D^0	Bic	0·0–2·4	5166	−3·1		−3·07			−3·08	<0·8	
2	z^7F^0	Bic	2·8	4375	−2·21		−2·27		−2·4	−2·26	<0·8	
3	z^7P^0	Bic	3·0	4216	−2·85		−2·93		−2·5	−2·86	<0·8	
4	z^5D^0	B6	3·2	3859	−0·31	−0·26	−0·43		−1·4	−0·34	+0·85	+0·80
5	z^5F^0	B6	3·4	3719	−0·09	−0·10				−0·10	+0·99	+0·97
6	z^5P^0	B6	3·6	3440	−0·6	−0·53				−0·58	+0·62	+0·65
7	z^3F^0	Bic	3·9	3193	−1·80					−1·8	<0·8	
8	z^3D^0	Bic	3·9	3191	−2·01					−2·0	<0·8	
9	y^5D^0	dj	4·1	3020	−0·68					−0·7	<0·8	
10	y^5F^0	dj	4·2	2966	−0·92					−0·9	<0·8	
11	z^3P^0	Bic	4·2	2981	−1·73					−1·7	<0·8	
15	a^5F–z^5D^0	C	0·9–3·2	5269	−0·61	−0·74	−0·62			−0·66	+0·7	

16	z^5F^0	C	3·4	5012	−1·8		−1·74			−1·77	+0·7		
20	y^5D^0	A	4·1	3820	+0·62	+0·65	+0·66			+0·64	+0·76	+0·81	
21	y^5F^0	A	4·2	3734	+0·92	+0·85				+0·89	+0·91	+0·96	
22	z^3P^0	Cic	4·2	3812	−0·61	−0·64				−0·63	<0·9		
23	z^5G^0	A	4·4	3581	+0·96	+0·88				+0·93	+1·02	+1·09	
24	z^3G^0	Aic	4·4	3513	+0·39	+0·40				+0·39	<0·9		
25	y^3F^0	Aic	4·6	3359	−1·4					−1·4	<0·9		
28	x^5D^0	C	4·9	3057	+0·23					+0·2	+0·7		
30	x^5F^0	C	5·0	2999	+0·06					+0·1	+0·7		
36	a^3F–z^3F^0	C	1·5–3·9	5171	−1·0		−1·3	−1·3		−1·2	+0·5		
37	z^3D^0	C	3·9	5167	−0·53		−0·52			−0·52	+0·5		
39	y^5F^0	Aic	4·2	4602	−0·9		−1·43	−1·2	−0·8	−1·05	<0·7		
41	z^5G^0	Aic	4·4	4383	+0·64	+0·63	+0·75		−0·3	+0·65	<0·7		
42	z^3G^0	A	4·4	4271	+0·67	+0·65	+0·73		−0·3	+0·68	+0·80	+0·86	
43	y^3F^0	A	4·6	4045	+0·86	+0·84	+0·85		+0·3	+0·84	+0·69	+0·78	
45	y^3D^0	A	4·8	3815	+0·86	+0·83	+0·66			+0·77	+0·54	+0·65	
66	a^5P–y^5P^0	C	2·2–4·6	5202				−0·98		−1·0	+0·5		
68	x^5D^0	C	5·0	4528				+0·14	+0·3	+0·20	+0·5		
71	z^5S^0	C	5·0	4282				0·0	0·0	0·0	0·0		
152	z^7D^0–e^7D	E	2·4–5·3	4260		+1·07		+0·94	+0·9	+0·97	+0·47	+0·24	
350	b^3P–x^3D^0	C	2·8–5·6	4466				+0·6	+0·8	+0·7	+0·2		
383	z^7P^0–e^7D	E	3·0–5·3	5232				+0·65		+0·6	+0·25	+0·20	
553	z^5D^0–e^5D	E	3·2–5·6	5324				+0·63		+0·6	+0·33	+0·23	
686	z^5F^0–e^5D	E	3·4–5·6	5615		+0·8				+0·8	+0·47	+0·41	
693	e^5G	F	6·3	4227				+1·17	+1·7	+1·3	+1·33		

Co	$(n=8)$				KPDO	AA	Ost	OB*				
					−4·64	+0·05	−4·63	−5·80				
1	a^4F–z^4F^0	Bic	0·1–3·0	4233	−2·50		−2·2	−2·4	−2·40	<0·8		
2	z^6D^0	Bic	3·1	4059	−3·2			−3·3	−3·23	<0·8		
3	z^6G^0	Bic	3·2	3909	−2·09	−2·00	−1·9	−2·1	−2·03	<0·8		
4	z^4F^0	B5	3·6	3526	−0·10	−0·26	−0·20	0·0	−0·16	+0·91		
5	z^4G^0	B5	3·6	3465	−0·06	−0·15	−0·18	−0·3	−0·14	+1·02	+1·17	
6	z^4D^0	B5	3·7	3412	−0·14	−0·29	−0·29	−0·1	−0·21	+0·76	+0·92	

TABLE I (*continued*)

Mult. No.	Terms	Transition	E.P.	λ	log $g_t f$ measured					log $g_t f$ calculated	
					Individual observers				Mean		
Co	(n=8)		Volts	A	KPDO	AA	Ost	OB*		f-sum	B.D.
					−4·64	+0·05	−4·63	−5·80			
7	a^4F–z^2G^0	Bic	0·1–4·0	3153	−2·2			−1·9	−2·1	<0·8	
8	z^2F^0	Bic	4·0	3136	−2·1			−1·9	−2·05	<0·8	
9	y^4D^0	dj	4·0	3121	−1·29		−1·00	−1·2	−1·14	<0·8	
10	y^4G^0	dj	4·1	3082	−0·89		−0·60	−0·5	−0·72	<0·8	
11	y^4F^0	dj	4·1	3044	−0·08		−0·05	−0·4	−0·09	<0·8	
12	z^2D^0	Bic	4·2	3062	−2·0			−1·6	−1·9	<0·8	
13	y^2G^0	dj	4·2	2989	−1·3		−1·15	−1·5	−1·28	<0·8	
14	b^4F–z^6F^0	Cic	0·5–3·0	4966	−2·9				−2·9	<0·8	
15	z^6D^0	Cic	3·1	4727	−2·8			−3·1	−2·9	<0·8	
16	z^4F^0	C	3·6	4020	−1·50		−1·43	−1·6	−1·48	+0·7	
17	z^4G^0	C	3·6	3941	−1·19	−1·28	−0·6	−1·4	−1·16	+0·8	
18	z^4D^0	C	3·7	3872	−0·22	−0·13	−0·27	−0·3	−0·22	+0·6	
19	z^2G^0	Cic	4·0	3542	−0·64	−0·65	−0·48	−0·6	−0·60	<0·8	
20	z^2F^0	Cic	4·0	3521	−0·64	−0·54	−0·48	−0·5	−0·55	<0·8	
21	y^4D^0	A	4·0	3502	+0·63	+0·52	+0·62	+0·5	+0·59	+0·67	+0·73
22	y^4G^0	A	4·1	3453	+1·01	+0·75	+0·85	+0·9	+0·88	+0·92	+1·00
23	y^4F^0	A	4·1	3405	+0·82	+0·94	+0·71	+0·6	+0·81	+0·81	+0·89
24	z^2D^0	Cic	4·2	3409	−1·8			−1·6	−1·75	<0·8	
25	y^2G^0	Aic	4·2	3337	+0·2	+0·1	+0·27	0·0	+0·18	<0·8	
26	y^2F^0	Aic	4·4	3127	−1·4			−1·6	−1·45	<0·8	
27	a^2F–z^4G^0	Cic	1·0–3·7	4580	−2·4			−2·5	−2·43	<0·5	
28	z^2G^0	C	4·0	4121	+0·08	+0·13	+0·01	+0·4	+0·07	+0·3	
29	z^2F^0	C	4·0	4092	−0·62	−0·66	−0·70	−0·4	−0·64	+0·4	
30	y^4D^0	Aic	4·0	4066	−1·39			−1·4	−1·39	<0·5	
31	y^4G^0	Aic	4·1	3995	+0·1	−0·03	+0·02	+0·2	+0·03	<0·5	
32	y^4F^0	Aic	4·1	3935	−0·39	−0·37	−0·40	−0·1	−0·37	<0·5	

33	z^2D^0	C	4·2	3842	−0·41	−0·33	−0·36	−0·3	−0·35	+0·2		
34	y^2G^0	A	4·2	3845	+0·48	+0·47	+0·47	+0·4	+0·47	+0·62	+0·69	
35	y^2F^0	A	4·4	3569	+0·63	+0·76	+0·70	+0·4	+0·66	+0·51	+0·61	
36	y^2D^0	A	4·5	3489	+0·49	+0·55	+0·58	+0·4	+0·52	+0·37	+0·46	
37	a^4P–z^4D^0	B5	1·7–3·7	6450	−1·9				−1·9	+0·76	+0·63	
38	z^2F^0	Bic	4·0	5530	−2·1				−2·1	<0·4		
39	y^4D^0	dj	4·1	5483	−0·86				−0·9	<0·4		
41	z^4P^0	B5	5·2	3548	−0·96			−0·7	−0·9	+0·54	+0·59	
57	b^4P–y^2D^0	Aic	1·9–4·5	4781	−1·49			−1·8	−1·55	<0·4		
58	x^4D^0	C	5·0	4086	−0·06	−0·01		−0·1	−0·05	+0·4		
59	z^4S^0	C	5·0	3930	−1·0			−1·4	−1·1	+0·2		
62	z^4P^0	C	5·2	3732	+0·20	+0·23		+0·3	+0·23	+0·3		
64	w^4D^0	C	5·3	3543	−0·08	−0·02		0·0	−0·04	+0·4		
66	x^2F^0	Cic	5·4	3523	−0·7			−0·8	−0·73	<0·4		
67	x^2D^0	Aic	5·4	3478	−0·5			−0·1	−0·4	<0·4		
69	x^4P^0	C	5·7	3243				+0·2	+0·2	+0·3		
70	v^4D^0	A	5·7	3247				+0·1	+0·1	+0·67		
77	t^4D^0	C	6·0	3026				0·0	0·0	+0·4		
83	a^2G–y^2F^0	dj	2·1–4·4	5266	−0·8				−0·8	<0·6		
92	a^2D–y^2D^0	Aip	2·1–4·5	5176	−1·3				−1·3	<0·4		
95	z^2P^0	A	5·3	3735	−0·26	−0·34		−0·24	−0·28	+0·15		
96	w^4D^0	Cic	5·3	3755	−0·3			−0·5	−0·35	<0·4		
97	w^4F^0	Cic	5·4	3693	−0·3			−0·25	−0·28	<0·4		
98	x^2F^0	C	5·4	3733	−0·20	−0·05		−0·02	−0·10	+0·2		
99	x^2D^0	A	5·4	3683	+0·1			+0·08	+0·09	+0·37	+0·30	
112	a^2P–y^2D^0	Aip	2·3–4·5	5647	−1·2				−1·2	<0·1		
113	x^2D^0	Aip	5·4	3915	0·0			−0·4	−0·1	<0·1		
115	w^2D^0	A	5·7	3662	+0·18	+0·23		+0·2	+0·20	+0·37	+0·45	
128	b^2P–w^2D^0	dj	2·6–5·7	3969	−0·06			−0·1	−0·07	<0·1		
145	b^2G–y^2H^0	dj	2·9–6·2	3676	+1·4	+0·8		+0·6	+1·0	<0·6		
146	u^2F^0	dj	6·2	3649				+0·3	+0·3	<0·6		
147	x^2H^0	B3	6·3	3632				+0·2	+0·2	+0·89		
149	v^2G^0	dj	6·6	3322				+0·8	+0·8	<0·6		
150	z^4F^0–e^4F	E	3·0–5·8	4530				+1·1	+1·1	+0·56		
152	f^4F	F	6·7	3326				+0·8	+0·8	+1·12		

TABLE I (*continued*)

Mult. No.	Terms	Trans-ition	E.P. Volts	λ A	log $g_t f$ measured: Individual observers KPDO	AA	Ost	OB*	Mean	log $g_t f$ calculated: f-sum	B.D.
Co	$(n=8)$				−4·64	+0·05	−4·63	−5·80			
153	z^6F^0–e^6D	F	3·0–6·7	3319				+0·9	+0·9	+0·70	
154	e^6G	F	6·7	3319				+0·8	+0·8	+1·23	
155	e^6P	Fml	6·7	3339				+0·6	+0·6	<1·0	
156	z^6D^0–e^6F	E	3·1–5·7	4749				+0·6	+0·6	+0·41	
158	z^6G^0–e^6F	E	3·2–5·8	4867	+1·3			+0·8	+1·1	+0·66	+0·58
161	e^6G	F	6·8	3496				+0·7	+0·7	+1·01	
162	e^6H	F	6·8	3485				+1·3	+1·3	+1·53	
171	z^4F^0–f^4G	F	3·6–6·7	3972				+0·5	+0·5	+1·06	
173	z^4G^0–f^4H	F	3·6–6·7	4035				+0·7	+0·7	+1·35	
176	z^4D^0–e^4D	dj	3·7–6·3	4594				0·0	0·0	<0·7	
177	e^4P	dj	6·4	4596				+0·1	+0·1	<0·7	
178	g^4F	dj	6·3	4570				−0·3	−0·3	<0·7	
182	z^2G^0–g^2F	E	4·0–6·6	4746				−0·1	−0·1	+0·18	
Ni	$(n=9)$				King	VD	AA	HD*	OB*		
					−3·57	−3·63	+0·36	−7·30	−5·20		
1	a^3F–z^5D^0	Bic	0·1–3·3	3946	−2·42				−2·6	−2·45	<0·7	
2	z^5G^0	Bic	3·5	3624	−1·39				−1·5	−1·42	<0·7	
3	z^5F^0	Bic	3·6	3502	−0·55	−0·60	−0·61		−0·6	−0·59	<0·7	
4	z^3P^0	dj	3·6	3670	−1·23		−1·14		−1·5	−1·24	<0·7	
5	z^3F^0	dj	3·7	3391	−0·21	−0·32	−0·33		−0·4	−0·29	<0·7	
6	z^3D^0	dj	3·7	3369	−0·07	−0·11	−0·12		−0·1	−0·10	<0·7	
7	z^3G^0	B2	3·9	3232	−0·31	−0·15	−0·54		−0·5	−0·35	+0·62	+0·59
8	z^1F^0	dj	3·8	3221	−0·72	−0·91	−0·84		−0·8	−0·82	<0·7	
9	z^1D^0	dj	3·9	3320	−0·97	−1·05	−0·91		−0·7	−0·96	<0·7	
10	z^1P^0	dj	4·1	3249	−2·07				−2·0	−2·05	<0·7	

11	y^3F^0	B2	4·1	3031	−0·7				−0·5	−0·65	+0·52	+0·53
12	y^3D^0	B2	4·2	2984	−0·55				−0·5	−0·53	+0·37	+0·42
13	z^1G^0	Bic	4·2	3099	−1·09				−1·0	−1·07	<0·7	
15	a^3D–z^5D^0	Cic	0·1–3·3	3912	−1·87				−2·2	−1·93	<0·5	
16	z^5G^0	Cic	3·5	3587	−1·25				−1·3	−1·27	<0·5	
17	z^5F^0	Cic	3·7	3461	+0·04	+0·08	+0·03		−0·2	+0·05	<0·5	
18	z^3P^0	A	3·6	3524	+0·48	+0·48	+0·47		+0·4	+0·48	+0·32	+0·36
19	z^3F^0	A	3·7	3414	+0·59	+0·63	+0·48		+0·4	+0·56	+0·69	+0·75
20	z^3D^0	A	3·7	3392	+0·29	+0·42	+0·34		+0·1	+0·35	+0·54	+0·63
21	z^3G^0	Cml	3·9	3248	−1·11				−1·1	−1·11	<0·5	
22	z^1F^0	Aic	3·8	3243	−0·62	−0·73	−0·6		−0·6	−0·65	<0·5	
23	z^1D^0	Aic	3·9	3200	−1·67				−1·6	−1·65	<0·5	
24	z^1P^0	Aic	4·1	3114	−0·99				−0·8	−0·95	<0·5	
25	y^3F^0	C	4·1	3050	+0·78				+0·3	+0·7	+0·6	
26	y^3D^0	C	4·2	3005	+0·71				+0·1	+0·6	+0·6	
30	a^1D–z^5F^0	Cic	0·4–3·7	3783	−0·67	−0·73	−0·7		−0·7	−0·70	<0·1	
31	z^3P^0	Aic	3·6	3973	−1·22		−1·34		−1·4	−1·30	<0·1	
32	z^3F^0	Aic	3·7	3858	−0·35	−0·73	−0·49			−0·52	<0·1	
33	z^3D^0	Aic	3·7	3807	−0·45	−0·71	−0·53		−0·2	−0·51	<0·1	
34	z^3G^0	Cic	3·9	3523	−2·7				−1·9	−2·5	<0·1	
35	z^1F^0	A	3·8	3619	+0·21	+0·27	+0·24		+0·4	+0·26	+0·21	+0·28
36	z^1D^0	A	3·9	3566	+0·03	+0·02	+0·01		+0·3	+0·05	+0·07	+0·13
37	z^1P^0	A	4·1	3380	+0·15	+0·03	+0·23		+0·5	+0·18	−0·15	−0·07
38	y^3F^0	Cic	4·1	3365	−0·93	−0·91			−0·6	−0·89	<0·1	
39	y^3D^0	Cic	4·2	3322	−0·57	−0·68			−0·3	−0·58	<0·1	
40	y^1F^0	C	4·4	3101	+0·18				+0·2	+0·19	+0·2	
41	y^1D^0	C	4·5	3012	+0·33				+0·2	+0·30	+0·2	
46	b^1D–z^1F^0	dj	1·7–3·8	5709				−1·8		−1·8	<0·1	
47	z^1D^0	dj	3·9	5578				−2·4		−2·4	<0·1	
48	z^1P^0	dj	4·1	5137				−1·5		−1·5	<0·1	
49	y^3F^0	Bic	4·1	5102				−2·3		−2·3	<0·1	
50	y^3D^0	Bic	4·2	5003				−2·3		−2·3	<0·1	
59	a^1S–z^1P^0	D	1·8–4·1	5476				−0·37		−0·4	+0·2	
60	y^3D^0	dj	4·2	5079				−0·8		−0·8	<0·6	
68	a^3P–z^1P^0	dj	1·9–4·1	5754				−1·5		−1·5	<0·3	

TABLE I (*continued*)

Mult. No.	Terms	Transition	E.P.	λ	log $g_t f$ measured						log $g_t f$ calculated	
					Individual observers					Mean	*f*-sum	B.D.
Ni	(n=9)		Volts	A	King	VD	AA	HD*	OB*			
					−3·57	−3·63	+0·36	−7·30	−5·20			
69	a^3P–y^3F^0	Bml	1·9–4·1	5711				−1·65		−1·6	<0·3	
70	y^3D^0	B2	4·2	5587				−1·57		−1·6	+0·37	
77	x^3P^0	B4	5·8	3176					−0·6	−0·6	+0·45	
78	v^3D^0	B4	5·8	3181					−0·2	−0·2	+0·67	
91	z^5D^0–e^5P	F	3·3–7·1	3217					+1·1	+1·05	+0·89	
93	e^5D	F	7·1	3214					+0·9	+0·92	+0·93	
94	f^5F	F	7·2	3202					+0·8	+0·78	+0·71	
106	z^5G^0–e^5H	F	3·4–7·2	3374					+1·6	+1·55	+1·45	
107	f^5F	F	7·2	3364					+1·0	+1·0	+0·20	
108	e^5G	F	7·2	3366					+1·4	+1·3	+0·93	
111	z^5F^0–e^5F	E	3·6–6·1	5017				+0·89		+0·8	+0·47	+0·40
121	e^5D	F	7·1	3530					+0·6	+0·61	+0·63	
123	f^5F	F	7·2	3516					+1·2	+1·16	+1·05	
124	e^5G	F	7·2	3518					+1·0	+1·04	+1·16	
129	z^3P^0–e^3S	H	3·6–6·0	4904				−0·1		−0·1	+0·18	
130	e^3P	H	6·1	4855				+0·7		+0·66	+0·54	
131	f^3D	H	6·2	4829				+0·5		+0·48	+0·43	+0·26
137	f^3S	Hh	6·7	3844					−0·3	−0·3		−0·64
141	z^3F^0–e^3F	dj	3·7–6·1	5265				+0·2		+0·2	<0·7	
142	e^3P	Hml	6·1	5039				−0·7		−0·7	<0·7	
143	e^3G	H	6·1	5080				+1·26		+1·23	+1·14	
144	f^3D	H	6·2	5051				−1·0		−1·0	−0·30	−0·46
145	e^3F	H	6·2	5035				+0·9		+0·8	+0·56	
150	g^3F	dj	6·8	4038					−1·7	−1·7	<0·7	
151	f^3G	Hh	6·8	3970					+0·3	+0·30		+0·30
159	z^3D^0–e^3P	H	3·7–6·1	5129				+0·20		+0·16	+0·06	

160		e^3G	Hml	6·1	5125	−0·1		−0·1	<0·5	
161		f^3D	H	6·2	5099	+0·68		+0·67	+0·65	
162		e^3F	H	6·2	5084	+0·83		+0·84	+0·85	
164		e^1P	Hic	6·2	4841	−0·5		−0·5	<0·5	
166		f^1D	Hic	6·3	4741	0·0		0·0	<0·5	
171		h^3F	Hh	6·8	3984		−0·1	−0·06		+0·01
173		i^3F	dj	7·1	3689		+0·4	+0·4	<0·5	
175		z^3G^o–e^3F	Eic	3·8–6·1	5521	−1·2		−1·2	<0·8	
177		f^3F	Eip	6·3	5115	+0·88		+0·9	<0·8	
180		e^3H	Fip	7·1	3889		+0·6	+0·6	<0·8	
181		g^3G	Fip	7·1	3863		+0·4	+0·4	<0·8	
194		z^1F^o–e^1G	H	3·8–6·3	5081	+0·88		+0·83	+0·66	+0·54
195		e^1F	H	6·3	5048	+0·09		+0·08	+0·07	
208		z^1D^o–e^1P	H	3·9–6·2	5235	−0·59		−0·54	−0·42	
209		f^1D	H	6·3	5176	0·00		+0·05	+0·17	
210		e^1F	H	6·3	5155	+0·41		+0·40	+0·38	
220		z^1P^o–e^1P	H	4·1–6·2	5694	−0·19		−0·15	+0·06	
221		f^1D	H	6·3	5625	−0·26		−0·20	−0·05	−0·32
222		e^1S	H	6·4	5411	−0·31		−0·30	−0·29	
231		y^3F^o–f^3F	Eip	4·1–6·3	5715	+0·62		+0·6	<0·7	
250		y^3D^o–f^3F	Eip	4·2–6·3	5892	+0·82		+0·8	<0·5	
273		y^1D^o–f^1F	E	4·5–6·9	5268	−0·14		−0·20	−0·37	−0·43

The corrections and factors in Table II *have been applied* in Table I and are discussed below or in Section 4.

TABLE II

Boltzmann corrections and factors

	$\Delta(5040/T)$
Cr HK*	−0·30
Cr AA*	−0·07
Cr Mit*	−0·50

	$\Delta(5040/T)$
Fe AA*	−0·05
Fe Mit*	−0·20

	$(5040/T)$
Co OB*	1·00
Ni OB*	0·95
Ni HD*	1·00

The differential temperature corrections $\Delta(5040/T)$ and the experimental accuracy may both be studied by plotting observer comparisons against excitation potential. In Fig. 1 we give a plot of log ($g_t f$ 1st observer/$g_t f$ 2nd observer) against E.P. for those cases in Table I where a number of multiplets have been observed by several authors. An upward slope means that the 1st observer has used a temperature that is low on the standard represented by the 2nd observer. We note for example for Ti that the OPP temperature is low by comparison with KK whereas vSS and KK agree. More details will be considered in Section 4 when the results are compared with calculations.

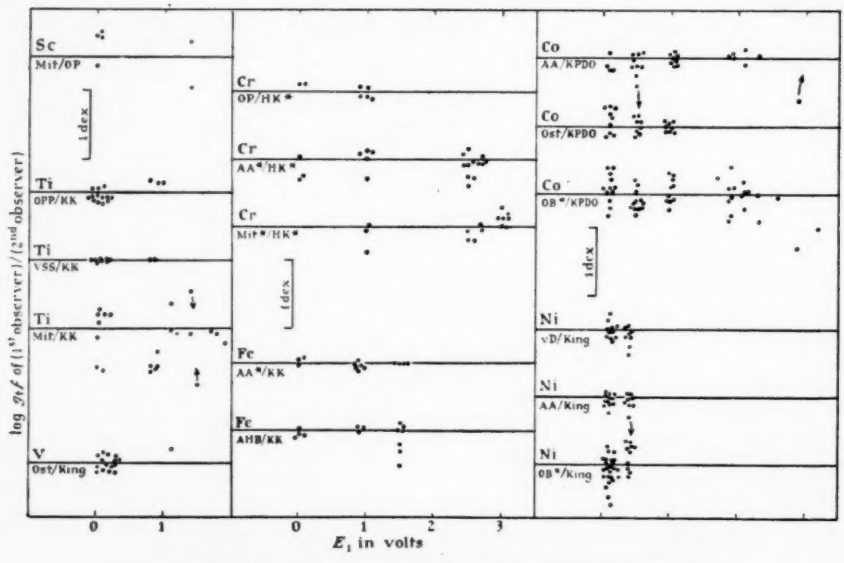

FIG. 1.—*Comparison of observers plotted against lower excitation potential. The logarithmic scale is indicated by* 1 *dex* (=$\log_{10}$ 10).

Several of the experimental excitation temperatures have been derived by comparison with the work of King and his collaborators and therefore agreement of slope in Fig. 1 does not necessarily mean independent temperature confirmation. The measurements by Mitrofanova appear to be seriously influenced by self-absorption. Without allowing for this her excitation temperatures are derived

by comparison with King. This procedure apparently leads to large errors in the derived values of $g_t f$ and a further empirical temperature correction is sometimes required to make her results fit other work and become usable. Some of the Allen and Asaad results have been subject to some revision which has resulted in minor changes of temperature.

The scatter of the points in Fig. 1 gives an indication of the accuracy of the experimental work, and leads to the approximate errors in $\log g_t f$ given in Table III.

TABLE III

Approximate standard errors in log $g_t f$

KK, King, HK, KPDO	±0·09	OB	±0·25
OPP, OP, Ost	±0·12	vD	±0·18
AA	±0·15	AHB	±0·13
Mit	±0·5	Car	±0·18
vSS	±0·08	HD	±0·18

3. *Calculations.*—Two approaches to the calculation of oscillator strengths that have some prospect of general applicability in the iron-group atoms are (*a*) the *f*-sum rule, and (*b*) the wave-function method systematized for a coulomb approximation by the Bates–Damgaard (1949) procedure. Since we cannot expect results to be more accurate than about ±0·1 dex (i.e. ±0·1 in the 10-based logarithm) we are entitled to introduce various simplifying approximations.

f-sum rule

The *f*-sum rule (Unsöld 1955, p. 350), written in terms of $g_t f$ becomes

$$\sum_u g_t f + \sum_c g_t f + \sum_l g_t f = r g_t \qquad (1)$$

where t represents the atomic term for which the summation is being made and g_t is the total weight of that term; u signifies transitions to upper terms, c to the continuum and l to lower terms; r is the number of electrons involved in the transition. The summation $\sum_l g_t f$ is an emission oscillator strength and therefore negative. The other summations include transitions to high series members and to the continuum. However, the spectrum lines that concern us in the iron-group atoms are mainly lowest members of their particular series and as such they contain most of the total oscillator strength. We suppose the oscillator strength of the lowest member to be b times the total of upward transitions (including the continuum), where $b < 1$, then

$$\sum_a g_t f = b r g_t - \sum_l g_t f \qquad (2)$$

where the summation on the left is now for the lowest member in each series and is usually over one or two arrays (hence subscript a). We adopt $b = 0{\cdot}7$ on the argument that in simpler atoms where b can be determined it is between 0·4 and 1·0. Later we compare this adopted value of b with both Bates–Damgaard calculations and experiment. The emission component $-\sum_l g_t f$ is often zero for the arrays with which we are concerned; otherwise it is positive. Apart from sign the numerical values of $g_t f$ are the same in emission and absorption.

The expression (2) enables us to compute a value of $g_t f$ (though not necessarily a sound one) for nearly all multiplets that are amenable to any sort of calculation. The formula is of very general use when applied to iron-group atoms. It is convenient to distinguish the atoms by n as follows:

	Sc	Ti	V	Cr	Mn	Fe	Co	Ni
$n=$	2	3	4	5	6	7	8	9

Results of calculations are often expressed in relation to the weights of various terms, $g_t=(2S_t+1)\,(2L_t+1)$ where $2S_t+1$ is the multiplicity and L_t is the total orbital quantum number for the term t.

We give below the notation and the method of calculating $g_t f$ for the various transitions:

A $=d^n s-d^n p$ (examples in all atoms Sc to Ni); $r=1$ since only 1 non-equivalent electron moves; $\sum 1=0$; $b=0{\cdot}7$. All transitions are from lower unit terms to upper triads with three times the total weight of the lower term. $g_t f$ is proportional to g_{ut} the weights of the upper terms. From (2) we have

$$g_t f=0{\cdot}7 g_{ut}/3=0{\cdot}233 g_{ut}.$$

B $=d^{n-1}s^2-d^{n-1}sp$ (examples in all atoms Sc to Ni); $r=2$; $\sum 1=0$; $b=0{\cdot}7$. Each term t combines with two upper triads. For one of these the parent multiplicity is $(2S_t+1)+1$ and for the other $(2S_t+1)-1$. Assuming the $g_t f$ to be proportional to the parent multiplicity (see Rohrlich 1948) we obtain

$$g_t f=0{\cdot}233 g_{ut}(2S_t+1\pm 1)/(2S_t+1)$$

where the + and − refer to the higher and lower parent multiplicities. The number following B in Table I is $(2S_t+1\pm 1)$.

C $=d^n s-d^{n-1}sp$ (examples in Ti, V, Cr, Fe, Co, Ni); $r=n$; $\sum 1=0$; $b=0{\cdot}7$. To apply the f-sum rule for the moving d electron one must add the transitions to both $d^{n-1}sp$ and $d^{n-1}sf$ which are in the ratio $1:3\frac{1}{2}$ (see Allen 1955, p. 60). The total $g_t f$ in the $d^n s-d^{n-1}sp$ array will then be $0{\cdot}7(2/9)ng_t$. Comparing this with $\mathscr{S}(\mathscr{M})$, the sum of the angular matrices as published by Goldberg (1935) with the correcting factors (Goldberg 1936, Allen 1955, p. 60), we obtain the generalization

$$g_t f=0{\cdot}7\mathscr{S}(\mathscr{M})/27=0{\cdot}026\mathscr{S}(\mathscr{M}).$$

When the $\mathscr{S}(\mathscr{M})$ for the individual multiplet is not given, but only the sum of x multiplets, it has been assumed that the multiplets actually concerned are stronger than the average. To cater for this effect I have divided the total by $\sqrt{x}$; not by x. Large errors in the calculations are inevitable.

D $=d^{n+1}-d^n p$ (one example in Ni); $r=10$; $\sum 1=0$; $b=0{\cdot}7$; (2/9) of total $g_t f$ as in C.

E $=d^{n-1}sp-d^{n-1}ss$ (examples in V, Cr, Mn, Fe, Co, Ni),

F $=d^{n-1}sp-d^{n-1}sd$ (examples in Ti, V, Mn, Fe, Co, Ni),

G $=d^n p-d^n s$ (example in Cr),

H $=d^n p-d^n d$ (examples in Cr, Ni); $r=1$; $-\sum g_t f\simeq 0{\cdot}233 g_t$; $b=0{\cdot}7$. The ratio of the p–s to p–d transitions is 1 to 10. Hence the f-sum rule gives

E and G $\quad \sum g_t f=(1/11)(0{\cdot}7g_t+0{\cdot}233g_t)$,

F and H $\quad \sum g_t f=(10/11)(0{\cdot}7g_t+0{\cdot}233g_t)$.

Comparing these values with $\mathscr{S}(\mathscr{M})$ as obtainable from Goldberg's tables (1935, 1936) we obtain for E, F, G, H

$$g_t f = 0{\cdot}085\mathscr{S}(\mathscr{M}).$$

J $= d^{n-1}sp - d^{n-1}p^2$ (one example in Ti); $r=2$; $\sum_t g_t f \simeq 0{\cdot}233 g_t$; $b=0{\cdot}7$. The f-sum rule (2) gives $\sum_a g_t f = 0{\cdot}7 \times 2g_t + 0{\cdot}233 g_t$. Comparing such values with the tabulations of $\mathscr{S}(\mathscr{M})$ we obtain

$$g_t f = 0{\cdot}817\mathscr{S}(\mathscr{M}).$$

h The symbol h is added to transitions which are not the lowest members of the series and to which therefore the above rules do not apply. B.D. calculations are used in such cases.

In addition to the transitions permitted in LS-coupling there are many strong transitions that violate the LS rules. The following notation is used:

ic = intercombination line,

ip = interparent transition,

ml = multiple change in L,

dj = double jump. The main such transitions are of the forms $d^{n-1}s^2 - d^n p$, $d^{n-1}sp - d^n d$, $d^n p - d^{n-1}ss$.

In such cases, the f-sum rule can give an approximate maximum value. By comparison with permitted multiplets it would appear reasonable to adopt for our calculations $g_t f < 0{\cdot}233 g_t$ where we select t to be the lower term of the transition.

Calculated values of $g_t f$ in accordance with these f-sum applications are given in the f-sum columns of Table I.

Bates–Damgaard calculations

The Bates–Damgaard (1949) method of calculating the radial integral designated σ^2 may be used for many of the multiplets permitted in LS-coupling. The multiplet strength is then given by $\sigma^2\mathscr{S}(\mathscr{M})$ and the weighted oscillator strength by

$$g_t f = 0{\cdot}0304\sigma^2\mathscr{S}(\mathscr{M})/\lambda$$

with σ^2 and $\mathscr{S}(\mathscr{M})$ in atomic units, and λ in microns.

The B.D. results quoted in Table I have been taken from any available calculations (many from Asaad 1956) and may not be entirely consistent. They are not required for the main part of the present analysis.

Comparison of f-sum and B.D. calculations

The f-sum and B.D. calculations are compared logarithmically in Fig. 2. For the A transitions the two calculations would have been almost identical if b had been taken as 0·82 instead of 0·70. For the B transitions there is considerable spread between the two calculations; the choice of $b=0{\cdot}76$ would have produced slightly better mean agreement. For the E, F, G, H transitions the two calculations are in good proportion and absolute agreement would have been obtained by selecting $b=0{\cdot}50$. Our choice of $b=0{\cdot}70$ gives fair overall agreement between f-sum and B.D. calculations. The disagreement in calculated values is small by comparison with the disagreement between observation and calculation.

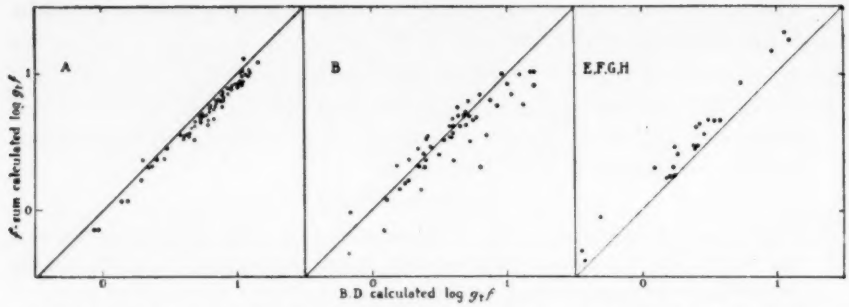

FIG. 2.—*Comparison of log $g_1 f$ calculated from the f-sum rule and from the Bates–Damgaard (1949) procedure. Transition types are A; B; and E, F, G, H.*

It should be noticed that the agreement between *f*-sum and B.D. calculations is valid over a considerable wave-length range. The B.D. procedure has been recomputed for each line or multiplet and should not produce an error that changes systematically with wave-length. Hence when a wide wave-length range is to be considered, sum rules should be applied in terms of *f*-values, as has been done here—not in terms of line strengths which are proportional to $gf\lambda$.

To represent the calculated values I have chosen the *f*-sum procedure because it is very general, quite consistent, and easy to compute. It agrees slightly better with unadjusted experimental values than the B.D. procedure.

4. *Comparison of observations and calculations.*—In Fig. 3 the observed values taken from the "mean" column of Table I (and therefore adjusted to a

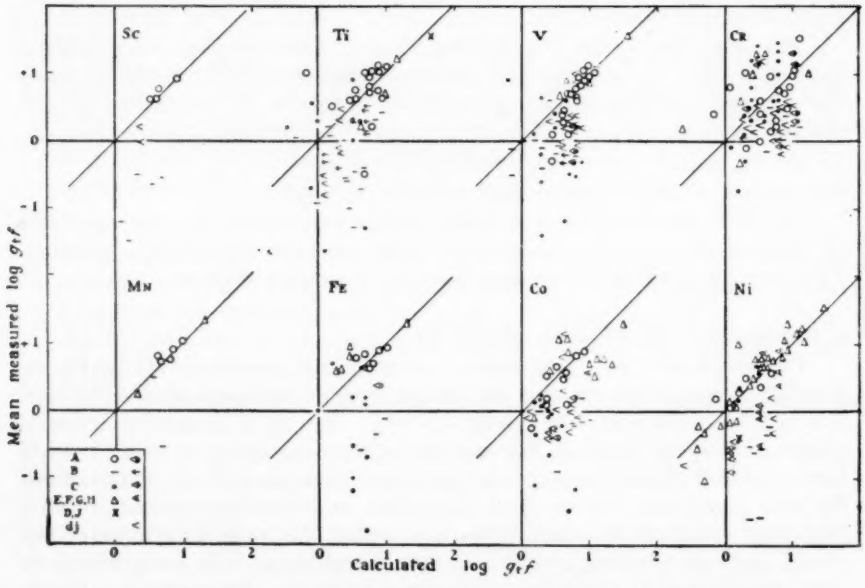

FIG. 3.—*Comparison of measured and calculated values of the weighted oscillator strength. Arrowed signs (<, ←, etc.) are violations of LS-coupling.*

calculated scale) are plotted logarithmically against the adopted (f-sum) calculations. The transition types are sub-divided by symbols. Arrowed signs (e.g. $<$, $\leftarrow$, etc.) indicate that LS-rules are violated and that calculations can give an indication of only the maximum value. Such multiplets are included in Figs. 3, 4, 5 and 6 only if the log (observed/calculated) value is greater than $-1{\cdot}0$.

In considering Fig. 3 and later diagrams, it is well to remember that even for genuine regularities several exceptions may be expected. These may be due to interactions between terms and to unsuitable designations. Such intensity effects may be large and one could not expect the consequent scatter to follow random laws. We will therefore look for regularities that relate to the majority, but not all, of the multiplets. The multiplets that are strong both by observation and calculation are likely to be well designated and unaffected by interaction. These, which will appear on the top-right of each plot in Fig. 3, should show the best agreement.

The agreement shown in Fig. 3 varies from atom to atom but we can draw the following generalizations:

(i) The transitions A, E, F, G, H, involving the movement of a non-equivalent electron, show observations and calculations in fair agreement. The absolute scale of the observations has been adjusted to make *this* agreement as close as possible.

(ii) The transitions B, C, involving the movement of an equivalent electron, show much larger scatter and the observed values are systematically smaller than the calculations.

(iii) The most intense of the observed multiplets that violate LS-coupling are in near agreement with calculated maximum value.

In Fig. 4 the log (observed/calculated) values for each atom are plotted against the lower excitation potentials, E_1. We see that for most atoms the A, E, F, G, H transitions (non-equivalent electrons) do not change systematically with excitation potential (E.P.), while for the B, C transitions (equivalent electrons) the low voltage multiplets have low observed intensities. To show

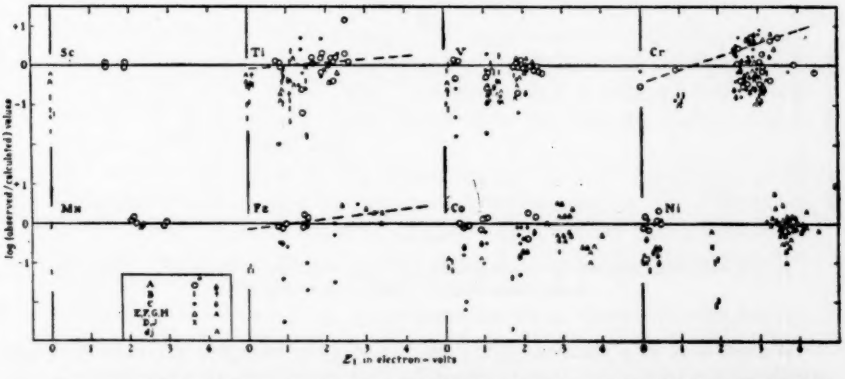

FIG. 4.—*Relation between the (observed/calculated) gf ratio and E_1 the lower excitation potential. Broken lines show possible trends. Arrowed signs (∧, ↑, etc.) are violations of LS-coupling.*

the trends more clearly, Fig. 5 collects for all atoms (i) the A, E, F, G, H transitions, (ii) the B, C transitions, and (iii) the more intense of those multiplets that violate *LS*-coupling. In Fig. 5 (i) there appears to be no systematic departure from the zero ordinate (i.e. obs.–calc. agreement). However, in interpreting this diagram we should remember that the absolute values have been chosen to render good absolute agreement and this may have some effect on the apparent change with E.P. Fig. 5 (ii) shows that the characteristics of the B and C transitions

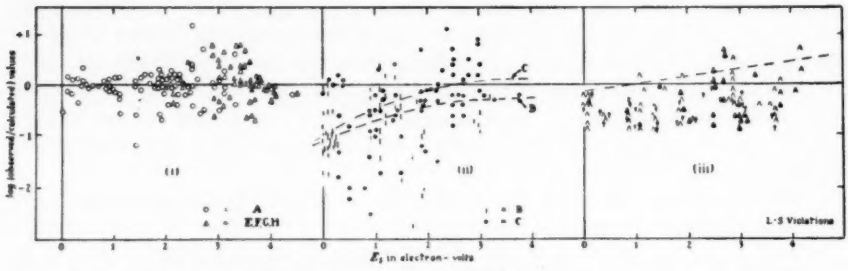

FIG. 5.—*General relation between the (observed/calculated) $g_1 f$ ratio and E_1 the lower excitation potential. Broken lines show possible trends (see text). Symbols as in Fig. 4.*

are somewhat similar. They both have systematically low observed values at low E.P. but tend towards agreement with calculations for $E_1 > 2$ eV. We see later, Fig 7, that the scatter of the values is somewhat reduced if we use the upper E.P., E_2, instead of the lower. From Fig. 5 (iii) there appears to be an upward trend of the highest observed–calculated values for multiplets forbidden in *LS*-coupling.

In Fig. 6 the log (observed/calculated) values for all atoms are plotted against wavelength. There appears to be no significant trend for A, E, F, G, H transitions while the trends for B and C are somewhat similar. Any apparent trend for the multiplets violating *LS*-coupling is probably not significant.

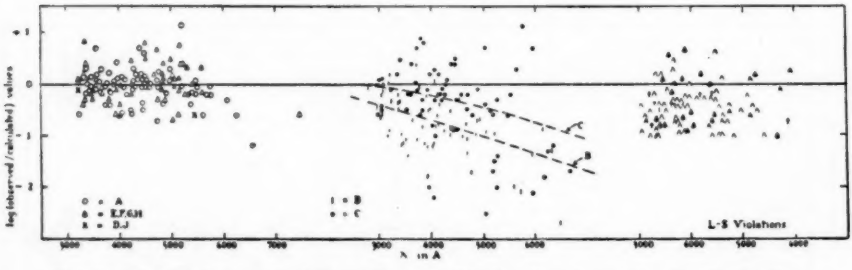

FIG. 6.—*Relation between the (observed/calculated) $g_1 f$ ratio and wave-length. Broken lines show possible trends. Symbols as in Fig. 4.*

We are now in a position (ref. Figs. 1 and 4) to compare the measured and calculated values for the individual atoms and to investigate what effects might have been caused by the temperature adjustments that have been made to the experimental results.

Sc. The A transitions agree while the B disagreement is large and typical. No temperature adjustment has been made to the OP observations and there is no evidence that any is necessary. If x^2P^0 is designated (from Sc II) as configuration $4s^2(^1S)4p$ the calculated $\log gf$ becomes 0·19 in agreement with observation.

Ti. The A, F and J transitions are mostly in agreement and the B disagreement is typical. Some C measurements are high. The pattern of agreement is not greatly changed if the Rohrlich (1948) classification is introduced instead of that tabulated by Moore (1949). The upward trend of the A transitions in Fig. 4 suggests that a higher temperature would improve the agreement. However the results are dominated by the KK observations and Fig. 1 shows that the OPP temperature standard is lower still. There is therefore no experimental justification for making an upward temperature adjustment.

V. The agreement is good for the strong multiplets of the A, E, F types but the weaker A measurements are systematically small. Fig. 4 shows that no temperature change would improve the agreement and therefore this atom confirms the King temperature scale. Fig. 4 shows no upward trend in the B multiplets which is unusual.

Cr. The general disagreement between measurement and calculation in Cr is too large for any precise conclusions to be drawn. Fig. 4 shows an upward slope if the highest values are used but this may be associated with the general scatter. In any case Fig. 4 implies that the upward temperature correction given to the HK measurements was necessary, and furthermore Fig. 1 shows that the OP temperature scale is higher than HK* (even after correction). There is other evidence (Allen and Asaad 1957, pp. 39, 41) that the HK temperature used for Cr was abnormally low.

Mn. Agreement for the A, E, F type transitions is surprisingly good for this atom. A zero E_1 B transition also agrees which is unusual. No temperature adjustment has been made to the AA scale, which is effectively the King scale, and none appears necessary.

Fe. The A, E, F transitions are in fair agreement and the C transitions rather fainter than in some other atoms. The experimental temperature agreement shown in Fig. 1 is satisfactory but the temperatures used are not independent. The trend in Fig. 4 shows that a higher temperature (about $-0{\cdot}13$ in $5040/T$ fitting the broken line) would lead to better agreement with calculations.

Co. The general agreement is rather poor for the A, E, F transitions. The other transitions are low and typical. The character of Fig. 4 is rather dominated by the selection of $5040/T = 1{\cdot}0$ for OB* but Fig. 1 shows this selection to be in reasonable agreement with KPDO. Therefore the absence of any trend in Fig. 4 is probably correct.

Ni. The right-hand side of Fig. 4 has been forced to agree with the left by selecting the temperature of OB* and the reduction factor for HD*. There is therefore no unbiased experimental evidence for the good general agreement that appears in Fig. 3 for the A, E, F, H transitions. More experimental work is needed to connect the observations in the violet

with those in the green–red. It is unusual for the low-E_1 C transitions to agree, but the low B values are typical. The E_1 range in Fig. 1 is too small for any effective temperature comparison.

5. *Absolute experimental values.*—The absolute oscillator strength measurements that are thought to have useful accuracy for iron-group atoms are from the authors (with abbreviations) listed below:

KW	Kopfermann and Wessel (1951)	Fe.
HL	Huldt and Lagerqvist (1952)	Mn.
Est	Estabrook (1952)	Cr.
DRK	Davis, Routly and King (1954)	Cr.
King	King (1942, 1956). King's (1956) letter amends DRK and King values	Cr, Fe, Mn.
AA	Allen and Asaad (1957), giving absolute comparisons but dependent on other absolute values	Cr, Mn, Fe, Co, Ni.
Z	Ziock (1957)	Fe.
OP	Ostrovsky and Penkin (1957a)	Cr, Mn.
BDKR	Bell, Davis, King and Routly (1958, 1959)	Fe, Mn.

We summarize in Table IV the latest values published or available and the mean experimental values adopted for the present comparisons.

TABLE IV

Absolute f and log $g_t f$ values

Cr Mult. No. 1	Est.	King	OP	Adopted	
f(4254)	0·086	0·055	0·15		
f(4275)	0·069	0·043	0·11		
f(4290)	0·048	0·032	0·082		
log $g_t f$	+0·15	−0·04	+0·38	+0·12	
Mn Mult. No. 2	**BDKR, King**	**HL**	**OP**	**Adopted**	
f(4030)	0·061	0·062	0·056		
f(4033)	0·034	0·047	0·040		
f(4034)	0·032	0·032	0·027		
log $g_t f$	−0·12	−0·07	−0·13	−0·11	
Fe Mult. No. 5	**King**	**BDKR**	**KW**	**Z**	**Adopted**
f(3720)	0·033, 0·022	0·032	0·043	0·046	0·036
log ($g_t f/gf$)	0·58			0·51	0·53
log $g_t f$					+0·04

In Table V the observed values of Table IV are compared with mean values in Table I, which are observed values on a calculated absolute scale. They are also compared with the AA values which are all on a consistent scale.

TABLE V

Comparisons of absolute log $g_t f$

Element and (Multiplet)	log $g_t f$			log differences		
	Observed Table III	Calc. scale Mean of Table I	AA	Obs.–calc.	Obs.–AA	AA–calc. All multiplets
Cr (1)	+0·12	+0·14	−0·09	−0·02	+0·21	−0·22
Mn (2)	−0·11	−0·54	−0·24	+0·43	+0·13	+0·32
Fe (3)	+0·04	−0·10	0·00	+0·14	+0·04	+0·10
Co						−0·05
Ni						−0·36
Mean				+0·18	+0·13	−0·04

The greatest difference quoted in Tables IV or V is 0·43 dex or a factor of 2·7. From this general agreement we might infer that the standard error of obtaining absolute values by (i) *f*-sum calculations on several well-designated multiplets, (ii) well-executed absolute observations, or (iii) the AA dilute alloy procedure, is not likely to be greater than ±0·3 dex. We must investigate however whether any of the three methods can be substantially more accurate than this, and whether the larger differences are due to faults in measurement or calculation.

The systematic difference between observations and calculations, log (obs./calc.) = +0·18, is not very large and is due mainly to Mn. We see from the last column of Table V that Ni differs in the opposite direction and we reach the conclusion that there is no substantial systematic difference between absolute measured and calculated values.

Mn is the only atom for which the log (obs./calc.) is large enough to attempt a decision on whether the fault lies in the observations or calculations. For Mn three independent absolute observations are in very good agreement and furthermore the AA observations give further support to the high measured values. On the other hand the relative calculated values agree well with the relative observations. We must conclude that, either (*a*) for all seven of the used A, E, F multiplets the *f*-sum (and also B.D.) calculations chance to be too low by about the same amounts, or (*b*) the relative measurements do not give a satisfactory connection between the multiplet 2 and the rest of the spectrum. Probably both of these points are involved to some extent. With regard to the first we might note in Fig. 4 that for all the relevant Mn multiplets E_1 is in the 2–3 eV range. If all of the points were raised by about 0·3 dex (to meet most of the discrepancy), they would not be out of keeping with the pattern for Ti, Cr, Fe and Co in this E_1 range.

6. *Discussion.*—Rohlich (1948) has made a study of the terms in Ti and finds that a redesignation of the odd terms will improve the relative *f*-values of several multiplets. The use of Rohlich's designations reduces the scatter of the Ti points in Figs. 3 and 4 to some extent but does not alter the general pattern.

His calculations for inter-parent multiplets are very satisfactory but are not included in our analysis because there are no corresponding results for other iron-group atoms. His investigation leaves the impression that in Ti there is no set of designations that can be regarded as completely correct.

Without doubt the same designation difficulty applies in other iron-group atoms. The experience in Ti makes it reasonable to suppose that interactions and designation faults can account for most of the *scatter* of at least the A, E, F, G, H multiplets in Figs. 3 and 4.

We are left with a need to consider the general trends.

Fig. 5 (i) gives the impression that there is no general trend of log (obs./calc.) against E_1 for the A, E, F, G, H multiplets. However when the high absolute values of Mn are taken into consideration (see end of Section 5) seven points in the range $E_1 = 2$–3 eV may need to be raised by about 0·3 dex. Also the level of the cluster of points due to Ni near $E_1 = 3{\cdot}6$ eV has not been determined experimentally. It is therefore still possible that there is a vestige of E.P. dependence among the A, E, F, G, H multiplets. It could not be more than about $+0{\cdot}2$ dex/eV and therefore very much less than the effect first exhibited by Allen and Asaad (1955). Experiments with higher temperature sources and independent temperature standards are perhaps the best means of resolving final doubts on this question.

On the other hand the change of the observed/calculated ratio with excitation potential is considerable for the B and C multiplets as can be seen from Fig. 5 (ii). Also these two transition types are distinguished by having a variation with wavelength, as seen in Fig. 6. It seems unlikely that the E and λ variations are physically independent and there is no correlation between E_1 and λ that could account for the two trends. However, both could be explained by one cause

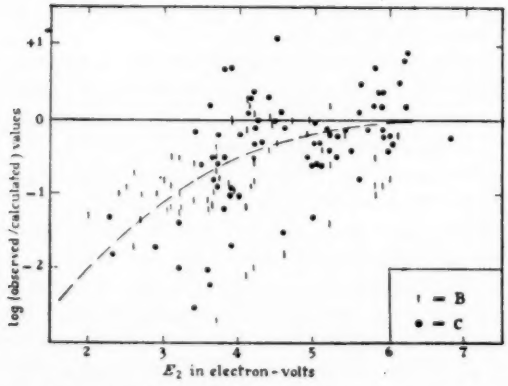

FIG. 7.—*Relation between (observed/calculated) values (for B and C transitions) and the upper excitation potential. The broken line represents the main trend.*

if the departure from agreement were due entirely to the *upper* level. This does correlate with wavelength and could account for the λ variation. Furthermore if the ratio obs./calc. be plotted against E_2, the upper E.P., see Fig. 7, the relation becomes

clearer and the variation larger. This argument suggests fairly strongly that it is the position of the upper level that is important in deciding the intensity; that for $E_2 > 4$ eV the B and C intensities agree absolutely with calculations (though with a large scatter), and that for $E_2 < 4$ eV intensities are diminished by systematic factors that can be as much as 1·5 dex at $E_2 \simeq 2{\cdot}5$ eV. Although this argument points to the position of the upper level as being responsible for the depression of intensities of both the B and C transitions there is no evidence of a correlation for individual B and C transitions that have the same upper level.

Finally we should give an indication of what values might be regarded as the best available. Except for a possible scale correction these are given in the 'mean' column of Table I. To obtain a scale correction it seems safest to make a compromise between observed and calculated values. From the foregoing discussion and Table V, I offer the following corrections as the best available at present. When no absolute observations are available there seems no reason to make any correction.

Element	Sc	Ti	V	Cr	Mn	Fe	Co	Ni
Correction in dex	0·0	0·0	0·0	0·0	+0·25	+0·10	0·0	−0·1

University of London Observatory,
Mill Hill Park,
London, N.W.7:
1960 *May.*

References

Aarts, J., Harting, D. and Bakker, C. J., 1954, *Physica*, **20**, 1250.
Allen, C. W., 1955, *Astrophysical Quantities*, Athlone Press, London.
Allen, C. W. and Asaad, A. S., 1955, *M.N.*, **115**, 571.
Allen, C. W. and Asaad, A. S., 1957, *M.N.*, **117**, 36.
Asaad, A. S., 1956, Thesis, London.
Bates, D. R. and Damgaard, A., 1949, *Phil. Trans.*, A, **242**, 101.
Bell, G. D., Davis, M. H., King, R. B. and Routly, P. M., 1958, *Ap. J.*, **127**, 775.
Bell, G. D., Davis, M. H., King, R. B. and Routly, P. M., 1959, *Ap. J.*, **129**, 437.
Carter, W. W., 1949, *Phys. Rev.*, **76**, 962.
Condon, E. U. and Shortley, G. H., 1935, *Theory of Atomic Spectra*, p. 241, Cambridge.
Davis, M. H., Routly, P. M. and King, R. B., 1954, Stellar Atmospheres Conference, Indiana, p. 47.
Estabrook, F. B., 1952, *Ap. J.*, **115**, 571.
Goldberg, L., 1935, *Ap. J.*, **82**, 1.
Goldberg, L., 1936, *Ap. J.*, **84**, 11.
Heid, R. L. and Dieke, G. H., 1954, *J.O.S.A.*, **44**, 402.
Hill, A. and King, R. B., 1951, *J.O.S.A.*, **41**, 315.
Huldt, L. and Lagerqvist, A., 1952, *J.O.S.A.*, **42**, 142.
King, R. B., 1942, *Ap. J.*, **95**, 78.
King, R. B., 1947, *Ap. J.*, **105**, 376.
King, R. B., 1948, *Ap. J.*, **108**, 87.
King, R. B., 1956, private communication, Nov. 27.
King, R. B. and King, A. S., 1935, *Ap. J.*, **82**, 377.
King, R. B. and King, A. S., 1938, *Ap. J.*, **87**, 24.
King, R. B., Parnes, B., Davis, M. and Olsen, K., 1955, *J.O.S.A.*, **45**, 350.
Kopfermann, H. and Wessel, G., 1951, *Z. f. Phys.*, **130**, 100.
Mitrofanova, L. A., 1952, *Izv. Ob. Pulkova*, **19**, No. 149, 81.
Mitrofanova, L. A., 1954, *Izv. Ob. Pulkova*, **19**, No. 152, 100.

Mitrofanova, L. A., 1955, *Izv. Ob. Pulkova*, **19**, No. 153, 107.
Mitrofanova, L. A., 1958, *Izv. Ob. Pulkova*, **21**, No. 162, 159.
Moore, C. E., 1945, *Revised Multiplet Table*, Contr. Princeton Univ. Ob., No. 20.
Moore, C. E., 1949, *Atomic Energy Levels*, NBS Circ. 467.
Moore, C. E., 1952, *Atomic Energy Levels*, NBS Circ. 467.
Ornstein, L. S. and Bouma, T., 1930, *Phys. Rev.*, **36**, 679.
Ostrovsky, Yu. I., 1958, *Oscillator strength measurements*, Thesis, Leningrad.
Ostrovsky, Yu. I., Parchevsky, G. F. and Penkin, N. P., 1956, *Opt. i. Spek.*, **1**, 821.
Ostrovsky, Yu. I. and Penkin, N. P., 1957 a, *Opt. i. Spek.*, **3**, 193.
Ostrovsky, Yu. I. and Penkin, N. P., 1957 b, *Opt. i. Spek.*, **3**, 391.
Rohrlich, F., 1948, *Phys. Rev.*, **74**, 1381.
Unsöld, A., 1955, *Physik der Sternatmosphären*, 2nd Ed., Springer.
van Driel, H., 1935, Utrecht Dissertation.
van Stekelenburg, L. H. M. and Smit, J. A., 1948, *Physica*, **14**, 189.
Ziock, K., 1957, *Z. Phys.*, **147**, 99.

THE PHOTOELECTRIC LIGHT CURVE OF FU ARAE

G. G. Cillié and E. M. Lindsay

(Received 1960 May 26)

Summary

Photoelectric light curves have been obtained in blue and yellow light for the star FU Arae using the 60-inch Rockefeller reflector of the Boyden Observatory. There are two equal fairly flat topped maxima. Primary minimum is much deeper than secondary; the latter occurs at 0·5 phase. The light elements are Min. = JD 2426869·490 + 0^d·864500957*E*.

The variability of FU Arae was discovered by Miss Swope (1) in a search for variables in Harvard Milky Way Field 233. It was designated H*v* 6768 and is the star CPD −58°7173. From measurements on 106 plates taken with the 10-inch Metcalf telescope Miss Swope concluded that the star was an eclipsing binary, its magnitude varying between 11·2 and 11·6. She derived the following light elements for the system.

$$\text{Min.} = \text{JD } 2426869{\cdot}490 + 0^d{\cdot}86450E.$$

FU Arae was observed on 30 nights during 1954 and on 21 nights in 1956 using the 60-inch Rockefeller reflector and Linnell-King photoelectric photometer of the Boyden Observatory. The total number of individual observations was 1171 in blue and 874 in yellow light. The blue filter was a Corning No. 5551; the yellow a Corning No. 3385. Comparisons with a nearby standard star are expressed as magnitude differences Δm_b and Δm_y for blue and yellow light respectively.

From primary minima observed on two nights in 1956 the following light elements were computed:

$$\text{Min.} = \text{JD } 2426869{\cdot}490 + 0^d{\cdot}864500957E.$$

Table 1 gives the differences between the observed and predicted minima in heliocentrically corrected time.

TABLE I

Primary minima of FU Arae

Date of run	Observed time of prim. min.	Wt.	Min. = 2426869·490 + 0^d·864500957*E* Calc. min.	O–C
	243		243	
1956 August 27/28	5713·33335	3	5713·33479	−·00144
1956 September 3/4	5720·25224	3	5720·25080	+·00144

In Tables II and III the normal points of the blue and yellow light curve are given. The first and second columns give the phases and magnitude differences respectively of the normal points. The third column gives the mean error for each normal point and the fourth column its weight, that is, the number of observations used in forming it.

TABLE II

Normal points of blue light curve of FU Arae

Phase (period)	Δm_b	M.e. of normal pt.	Wt.	Phase (period)	Δm_b	M.e. of normal pt.	Wt.
	m	m			m	m	
0·0012	+0·893	±0·004	33	0·5018	+0·112	±0·002	54
·0185	·770	·007	21	·5344	·095	·004	31
·0376	·520	·003	35	·5614	+0·065	·004	23
·0608	·231	·004	26	·5890	−0·015	·004	33
·0850	+0·066	·003	25	·6120	·022	·003	24
·1128	−0·028	·003	25	·6361	·033	·004	23
·1384	·048	·002	36	·6638	·053	·004	39
·1620	·066	·003	31	·6869	·073	·003	37
·1883	·073	·003	27	·7104	·084	·003	35
·2105	·079	·003	23	·7384	·089	·003	25
·2358	·094	·005	13	·7628	·092	·002	40
·2644	·090	·002	26	·7882	·092	·003	43
·2868	·095	·004	30	·8121	·074	·004	33
·3111	·092	·003	35	·8370	·059	·003	27
·3363	·082	·002	35	·8612	·038	·004	23
·3608	·061	·004	29	·8881	·025	·006	20
·3881	+0·050	·005	22	·9113	·049	·004	25
·4130	−0·011	·003	24	·9371	·228	·005	32
·4386	+0·035	·003	29	·9631	·513	·005	27
·4648	·089	·005	31	·9829	·800	·004	21

TABLE III

Normal points of yellow light curve of FU Arae

Phase (period)	Δm_y	M.e. of normal pt.	Wt.	Phase (period)	Δm_y	M.e. of normal pt.	Wt.
	m	m			m	m	
0·0000	+0·394	±0·003	34	0·5383	+0·245	±0·005	30
·0272	·750	0·02	32	·5858	·146	·003	29
·0527	·446	·004	28	·6198	·119	·003	28
·0837	·204	·003	30	·6614	·089	·003	27
·1131	·111	·003	24	·6856	·072	·003	20
·1372	·096	·002	29	·7108	·060	·003	25
·1614	·077	·003	28	·7392	·064	·004	18
·1940	·063	·003	25	·7626	·054	·003	29
·2251	·058	·004	18	·7879	·062	·003	32
·2683	·050	·002	22	·8105	·068	·005	24
·2970	·064	·003	23	·8360	·092	·003	21
·3246	·068	·004	25	·8613	·125	·003	22
·3562	·087	·004	28	·8887	·134	·006	16
·3927	·116	·003	24	·9145	·210	·004	27
·4248	·154	·003	26	·9425	·398	·004	26
·4583	·241	·003	38	·9728	·739	·006	26
·5018	·287	·003	40				

Fig. 1 gives the blue light curve and Fig. 2 the yellow light curve of the star. The maxima are of equal height and to a small degree are flat topped. They are more so in blue than in yellow light. It would appear that the maximum preceding secondary minimum is flatter than that following secondary minimum,

particularly in blue light. A weakness in the observational material between phases 0·6 and 0·7 would result in such an apparent effect but there is no actual reason to suspect the accuracy of the observations within this phase range.

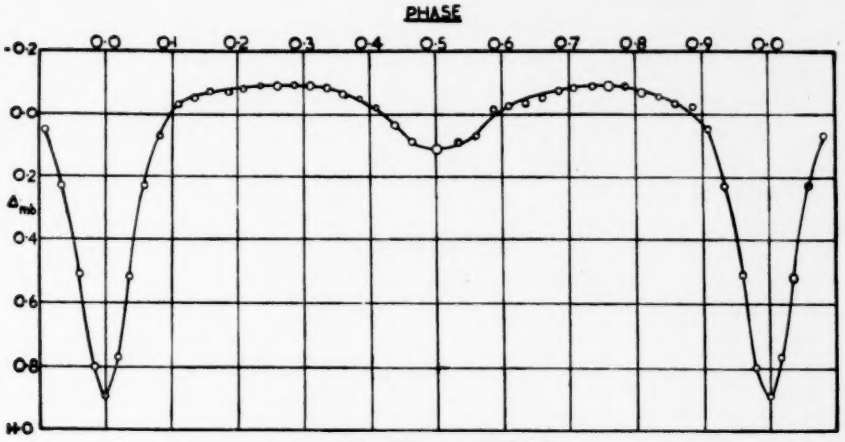

FIG. 1.—*Blue light curve of FU Arae.*

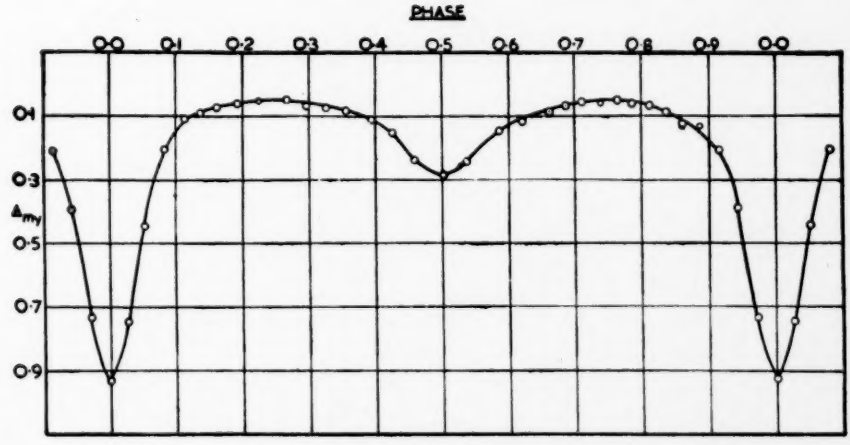

FIG. 2.—*Yellow light curve of FU Arae.*

The range in magnitude is very much greater than found by Miss Swope. At primary minimum it is $0^m{\cdot}97$ in blue light and $0^m{\cdot}89$ in yellow light. At secondary minimum the respective values are $0^m{\cdot}20$ and $0^m{\cdot}23$. Thus primary minimum is much deeper than secondary. So far as can be seen from the light curve the latter occurs at 0·5 phase.

We wish to thank Mr Bester of the staff of the Boyden Observatory for observing the variable for us on a number of occasions. We are also grateful to C.S.I.R. Pretoria for a grant to one of us (G. G. C.) for assistance towards completing the reductions.

The individual observations of FU Arae in blue and yellow light will be distributed with Armagh Contribution 30.

Department of Mathematics,
University of Stellenbosch,
Union of South Africa:

Armagh Observatory,
Northern Ireland:

1960 *May* 7.

Reference

(1) Henrietta H. Swope, H.A., **90**, No. 7, 1936.